VUV Reflectivity Spectra of Rare-Earth Sesquioxides II

Fumitaka ARAI, Shin-ichi KIMURA, Yasuhiko SATO,
Mikihiko IKEZAWA, Yuki CHIBA and Mareo ISHIGAME

Research Institute for Scientific Measurements, Tohoku University, Aoba-ku, Sendai 980

Rare-earth elements are characterized by the 4*f* electrons, and their compounds have some interesting properties such as the mixed valence state. So we measured a series of rare-earth sesquioxides (R_2O_3's), which are typical insulator compounds, for the purpose of investigating the fundamental electronic state of the rare-earth compounds. We have already reported the VUV reflectivity spectra of four kinds of R_2O_3 single crystals (R=La, Nd, Gd and Y) [1]. In this report, we measured the reflectivity spectra of another four kinds of R_2O_3 single crystals (R=Er, Tm, Yb and Lu) for the first time in the photon energy region between 4 eV and 35 eV at 300K at the beamline BL7B. We discuss the electronic structure of these materials including the 4*f* multiplet structure.

We made single crystals of all samples by the floating zone method using a Xe-arc lamp image furnace. All compounds form bcc type crystal structure, which is called the C-type. We measured the reflectivity spectra using the cleavage surface along to the (111)-plane.

Figure 1 shows reflectivity spectra of five kinds of R_2O_3 materials (R=Y, Er, Tm, Yb and Lu). Y_2O_3 has no 4*f* electron and has the same bcc crystal structure as other R_2O_3. We adopted Y_2O_3 as the reference material of R_2O_3 because the ionic radius of Y^{3+} is almost the same as that of Er^{3+}, Tm^{3+}, Yb^{3+} and Lu^{3+}. All spectra are similar to one another. This means that the origin of the main structure of these spectra is almost equal to one another.

We will make a detailed analysis using the optical conductivity spectra (Figure 2), which are derived from the Kramers-Kronig transformation of the reflectivity spectra in Figure 1. There are three peak structures in common, which are located around 10 eV (here called a), 18 eV (b) and 30 eV (c). In our previous papers, we have explained that the origin of the main part of the structure a is the excitation from the valence band (O-2*p*) to the conduction band (R-5*d*), that of the peak a' is the exciton of the peak a, and that of the peak c is the intra-atomic excitation from R-$5p_{3/2}$ to R-5*d* states [1, 2]. The structure due to the transition from R-$5p_{1/2}$ to R-5*d* is not seen in this figure because this peak is expected to be out of the observed energy range at about 38 eV. The origin of the peak b is considered to be the transition from O-2*s* to R-5*d* states, because this energy position and structure are almost the same among the materials and the energy position is expected from the atomic states of rare-earth and oxygen [3].

It can be seen that the detailed structure of peak a in each R_2O_3 spectrum is different from one another. It is obvious that the reason for this is the difference of the expanse of the R-4*f* states due to the 4*f* multiplet. The peak structure due to the transition from O-2*p* to Y-4*d* is thought to be almost equal to that from O-2*p* to R-5*d* because the band shape of 4*d* in Y_2O_3 is as almost same as that of 5*d* in R_2O_3. Therefore the difference structure of the peak a among each R_2O_3 is thought to be due to the expanse of R-4*f* electrons. We show the 4*f* multiplet structure which is estimated from the theoretical expectation [4] in Figure 2. The peak structure of R_2O_3 which is different from that of Y_2O_3 around 10 eV is thought to be explained by the R-4*f* multiplet structure. However, the peaks of R_2O_3 at about 7 eV indicated by a" are located at almost same energy position in each R_2O_3 spectrum, and can't be explained by this consideration. These peaks are thought to be due to the exciton of the transition from R-4*f* to R-5*d*.

References
[1] S. Kimura, F. Arai, M. Ikezawa, Y. Chiba and M. Ishigame, UVSOR Activity Report 1991, 86 (1992).
[2] S. Kimura, T. Nanba, T. Tomikawa, S. Kunii and T. Kasuya, Phys. Rev. **B46**, 12196 (1992)
[3] C. E. Moore, *Atomic Energy Levels vol. 1 and 3*, (U. S. Government Printing Office, Washington D. C., 1949)
[4] M. Campagna, G. K. Wertheim and Y. Bear, *Photoemission in Solids II*, L. Ley and M. Cardona (eds.) (Springer–Verlag, 222 1979)

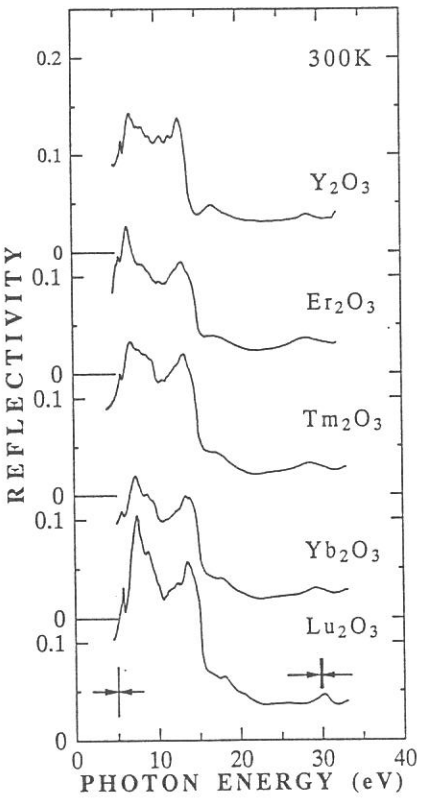

Fig.1. Reflectivity spectra of R_2O_3(R=Y,Er,Tm,Yb and Lu) single crystals in the photon energy region between 4 eV and 35 eV at 300K.

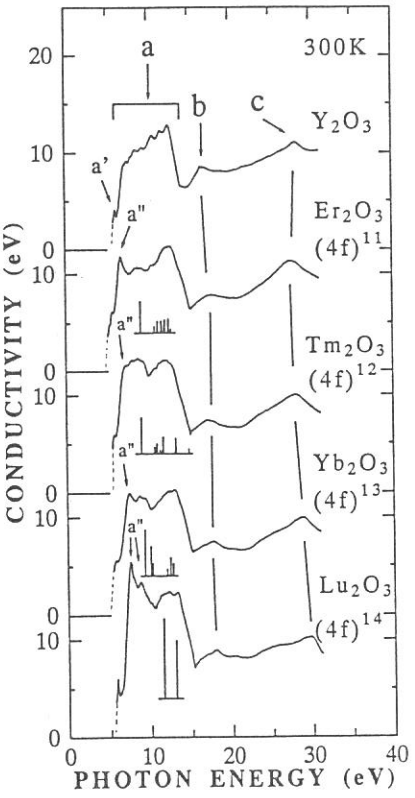

Fig.2. Optical conductivity spectra of R_2O_3's from the Kramers–Kronig transformation of the reflectivity spectra and 4*f* multiplet structures derived from theory (refer to [4]).

GENERATION OF OXYGEN DEFICIENT DEFECTS IN SYNTHETIC SILICA GLASS BY QUENCHING

Shigetosi Hayashi, Hiroshi Kawazoe*
Fine Ceramics Research Laboratory, Advanced Technology Research Laboratories of Sumitomo Metal Industries Ltd., 16-1 Sunayama, Hasaki, Kashima-gun, Ibaraki 314-02
*Research Laboratory of Engineering Materials, Tokyo Institute of Technology, Midori-ku, Yokohama 227

Informations on the generation mechanism and the properties of oxygen deficient defects in synthetic silica glass are very important in the use of the glass as optics in ultra-violet regions. We already reported that ≡Si-Si≡ (one type of the oxygen deficient defects) is generated by chlorine evaporation during sintering of the porous silica glass obtained by VAD (Vapor-phase Axial Deposition) method with several tens of ppm chlorine.

Another generation mechanism of ≡Si-Si≡ in synthetic silica glass was found in the present study. Samples were prepared by quenching the consolidated silica glass plates (from 1000 ℃ to 1500 ℃) These silica glasses contain less than 20 ppm of OH groups and less than 1 ppm of Cl. Absorption spectra of the samples were measured at the beam line BL1B.

Fig.1 shows absorption spectra of quenched silica glasses. In the sample heated at 1000 ℃ no optical absorption peak was observed, but in samples heated at higher temperature 7.6 eV absorption intensity (≡Si-Si≡) increased as raising their heating temperature.

Fig.2 shows Arrhenius' plots of the yields of ≡Si-Si≡ defects calculated by using absorption cross section 6 10^{-17} cm^2. It seems that the defects were generated by the thermally activated process.

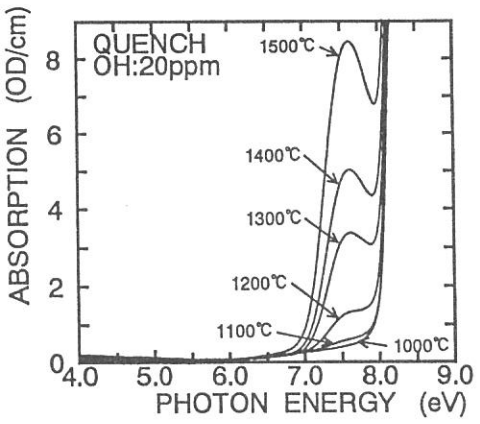

Fig.1 Generation of 7.6eV-absorption band in low OH-silica glass by quenching.

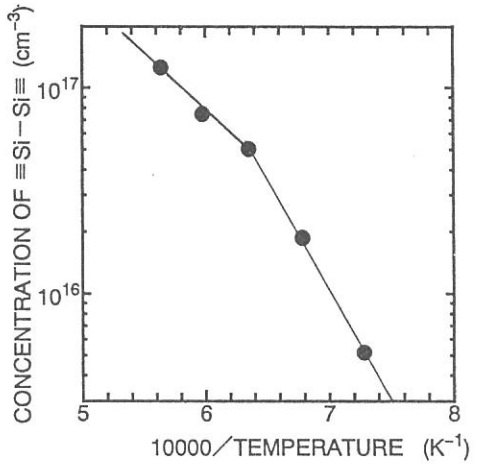

Fig.2 Arrhenius' plots of ≡Si-Si≡ yields in synthetic silica glasses by quenching.

CONVERSION OF OXYGEN VACANCY INTO E' CENTER INDUCED BY EXCIMER LASER IRRADIATION IN HIGH-PURITY SILICA

Hiroyuki NISHIKAWA, Takayuki SOTA, and Yoshimichi OHKI
Department of Electrical Engineering, Waseda University
3-4-1 Ohkubo, Shinjuku-ku, Tokyo 169

Optical absorption in ultraviolet (uv)-vacuum uv (vuv) regions were measured on high-purity silicas irradiated by excimer lasers. Samples investigated are oxygen-deficient silicas with low-OH ([OH]<1 ppm) and high-OH ([OH]≈ 20 ppm) concentrations. Irradiation was carried out with ArF (6.4 eV) or F_2 (7.9 eV) excimer laser at room temperature. Vacuum-uv-transmission measurements were done using synchrotron radiation from UVSOR as a light source. Shown in Figs.1 and 2 are uv-vuv absorption spectra obtained for the low-OH and high-OH oxygen-deficient silicas, respectively, after irradiation with 6.4-eV or 7.9-eV photons. Although the appearance of absorption bands at 5.0 and 5.8 eV can be seen, no significant change is observed in an absorption band at 7.6 eV in the low-OH sample. On the other hand, the decay of the 7.6-eV band is observed in conjunction with a significant growth of the 5.8-eV band in the high-OH sample, as shown in Fig.2. The 5.8-eV and 7.6-eV bands are considered to be due to E' center (≡Si·)[1] and oxygen vacancy (≡Si-Si≡)[2], respectively. Therefore, these results indicate that the conversion of the oxygen vacancies into E' centers is enhanced in the presence of hydrogen. The following mechanism is considered to be responsible for the conversion of the oxygen vacancy:

$$\equiv Si\text{-}Si\equiv + \cdot H \rightarrow \equiv Si\text{-}H \quad \equiv Si\cdot \qquad (1).$$

This mechanism involving the formation of the E' variant ($\equiv Si\text{-}H$ $\equiv Si\cdot$) in the high-OH sample is supported by the observation of a peak shift relative to the 5.8-eV band of the E'_{γ} center ($\equiv Si\cdot\ ^{+}Si\equiv$) by 0.1 eV to the lower energy.

References

1. C.M. Nelson and R.A. Weeks, J. Am. Ceram. Soc. 43, 396 (1960).

2. R. Tohmon et al. Phys. Rev. B 39, 1337 (1989).

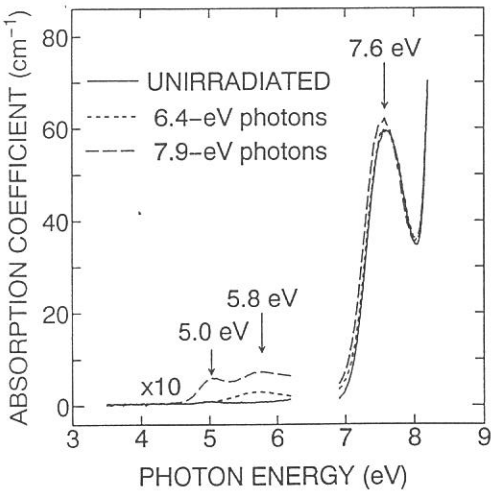

FIG.1 UV-VUV spectra of low-OH oxygen-deficient silica ([OH]<1 ppm) irradiated by 6.4-eV or 7.9-eV excimer laser

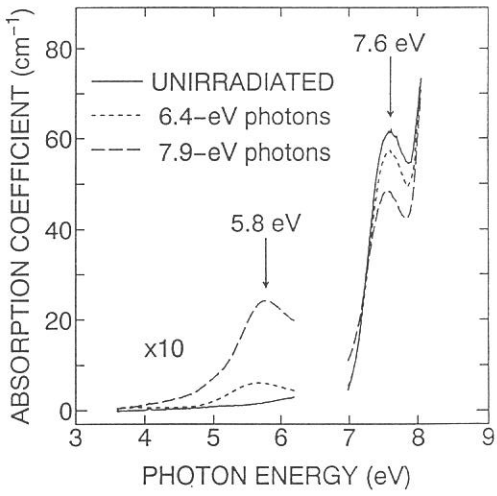

FIG.2 UV-VUV spectra of high-OH oxygen-deficient silica ([OH]≈20 ppm) irradiated by 6.4-eV or 7.9-eV excimer laser

REFLECTION SPECTRA OF Pb HALIDES AND BiI_3 IN THE 5*d* CORE EXCITON REGION

Masami FUJITA, Hideyuki NAKAGAWA,[+] Atsuhiko KASHINO,[+]
Kazutoshi FUKUI,[+] Takeshi MIYANAGA[++] and Makoto WATANABE[+++]

Maritime Safety Academy, Wakaba, Kure 737
[+]*Department of Electrical and Electronics Engineering, Faculty of Engineering, Fukui University, Fukui 910*
[++]*Department of Physics, Faculty of Education, Wakayama University, Wakayama 640*
[+++]*Institute for Molecular Science, Myodaiji, Okazaki 444*

The crystal structure of $PbCl_2$ and $PbBr_2$ belongs to orthorhombic (D_{2h}^{16}, *Pmnb*), while that of PbI_2 belongs to hexagonal (D_{3d}^{3}). BiI_3 has a rhombohedral (C_{3i}^{2}) crystal structure. The peaks due to the Pb^{2+} 5*d* core exciton are observed in the optical spectra of Pb halides in the 20-25 eV region.[1-3] In BiI_3, the Bi^{3+} 5*d* core exciton peaks are found in the 25-30 eV region.[1] In the present study, reflection spectra of these crystals were measured in order to investigate the crystal field effect on the core exciton.

Figure 1 shows reflection spectrum of BiI_3 single crystal below 12 eV. First exciton peak is seen at 2.0 eV. Sharp peak is also observed at 3.8 eV. Spectral features below 6 eV agree with those by previous study.[4] No distinct structure is observed between 10 and 25 eV.

In Fig. 2 are shown reflection spectra of Pb halides (upper part) and BiI_3 (lower part) in the metal 5*d* core exciton region. In addition to the three main peaks 1, 2 and 3, the small peak 0 is found in the low energy side of the peak 1 in each crystal. Weak shoulder 1' is observed at the high energy side of the peak 1 in PbI_2 and at the low energy side of the peak 1 in BiI_3. The structures 3 in PbI_2 and BiI_3 are broader than in $PbCl_2$ and $PbBr_2$.

The peaks 1, 2 and 3 are assigned to the transitions from the $^1S_0$ ground state to the $^3P_1$, $^1P_1$ and $^3D_1$ states, respectively. Energy splittings and relative intensities of these peaks in $PbCl_2$ and $PbBr_2$ are explained well based on the atomic excitation picture neglecting the crystal field effect.[3] This means that the anisotropic crystal field in $PbCl_2$ and $PbBr_2$ is weaker than in PbI_2 and BiI_3. The peak 0 in each material and the structure 1' in PbI_2 and BiI_3 are attributed to the transitions allowed by the anisotropic crystal field

effect. Broadness of the peak 3 in PbI_2 and BiI_3 is also ascribed to the crystal field effect. The splitting of the Pb^{2+} 6*p* level in PbI_2 due to the crystal field potential is supposed to be about 1 eV in order to explain the spectrum of PbI_2.

References

1) J. Bordas, J. Robertson and A. Jakobsson: J. Phys. C 11(1978)2607.
2) T. Hayashi, K. Toyoda and M. Itoh: J. Phys. Soc. Jpn. 57(1988)1861.
3) M. Fujita, H. Nakagawa, K. Fukui, H. Matsumoto, T. Miyanaga and M. Watanabe: J. Phys. Soc. Jpn. 60(1991)4393.
4) T. Komatsu and Y. Kaifu: J. Phys. Soc. Jpn. 40(1976)1062.

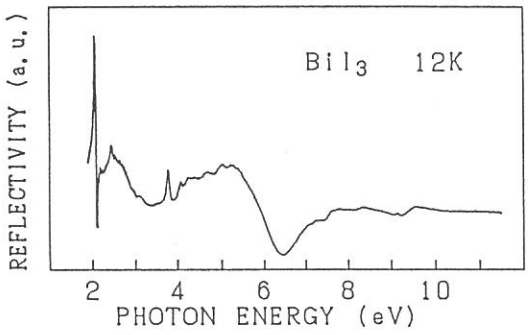

Fig. 1. Reflection spectrum of BiI_3 below 12 eV.

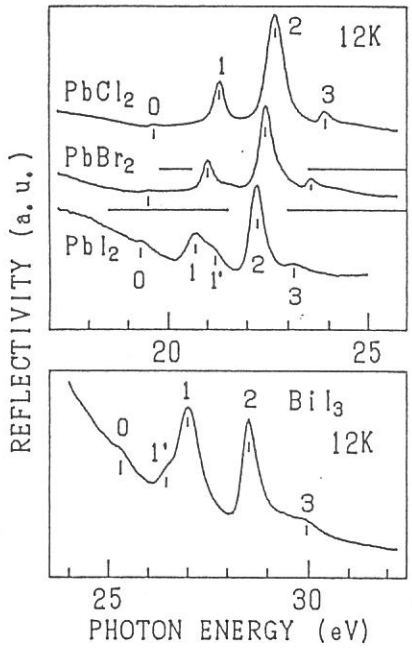

Fig. 2. Reflection spectra of Pb halides (upper part) and BiI_3 (lower part) in the 5*d* core exciton region.

VACUUM ULTRAVIOLET REFLECTANCE SPECTRA OF Mn_2Sb, MnAlGe, Superlattices (Mn/Sb, Fe/Gd, Fe/Nd) AND INTERCALATION COMPOUNDS (M_xTiS_2(M:Ni,Fe))

Shigemasa SUGA, Akio KIMURA, Tomohiro MATSUSHITA,
Yasuaki MORI, Hiroaki SHIGEOKA and Shin Imada

Department of Material Physics, Osaka Universitsy
Toyonaka, Osaka 560

The electronic structures of Cu_2Sb type compounds, magnetic superlattices and TiS_2 intercalation compounds were studied by means of the vacuum ultraviolet reflectance spectroscopy by use of synchrotron radiation from UVSOR electron storage ring. The measurement was done at BL-1B of UVSOR equipped with a Seya-Namioka monochromator. The higher order light was suppressed by use of pyrex, SiO_2 and LiF filters in the wavelength regions above 3000, 1500 and 1000 A. The incidence angle was set to 22.5 degrees and the p reflectance was measured by a photomultiplier. All measurement was done at room temperature. Cleaved surfaces were employed for the intercalation compounds and the as grown surfaces were used for the superlattices. For Cu_2Sb type materials polished surfaces were prepared for the reflectance measurement. The reflectance spectra were obtained by normalizing the spectra by the spectrum of the monochromator output.

Figure 1 shows the reflectance spectrum of $Fe_{1/3}TiS_2$ compared with that of the TiS_2. Since the electronic structure of TiS_2 has been well studied by many authors, the reflectance spectrum can be rather easily understood. The spectrum in the 2-30eV region can be separated into 4 regions with distinct dip structures:(I) the region extending up to 3eV, (II) the region up to 8eV, (III) the region extending up to about 12eV and finally the region extending from 12eV beyond 20eV (IV). According to the band calculation,[1] the transitions between S 3p valence bands and the lower Ti 3d conduction bands which have "t_{2g}" symmetry are dominant in the region I. The region II consists of the transitions from the S 3p valence bands to the higher Ti 3d states with "e_g" symmetry. The transition between the bonding and antibonding orbitals occur in the region III. In the spectrum of $Fe_{1/3}TiS_2$, the sharp peak around 3.5 eV appears in the energy region II. This structure may be related to the Fe 3d state.

The reflectance spectra of the superlattices, Mn/Sb, Fe/Nd and Fe/Gd as well as Mn_2Sb and MnAlGe are summarized in Figs.2 and 3. The similarity between the two spectra of Fe/Nd and Fe/Gd compared with that of Mn/Sb suggests that the spectra in the energy region up to 20eV is mostly governed by the excitation associated with Fe.

Reference
1) A.Zunger and A.J.Freeman, Phys. Rev. B **16**, 906 (1977).

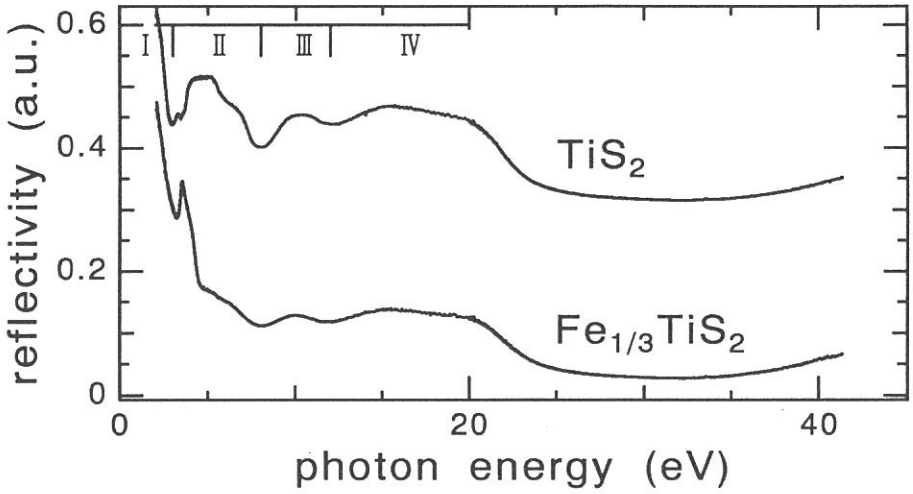

Fig.1

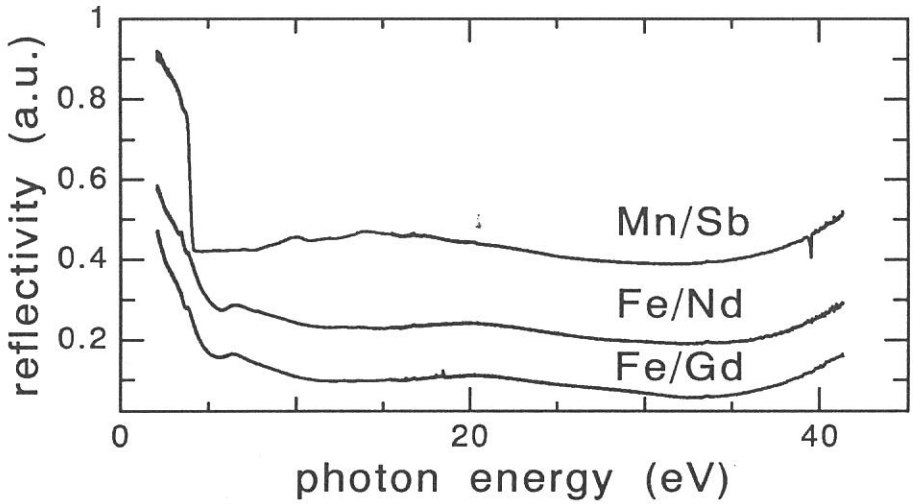

Fig.2

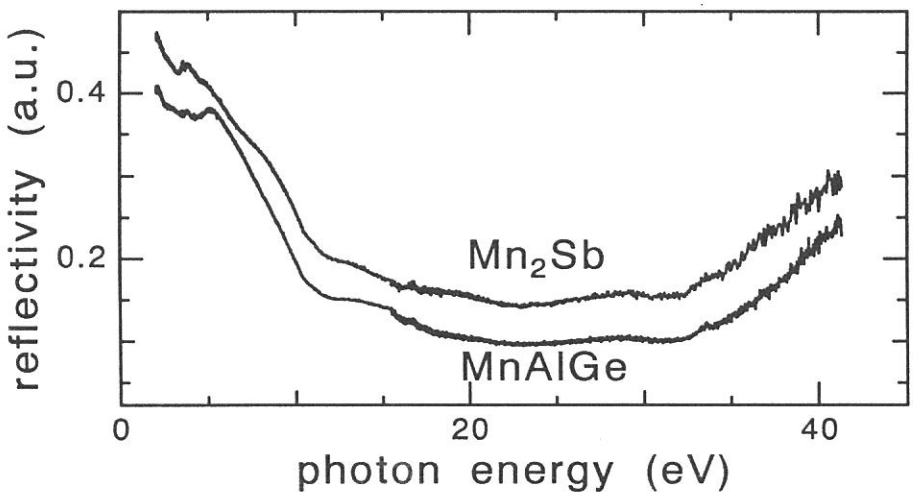

Fig.3

Contribution of Eu^{2+} to PSL Center Formation in $BaFBr:Eu^{2+}$ Single Crystal

Yasuo Iwabuchi, Nobufumi Mori,Terumi Matsuda
Tadaoki Mitani[1], Shigeo Shionoya[2]

Fuji Photo Film Co.,Ltd., Technology Development Center, Miyanodai, Kaisei, Kanagawa, 258 Japan
[1]Institute for Molecular Science, Myodaiji, Okazaki, 444 Japan
[2]Tokyo Engineering University, Department of Electronics, Hachioji, Tokyo, 192 Japan

Previous investigations showed that PSL centers are created efficiently at the energy of exciton formation in $BaFBr:Eu^{2+}$ single crystal.[1] Moreover, at the low energy side of the exciton band, a shoulder-like structure is observed. To clarify an origin of this structure,we measured the change of this structure with increasing the concentration of Eu^{2+}.

$BaFBr:Eu^{2+}$ single crystals were grown by the horizontal Bridgman method in a graphite boat. The various single crystals different in the Eu^{2+} concentration were made by changing the quantity of additional Eu^{2+} at preparation. The measurements using vacuum ultra violet (VUV) light were performed at the beam line BL-7B. The PSL center formation spectra which represents an efficiency of PSL center creation, were measured as follows. The samples were irradiated by chopped He-Ne laser at 10 Hz (633nm:NEC) as scanning the VUV light, and detected the signal of Eu^{2+} luminescence which was synchronized with chopped He-Ne laser excitation by using lock-in amplifier. Eliminating second diffractive light, VUV light was passed through a quartz filter. The electric vector E of the excitation light was always perpendicular to the c-axis of the single crystal.

Figure1 shows PSL center formation spectra in $BaFBr:Eu^{2+}$ single crystals of different concentration of Eu^{2+} at LNT. The concentration of doped Eu^{2+} analyzed by ICP method is (a)0.58% (b)0.15% (c)0.028% respectively. Spectra were normalized at the peak intensity concerning to the first exciton band at 7.2 eV. It is seen that the intensity of the structure at 6.6 eV grows as the concentration of Eu^{2+} increasing. The inset shows the relationship between the analyzed Eu^{2+} concentration in the $BaFBr:Eu^{2+}$ single crystal and the intensity of the structure at 6.6 eV.

As we can see the linear relationship, it is clear that the structure at 6.6 eV is due to the Eu^{2+}.

As to this structure at the low energy side of the exciton, the process of Eu^{2+} ionization is considered from the energy level scheme of $BaFBr:Eu^{2+}$.[2] That is to say, an electron generated by Eu^{2+} ionization is trapped by F^{+} center to form F center and Eu^{3+}. An ionization of Eu^{2+} was observed in alkaline-earth halides such as CaF_2[3], SrF_2, BaF_2[4], so it is sufficiently considered that the ionization of Eu^{2+} occurs in $BaFBr:Eu^{2+}$.

Reference

[1] Y.Iwabuchi, N.Mori, T.Matsuda, T.Mitani and S.Shionoya, UVSOR Activity Report 19 (1992) 128

[2] K.Takahashi, K.Kohda, J.Miyahara, Y.Kanemitsu, K.Amitani and S.Shionoya, J.Lumin. 31&32 (1984) 266

[3] C.Pendrini, F.Rogemond and D.S.McClure, J. Appl. Phys. 59 (1986) 1196

[4] B.Moine, C.Pedrni and B.Courtois, J.Lumin. 50 (1991) 31

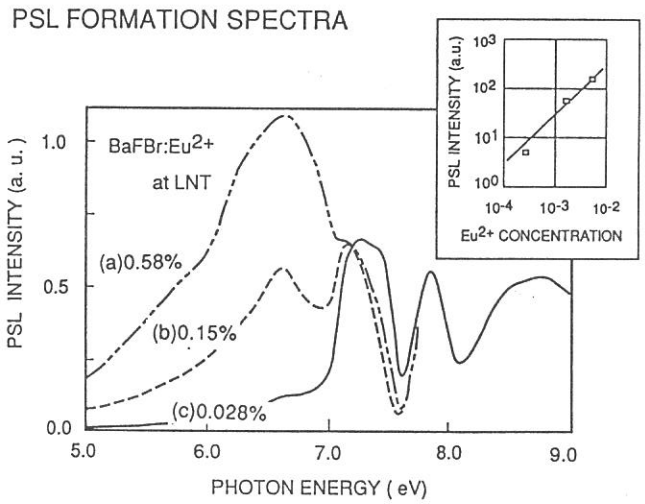

Figure 1 PSL center formation spectra in BaFBr single crystals of different concentration of Eu^{2+} at LNT. The concentration of doped Eu^{2+} is (a)0.58% (b)0.15% (c)0.028% respectively. Inset shows the relationship between the analyzed Eu^{2+} concentration in the $BaFBr:Eu^{2+}$ single crystal and the intensity of the structure at 6.6 eV .

Self-Trapped Excitons in $CdBr_2$ and $CdCl_2$

Hideyuki NAKAGAWA, Atsuhiko KASHINO, Junji YAMADA, Kazutoshi FUKUI, Takeshi MIYANAGA [A], Masami FUJITA [B], Makoto WATANABE [C]

Department of Electrical and Electronics Engineering, Fukui University, Fukui 910, Japan
[A] *Department of Physics, Faculty of Education, Wakayama University, Wakayama 640, Japan*
[B] *Maritime Safety Academy, Kure 737, Japan*
[C] *Institute for Molecular Science, Myodaiji, Okazaki 444, Japan*

Cadmium chloride and bromide are typical ionic crystals of layer structure, where one Cd^{2+}-ion sheet is sandwiched between two halogen ion sheets. A cadmium ion sits at the center of an octahedron composed of six halogen ions located at the vertices. The top of the valence band consists mainly of halogen np (n=3 or 4) orbitals while the bottom of the conduction band has cadmium 5s character. The lowest excitonic absorption corresponds to the transition from halogen np to cadmium 5s levels. Two luminescence bands are produced with excitation in the fundamental absorption region, that is, the one appears in near uv-region (UV-emission) and the other in yellow-region (Y-emission). They are associated with radiative decay of self-trapped excitons (STE). The STE-states in CdX_2(X=Cl or Br) are believed to be identical with the excited states of the $\left[Cd^{2+}X_6^-\right]^{4-}$-complex molecular ions which are formed through exciton-phonon interaction.

Decay profiles of UV and Y emission bands in $CdBr_2$ and $CdCl_2$ are shown in Fig. 1. Excitation was made with single-bunched pulses at 36 eV from an undulator of UVSOR which have 0.5 ns pulse duration and 178 ns pulse interval. The exsistence of long lived decay components gives rise to the piling-up of luminescence intensity. The decay curve of the UV-emission consists of two decay components, the fast(τ_F=11 ns for $CdBr_2$ and 2.0 ns for $CdCl_2$) and the slow($\tau_S \gg 178$ ns) ones. They are sttributed to the parity-allowed radiative decay of the spin singlet and triplet STE's. Detailed examination on the triplet components with use of N_2 gas laser pulses elucidates that the slow decay component is further decomposed into three ones, which indecates that the triplet STE state splits into three level system due to the spin-orbit and exciton-lattice interactions.

The decay curve of the Y-emission contains only the slow component, which is further decomposed into three decay components and is connected to the parity-forbidden radiative decay of STE's.

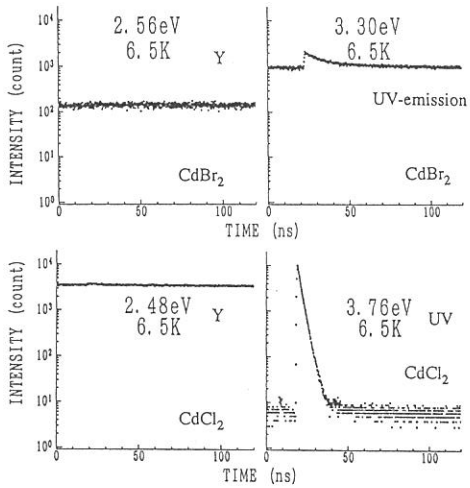

Fig.1 Decay curves of UV and Y emission bands in $CdBr_2$ and $CdCl_2$. Excitation was made with undulator radiation at 36eV. Piling-up arises from the existence of slow components with longer decay time than the pulse interval 178ns.

TIME-RESOLVED MEASUREMENTS OF EXCITATION SPECTRA FOR INTRINSIC EMISSION IN ALKALI IODIDES

Tamao MATSUMOTO, Akinori MIYAMOTO and Ken-ichi KAN'NO

Department of Physics, Kyoto University

We previously reported that the intrinsic emission bands of type I[1] in alkali halides, which are attributed to on-center self-trapped excitons (STE), consist of fluorescent (singlet) and phosphorescent (triplet) components.[2] In the present work, excitation spectrum for each component of these composite bands has been studied in three iodides; 4.21eV band (π_I) in NaI, 4.14eV band (σ) in KI and 3.90eV band (σ) in RbI. Spectra were obtained below and above the temperature at which resonance emission of free excitons (FE) disappears, using the time-resolved detection system of luminescence equipped at BL1B[2].

In Fig. 1 are shown excitation spectra obtained around 15K. Solid curves indicate singlet component and dotted curves indicate triplet components. By chain curves are shown excitation spectra for triplet emission bands from two different configurations of off-center STE's; 3.29eV band (π_{II}) in KI and 2.21eV band (π_{III}) in RbI. All excitation spectra are normalized at 7.0eV. Absorption spectra obtained by Teegarden and Baldini[3] are also shown by broken curves along with arrows indicating the energy positions of n=1 FE, n=2 FE and the onset of band-to-band transition. Both components of type I emission bands are efficiently excited in the whole energy region of band-to-band transition. Excitation spectra for them coincide above 7.0eV in NaI. In KI and RbI, excitation spectra for them and for π_{II} or π_{III} band coincide above 6.5eV. In the energy region between n=1 and n=2 FE, no intrinsic emission bands are excited efficiently. We observed emission bands related to impurities under excitation into this energy region.

In Fig. 2 are shown excitation spectra taken at higher temperature. As for NaI, only excitation spectrum for the triplet component is shown because singlet component disappears at this temperature. Shapes of all excitation spectra in band-to-band transition region are almost similar to those at low temperatures. Between n=1 and n=2 FE energy, however, π bands of three iodides are efficiently excited contrary to the result at low temperature. On the other hand, both components of σ bands in KI and RbI are still not efficiently excited there.

---

[1]K.Kan'no, K.Tanaka and T.Hayashi: Rev.Solid State Science **4,** 383 (1990)
[2]T. Matsumoto, T.Kawata, A.Miyamoto and K.Kan'no:J.Pys.Soc.Jpn. **61**,4229 (1992)
[3]K.Teegarden and G.Baldini: Phys.Rev. **155**,896 (1967)

At low temperature, it is clear that emission yield in the energy region between n=1 and n=2 FE are depressed by the presence of impurities. The n=1 FE, whose diffusion length is sufficiently large in iodides at low temperature,[4] are likely to have chances of being caught by impurities on their long free path.

At higher temperature, total intensity of intrinsic luminescence increases in three iodides in the energy region between n=1 and n=2 FE, reflecting the situation that almost all n=1 FE's immediately relax into STE state. In KI and RbI, it should be remarked that emission bands from off-center configuration increase but that both components of emission bands from on-center configuration do not. This suggests that n=1 FE preferentially relax into off-center configuration. The electron wavefunction of on-center STE is likely to be very diffuse.[5] We imagine that n=1 FE with small radius would not relax into on-center configuration when it can relax into off-center configuration.

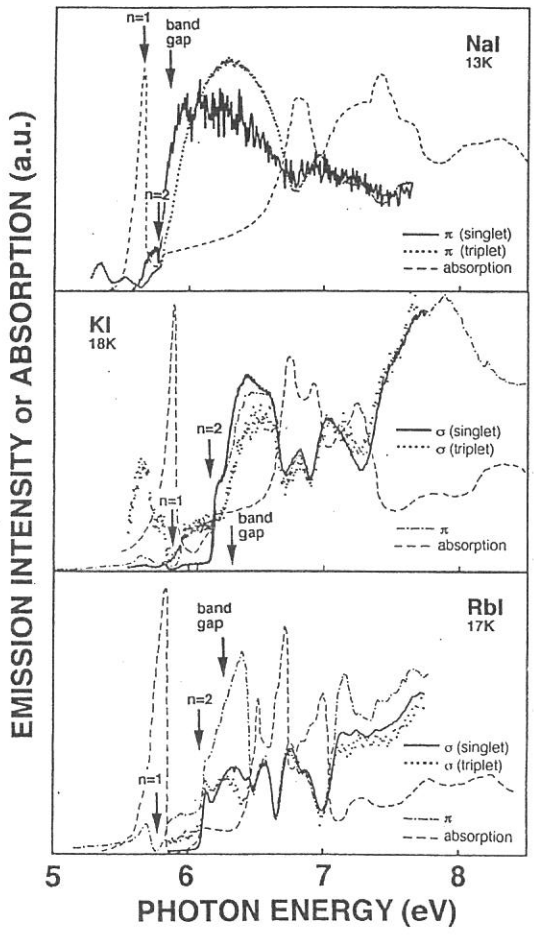

Fig. 1

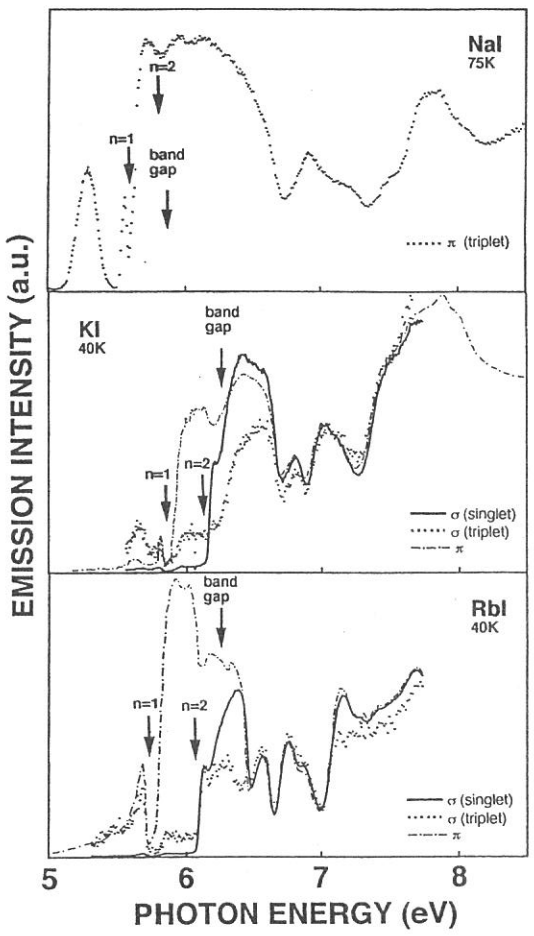

Fig. 2

[4]H.Nishimura: in Defect processes induced by electronic excitation in insulators, Edited by N. Itoh, p.56, World Scientific, (1989)
[5]T.Kawata, T.Mukai, T.Matsumoto and K.Kan'no: Proceedings of ICDIM92 (in press)

TEMPORAL BEHAVIOR OF THE RESONANT LUMINESCENCE OF EXCITONS IN KI AND RbI

Tetsusuke HAYASHI, Masayuki WATANABE, Ping GU*, and Toru TSUJIBAYASHI**

Faculty of Integrated Human Studies, Kyoto University, Kyoto 606-01.

**Department of Physics, Kyoto University, Kyoto 606-01.*

***Osaka Dental University, Hirakata, Osaka 573.*

Photo-excitation in the lowest (n=1) exciton absorption band of alkali iodide crystals induces resonant luminescence of free excitons (FE) together with the luminescence of self-trapped excitons (STE). The efficiency of the FE luminescence relative to the STE luminescence is less than 1×10^{-2}. It has been accepted that the FE state is separated from the STE state by an adiabatic potential barrier and a large part of FE at low temperatures relax to the STE state due to a tunneling process through the barrier.[1] In Fig.1 and 2 are shown the luminescence spectra of FE in KI and RbI. The main band at 5.828 eV in KI and that at 5.729 eV in RbI were identified recently as the emission from the triplet (J=2) state of FE.[2,3] We can observe a weak singlet emission on the high energy side of the main band. We have measured, for the first time, the temporal behavior of the triplet emission of FE, and examined the dynamical process of exciton relaxation.

Measurements were performed with BL1B of UVSOR under normal operation. The luminescence signal was collected through lenses set inside and outside of a sample chamber, and was dispersed with a single-path monochromator. Decay curves were measured with the time-correlated single photon counting method by using a MCP photomultiplier and a TAC system.

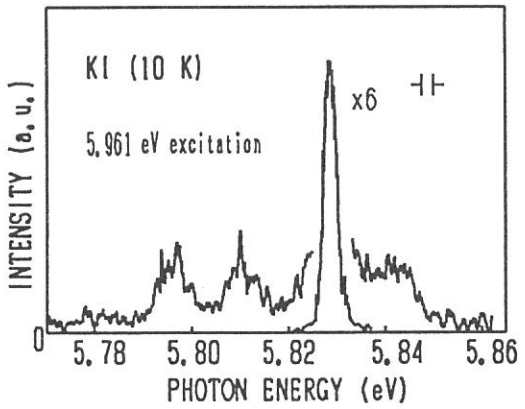

Fig.1 Emission spectrum of FE in KI at 10K.

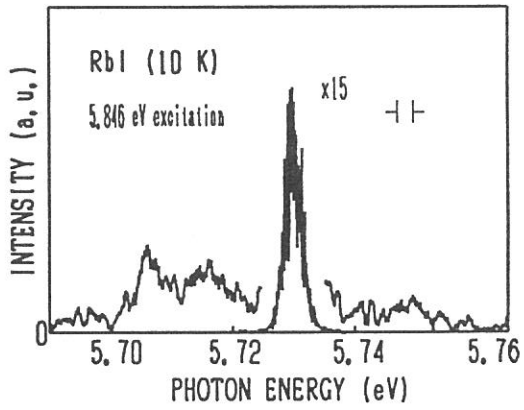

Fig.2 Emission spectrum of FE in RbI at 10K.

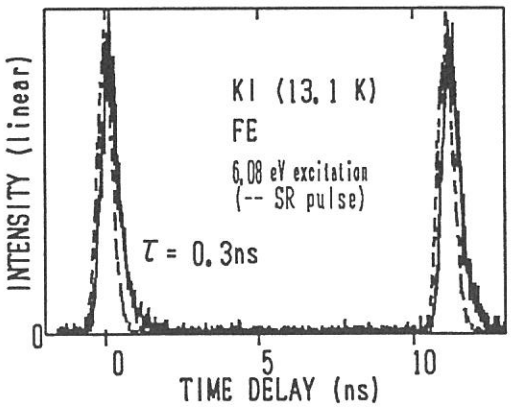

Fig.3 Temporal behavior of the FE luminescence in KI at 13.1K.

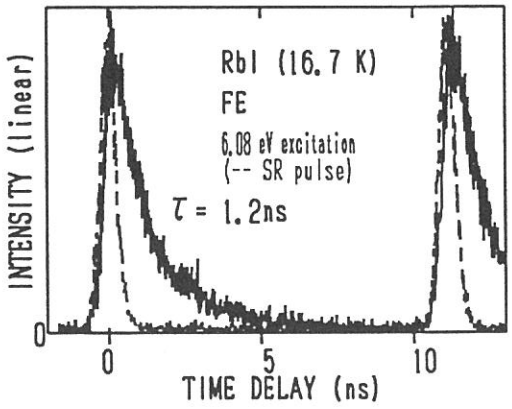

Fig.4 Temporal behavior of the FE luminescence in RbI at 16.7K.

The decay profiles of the FE luminescence at around 15 K in KI and RbI are presented in Figs.3 and 4. The excitation photon energy was 6.08 eV. The emission signals due to the two successive excitation pulses are shown together with the time response of the excitation pulse (dotted curve). The decay times of 0.3 ns for KI and 1.2 ns for RbI are obtained from the convolution analysis. We have obtained the yield of the FE luminescence of 2.5×10^{-3} for KI and 8.3×10^{-3} for RbI from the conventional measurement of the emission spectra on assuming the total luminescence efficiency to be unity. We can see that the difference in the luminescence yield between KI and RbI is roughly corresponding to the difference in the decay time. That is, the observed decay times are not the radiative lifetimes of FE, but they are determined by the self-trapping rate. The radiative lifetime of FE could be longer than 100 ns, which supports the identification of the relevant state of the FE luminescence as the triplet state.

References

1) K. Nasu and Y. Toyozawa: J. Phys. Soc. Jpn. **50** (1981) 235.
2) K. Tanimura and N. Itoh: Phys. Rev. **B45** (1992) 9417.
3) T. Kishigami-Tsujibayashi, K. Toyoda, and T. Hayashi: Phys. Rev. **B45** (1992) 13737.

VARIATION OF DECAY CURVES FOR AUGER-FREE LUMINESCENCE FROM BaF_2 AND CsCl CRYSTALS AGAINST EXCITING PHOTON ENERGY

Yoshihiko NUNOYA, Jian-zhi RUAN(GEN) and Shinzou KUBOTA

Rikkyo University, Nishi-Ikebukuro 3, Tokyo, 171

Decay curves for Auger-free luminescence from BaF_2 and CsCl crystals have been measured over the range of incident photon energy $h\nu$ from the threshold E_{th} of the luminescence to 30 eV. Motivation for this study is to explain the non-single exponential decay in luminescence intensity from BaF_2 and CsCl crystals under excitation of uv photons, as shown in Fig.1.[1] We should note that under excitation with 22 eV photons the decay curve for the 5.6 eV band from BaF_2 crystal has a short decay component with decaytime of 0.4 ± 0.1 ns together with the main decay component of 0.83± 0.02 ns. Under excitation of high-energy electrons due to 511 keV photons, the decay shows a single exponential decay with a decay time of 0.90 ± 0.05 ns. The difference in decay curves of the 4.5 eV band from CsCl is also observed in CsCl, as shown in Fig.1.

The experiment was carried out by using a 1-m Seya-Namioka monochromator at BL7B beam line of UVSOR. The experimental set up is similar to that described in Ref.2. Decay curves were measured by using 5.632 MHz UVSOR single bunch operation. Energy resolved luminescence photons were detected by a MCPPM (Hamamatsu R1564U-30).

For $E_{th} < h\nu < 20$ eV and $h\nu > 27$ ev, the measured decay curves of the 5.6 eV band from BaF_2 crystal show a single exponential decay down to the intensity of 1/500 of the peak intensity. The decay time is found to be 0.83 ±0.02 ns. For 20 eV < $h\nu$ < 26 eV a short component of decay time of 0.4 ns is observed together with the main decay component of 0.83 ns. The short component is also observed from BaF_2 crystal at liquid nitrogen temperature. The origin of the short decay component is unknown.

Decay curves of the 4.5 eV band from CsCl at room temperature have at least two exponential decay components with decay time of 0.6 ± 0.1 ns and 1.55 ± 0.05 ns. No appreciable energy dependence in decay curves is observed in the energy range from E_{th} to 30 eV which are related to different absorption coefficients. By considering no energy dependence in decay curves, the non-single exponential decay observed here can not be linked to the surface effect.[3] The surface

effect has been proposed to explain the faster decrease in luminescence intensity of the 4.5 eV band from CsCl under Cs^+ 4d core excitation of 80 eV < hν < 140 eV with increasing absorption coefficient. Under Cs^+ 4d core excitation decay curves have at least two exponential decay components of a short component with 0.1 - 0.2 ns decaytime and a second component with 1 - 1.5 ns decaytime. The decay curve under Cs^+ 4d core excitation is faster than that of uv photon excitation.

References:
1.S.Kubota, Proceedings of the tenth international conference on vacuum ultraviolet physics, Paris, 1992 (World Scientific Publication), in press.
2. S.Kubota, M.Itoh, J.Ruan(Gen), S.Sakuragi and S.Hashimoto, Phys. Rev. Letters (1988)183.
3. S.Kubota, M.MacDonald and I.H.MunroJ.Lum. 48 & 49(1991)589.

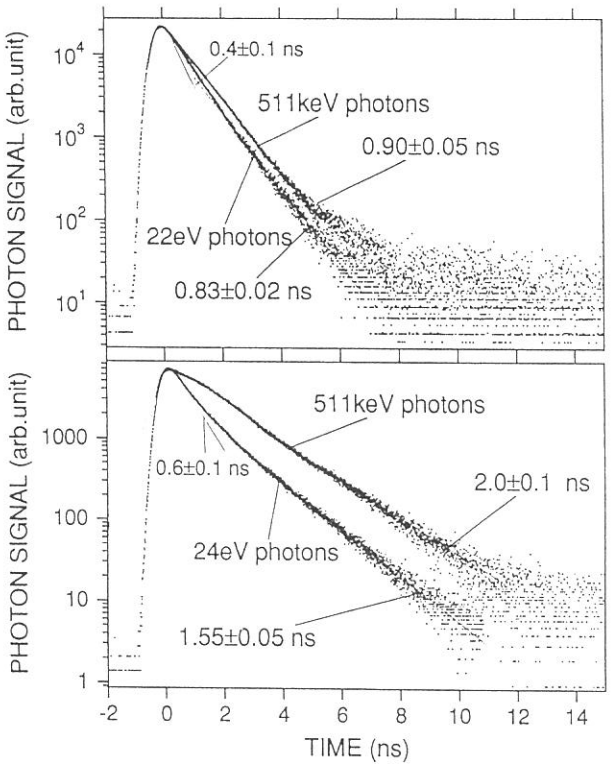

Fig.1. Decay curves for the 4.5 eV band from CsCl and for the 5.6 eV band from BaF_2 under uv photons and high-energy electron excitation by using 511 kev photons.

LIGHT AMPLIFICATION DUE TO POPULATION INVERSION BETWEEN THE VALENCE AND OUTERMOST-CORE BANDS IN BaF_2

Minoru ITOH and Hiroshi ITOH*

Faculty of Engineering, Shinshu University, Nagano 380
**Faculty of Education, Kagawa University, Takamatsu 760*

In BaF_2, a core hole created in the Ba^{2+} $5p$ band decays primarily through the radiative recombination with an F^- $2p$ valence electron, because the Auger decay process is energetically impossible. The resulting luminescence has been called "Auger-free (AF) luminescence ".[1] We notice that both the valence and core bands are completely filled with electrons at thermal equilibrium. As a result, it is likely that an inverted population between these two levels is easily realized at any intensity of excitation through which some electrons are elevated from the core band to the conduction band, leading to a laser oscillation of AF luminescence.

The present experiment was performed at room temperature by using an undulator radiation from the UVSOR ring as a pumping source. A 1-mm-thick plate of BaF_2 was mounted on a rotatable sample holder installed in a vacuum chamber. A flat multiple-dielectric coated mirror (R = 100% at 217 nm) and a quartz plate were placed close to the sample in the direction perpendicular to the exciting beam; see the inset in Fig. 1. Thus it was possible to form an optical cavity by suitably adjusting the orientation of the dielectric mirror. Without using lenses, the luminescence was observed through a grating monochromator, the entrance slit of which was 70 cm away from the sample.

Figure 1 shows luminescence spectra of BaF_2 measured under the core-band excitation with 36.0-eV photons; (a) no collimation and (b) best collimation. A broad band around 300 nm is due to the radiative annihilation of a self-trapped exciton. In (a), two emission bands are seen at 219 and 195 nm. These bands have been assigned to the AF luminescence of BaF_2. It is clear that the peak intensity of the 219-nm band is enhanced when the mirror is adjusted for best attainable collimation. In Fig. 2 we present decay behaviors of the 219-nm band taken under (a) no collimation and (b) best collimation. A pulse shape of the exciting light is also shown as (c) for reference. In (a), the luminescence exhibits a single-exponential decay, with a time constant of 0.8 ns. By adjusting the collimating mirror, the decay time becomes slightly fast [(b)]. However, such an appre-

ciable sharpening of the decay profile was not observable if the intensity of the undulator radiation was reduced to $\sim 1/3$ of the maximum value.

These observations suggest a possibility of the light amplification of AF luminescence (185-240 nm) in BaF_2. Although the data are still preliminary, the present work has demonstrated a new type of laser operation in which the core-valence transition plays an important role.[2)]

References

1) M. Itoh, S. Kubota, J. Ruan(Gen) and S. Hashimoto: Rev. Solid State Sci. **4** (1990) 467.

2) M. Itoh and H. Itoh: Phys. Rev. **B 46** (1992) 15509.

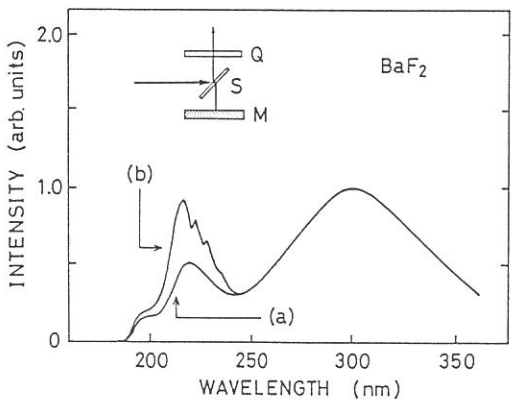

Fig.1. Luminescence spectra of BaF_2 excited with undulator radiation at 36.0 eV. The inset shows a cavity configuration (Q, quartz plate; S, BaF_2 crystal; M, adjustable mirror).

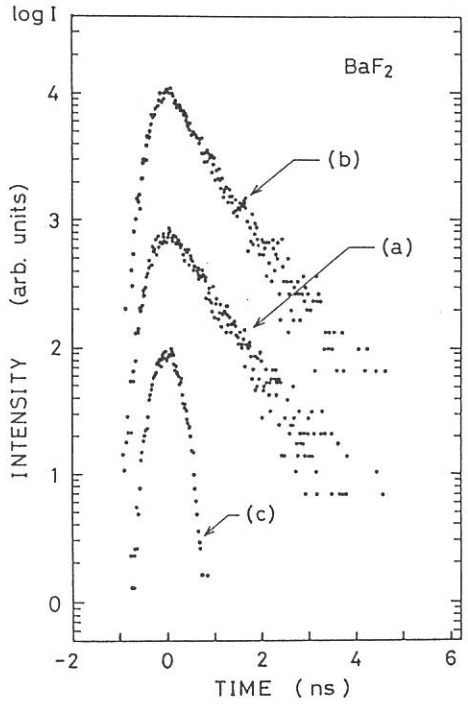

Fig.2. Decay profiles of the 219-nm band in BaF_2 [(a) and (b)]. A pulse shape of the exciting light is also shown as (c). For illustration purposes, the curves (a),(b) and (c) are shifted by one order, respectively.

XANES and EXAFS study of K_3C_{60}

Kazuyuki TOHJI and Hisanori SHINOHARA*

Department of Resources Engineering, Tohoku University, Sendai 980, Japan.
*Department of Chemistry for materials, Mi'e University, Tsu 514, Japan.

The Potassium L-edge EXAFS spectrum of microcrystalline potassium-doped K_3C_{60} has been measured using 250-500 eV synchrotron radiation. EXAFS is particularly useful to obtain the information of local structures around potassium in K_3C_{60}.

The XANES and EXAFS experiments have been performed on the BL-2B1 Beam Line of UVSOR at the Institute for Molecular Science. The beam line is equipped with a grasshopper monochromator. The energy resolution of the monochromator with the grating(600 lines/mm mechanically ruled grating) is 0.8 eV around the potassium L_{III} edge. In order to eliminate intensity variation due to carbon contaminants deposited on the optical elements, The background normalization-subtraction procedure is employed[1]. The background features are eliminated by subtracting the signal stemming from the Au-coated grid reference from that of C_{60} deposited on the Au substrate. This ensures optimum cancellation of all background structures. Energy calibration is performed by use of two transmission minima at 284.7 and 291.0 eV, which come from the carbon contamination.

Details of the production of fullerene-rich carbon soot by the contact arc method[2] have been described previously. Briefly, an arc between two graphite rods(13.5 mm in diameter) is sparked at 200-250 A in direct current (DC) mode in a He pressure of 100 Torr. Separation and purification of C_{60} are attained by column chromatography on neutral alumina (ICN Biomedicals Akt.I) with hexane/toluene solvent.

Fig.1 shows a XANES spectrum of potassium-doped K_3C_{60} microcrystals. The spectrum shows the carbon K-edge π^* resonance and σ^* resonance which are partly overlapped with the potassium L-edge absorption. The intensity of the potassium L-edge absorption increases as the number of potassium atoms (n) in K_nC_{60} . The results are consistent with a recent report on the XANES spectra on the same system with much higher spectral resolution[3].

Fig.2 exhibits EXAFS features of K_3C_{60} which are present at much higher energy regions. Fig.3 shows the extracts EXAFS oscillation $\chi(k)$ which is obtained after subtraction of the smooth X-ray absorption background and normalization[4-5]. Here, the wave vector k is defined by the following equation:

$k = \sqrt{2m(E-E_0)/h^2}$,

where E is the energy of the incident X-ray beam and E_0 is the threshold energy of L_{III} absorption of potassium atoms. The E_0 value was set to be 293 eV in the present analysis. The function $k^3\chi(k)$ was Fourier transformed over the range of $3.0<k<7.4$. The obtained magnitude, FT, is shown in the side of Fig.3. In the present calculations the values for the back scattering amplitude and the phase shift reported by Teo and Lee were used[6]. The obtained nearest-neighbor K-C distance is 3.06 A. The present value

is shorter than that obtained by an X-ray powder pattern analysis of K_3C_{60} (3.27 A for tetrahedral site), where the C_{60} molecules are assumed to be locked into a fixed position. The nearest-neighbor K-C distance decreases if the C_{60} molecules rotate in the K_3C_{60} crystals. The present results imply that the C_{60} molecules rotate in a cooperative manner (jump motion).

References
1) J. Store, R. Jaeger, Phys. Rev. B, 26, 4111, (1982).
2) R.E. Haufler, et al., Mat. Res. Soc. Proc. 206, 627, (1991).
3) C.T. Chen, et al., Nature, 352, 603 (1991).
4) F.W. Lytle, et al., Phys. Rev. B, 11, 4825, (1975).
5) K. Tohji, et. al., J. Am. Chem. Soc., 106, 612, (1984).
6) B.K. Teo and P.A. Lee, J. Am. Chem. Soc., 101, 2815, (1979).

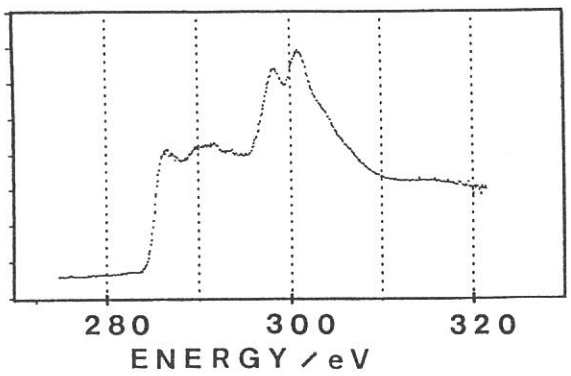

Fig.1
XANES spectrum of potassium-doped C_{60}. The intense peaks around 300 eV are due to potassium L-edge absorption. The K_3C_{60} sample is prepared ex-situ and shows a superconducting transition at 19 K.

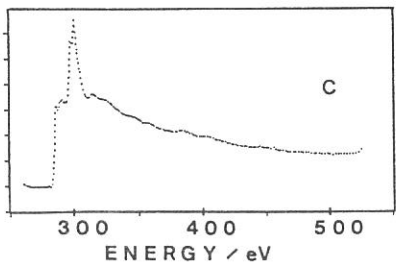

Fig.2
EXAFS feature of micro-crystalline K_3C_{60} at room temperature.

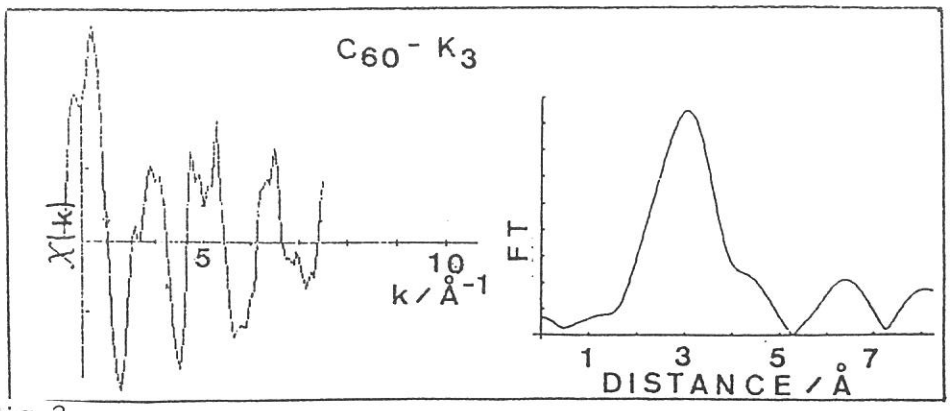

Fig.3
Extracted oscillation of Fig.2 and its Fourier transform.

Ni $L_{2,3}$ Absorption Spectra of $NiPS_3$

K.NOGUCHI, S.NAKAI, A.KAMATA, K.MATSUDA and K.SANO

Faculty of Engineering, Utsunomiya University, Utsunomiya 321

A layered 3*d* transition-metal thiophosphate crystallizes in the crystal structure belongs to the monoclinic space group with 4 formula units per unit cell and is related to the $CdCl_2$ structure. The sulfur atoms in the compound are cubically closed-packed, and the metal atoms and the phosphorus-phosphorus pairs occupy the cadmium positions. Furthermore, the crystal is constructed of a stack of sandwich layers each of which is weakly bonded by van der Waals forces. With in the layers the metal atoms are surrounded octahedrally by six sulfur atoms. The only difference is that a P_2 pair in $NiPS_3$ occupies one of the three metal-sites of the layered transition metal disulfides[1]. In this study, we have measured the linear polarized Ni $L_{2,3}$ absorption spectra in $NiPS_3$ single crystals.

Measurements have been performed by using synchrotron radiation at the BL-7A line of the Ultraviolet Synchrotron Radiation Facility (UV-SOR), Institute for Molecular Science. We have used a double crystal Beryl ($10\bar{1}0$) monochromator with an energy resolution about 0.4 eV at Ni *L* absorption peak. Spectra were measured by means of photoelectric yield from single crystal surfaces. The sample of $NiPS_3$ was cleaved in a vacuum by pealing off with Scotch tape along the sample surface (ab plane).

Figure 1 shows Ni 2*p* XAS spectra of $NiPS_3$. The upper solid curve (θ=70°) was taken for the polarization of electric field nearly parallel to the c-axis (E//c), and the lower dotted one (θ=0°) was taken parallel to the ab plane (E//ab). These spectra were normalized to the background. The first peak which appeared about 852eV corresponds to $2p_{3/2}$ absorption peak, and the second one which appeared about 870eV to $2p_{1/2}$ absorption peak. The satellite structure was appeared around 857eV. In Fig. 1, the polarization dependency is not clearly seen.

The $L_{2,3}$ absorption spectra are interpreted in terms of the multiplet structure which results from the interaction between a 2*p* hole and 3*d* electrons of localized metal ions[2]. It is well known that in a purely ionic configuration and in D_{Oh} symmetry the crystal field together with the *d*-*d* Coulomb interaction cause the ground state of a d^8 ion to be A_{2g} (ϵ_g). This state can mix with states $d^9\underline{L}$ and $d^{10}\underline{L}\,\underline{L}'$ of A_{2g} symmetry, where $\underline{L}$ denotes a ligand hole. The initial state covalency is related to the amount of d^8, $d^9\underline{L}$ and $d^{10}\underline{L}\,\underline{L}'$ character in ground state. The final state after absorption are of the form $\underline{c}\,d^9$ and $\underline{c}\,d^{10}\underline{L}$, where $\underline{c}$ denotes a core hole.

van der Laan et al.[3] reported the decrease in multiplet splitting which appeared in Ni $2p$ absorption spectra of Ni dihalides with decreasing anion electronegativity because of covalent mixing in both the initial and final states. Then, the relative intensities of the multiplet are reflect the covalent mixing. Comparing our experimental spectra with the calculated results by van der Laan, we can obtain the mixing amount of ground state for $NiPS_3$; the value of $3d$, $3d^9\underline{L}$, and $3d^{10}\underline{L}\,\underline{L}'$ characters as 0.47, 0.44 and 0.09, respectively.

However, the polarization dependency is not so clear in our result, so, improved experiments have to be done in future.

References

1) F.Hulliger , Physics and Chemistry of Materials with Layered Structures, ed. F.Levy (D.Reidel Pub. Com., Dordrecht,1967) Vol.5, P.217

2) S.Nakai et al. , J.Phys Soc. Jpn. 54 (1985) 4034

3) G.van der Laan et al., Phys. Rev. B33 (1986) 4253

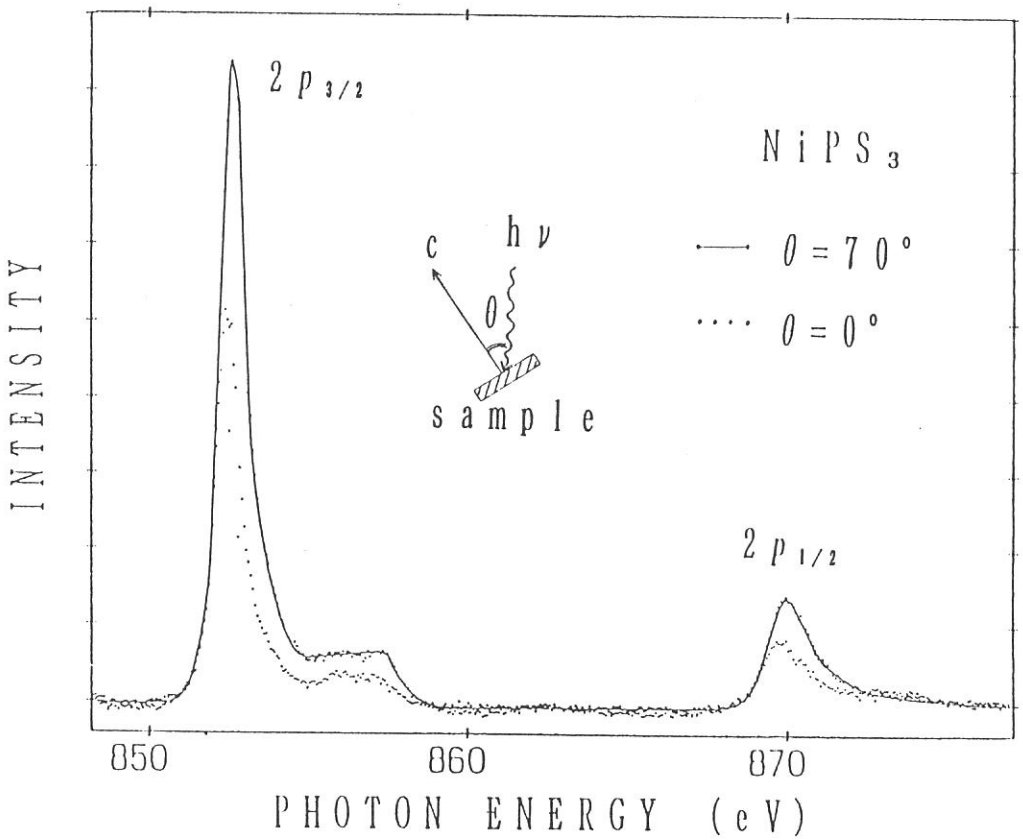

Fig. 1

Ni L-edge absorption spectra in Ni-MgO solid solutions

Tomoko HANADA, Tsunehiro TANAKA, Hisao YOSHIDA,
Takuzo FUNABIKI, and Satohiro YOSHIDA

Division of Molecular Engineering, Kyoto University, Kyoto 606

So far, we have studied solubility of Ni atoms into MgO matrix. We have found that nickel-ions-impregnated MgO powder forms a solid solution easily by calcination at 773 K at any ratio of Ni and Mg. Previous studies for Ni-MgO solid solutions concluded that nickel ions exist in divalent state in solid solutions of low nickel concentration. In fact, in our case, when the nickel concentration is lower than 50 % (Ni % = mole of Ni / (mole of Ni + mole of Mg) × 100) , the solid solution is pale green, indicating that nickel ions are present as Ni^{2+}. But at 50 %, the color is dark gray and gets darker with an increase in Ni concentration. Such a change in the color suggests that divalent and trivalent nickel ions coexist in the solid solutions. In the study of catalysis by the solid solutions, the quantitative analysis of divalent and trivalent nickel ions is very important. However, XPS can not be applied for the analysis because of little difference in the binding energy between Ni^{2+} and Ni^{3+}.

In this work, we measured $L_{3,2}$-edge XAFS including the bands due to $2p \rightarrow 3d$ transition and investigated a relation between the valence of nickel atoms and XAFS spectra, since the valence of nickel atom relates to the $2p \rightarrow 3d$ transition cross section.

Samples were prepared by impregnation of MgO powder with an $Ni(NO_3)_2$ aqueous solution, followed by calcination at 773 K for four hours in a dried air stream. Concentration of Ni ions was determined by X-ray fluorescence method.

Ni $L_{3,2}$-edge absorption measurements were carried out on BL-7A at UVSOR with a ring energy of 750 MeV and a stored current of 80-200 mA in a mode of total electron yields. Besides the samples, we recorded XAFS of $NiO(Ni^{2+})$ and $Ni_2O_3(Ni^{3+})$ as references. A double crystal beryl monochromater was used, and energy calibration was carried out using Al K-edge.

For all the samples including NiO and Ni_2O_3 references, spectra were very similar to each other. Figure 1 shows the spectrum of Ni $L_{3,2}$ absorption for $Ni_{0.5}Mg_{0.5}$ binary oxide as an example. Peaks are seen at around 853 and 855 eV in L_3-edge region, at around 870 and 871 eV in L_2-edge region. The positions of these peaks are the same for all samples within a resolution of the monochromater. That is, we could not observe any chemical shifts.

The white line in L_3-edge spectrum, the prominent peak at 853 eV, is assigned to $2p_{3/2} \rightarrow 3d$ transition. An Ni^{3+} ion has more unoccupied 3d orbitals than an Ni^{2+} ion and it is generally expected that the intensity of the white line associated with Ni^{3+} is higher than that associated with Ni^{2+}. To evaluate the intensity, we subtracted the backgrounds from recorded spectra and carried out deconvolution of the resultant spectra with Lorenzians. A typical deconvoluted spectrum is

shown in Fig. 2. Unfortunately, we failed the precise evaluation of intensity because of missing of an adequate normalizing procedure. However, we found that full width at half maximum (FWHM) of the white line changes with increasing nickel concentration as shown in Fig. 3. When nickel concentration is below10 %, samples are pale green, and FWHMs are found to be close to that of NiO(1.1 eV). Thus we suppose that nickel ions are almost divalent in these solid solutions. On the other hand, with an increase in the concentration, FWHM becomes larger, and converges on 1.25 eV above for samples contaning Ni ions 40 %. The broadening in the white line may result from formation of Ni^{3+} ions.

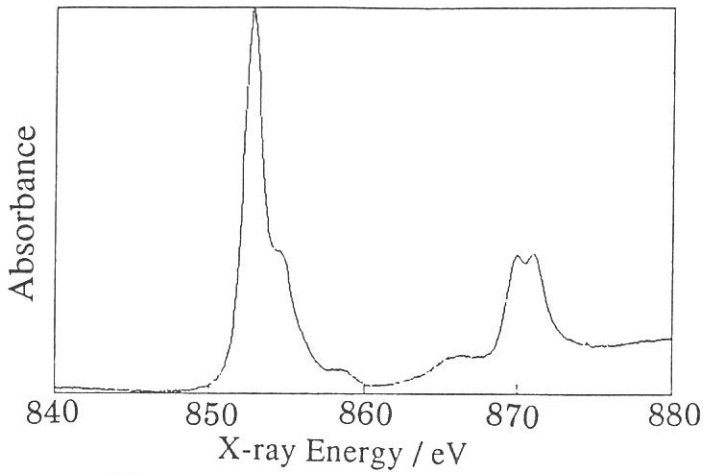

Fig.1 Ni $L_{3,2}$-edge absorption spectrum of $Ni_{0.5}Mg_{0.5}$ binary oxide.

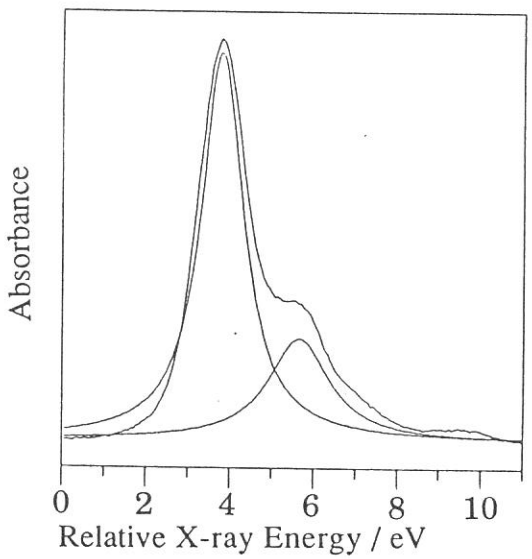

Fig.2 Ni L_3-edge absorption spectrum and its deconvoluted spectrum of $Ni_{0.5}Mg_{0.5}$ binary oxide. Energy offset is taken to be 849.0 eV.

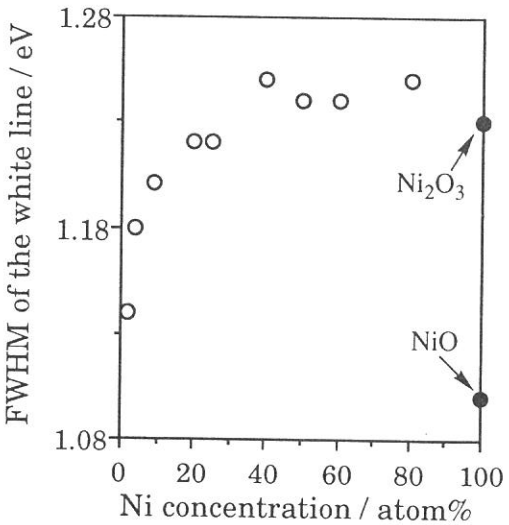

Fig.3 Variation of FWHM of the white line with Ni concentration in Ni_xMg_{1-x} binary oxide.

Cu $L_{2,3}$-edge Absorption Spectra of Cu-Au Alloys

T.K. SHAM[1,2,*], A. HIRAYA[1] and M. WATANABE[1]

1. UVSOR, Institute for Molecular Science, Myodaiji, Okazaki 444
2. Department of Chemistry, University of Western Ontario, London, Ontario, N6A 5B7 Canada

Electronic charge redistribution upon alloying of Au and Cu has been a subject of considerable interest for many decades in connection with the study of Friedel charge screening, effect of d-d interaction upon dilution and the local charge redistribution in view of chemical effects such as electronegativity difference. The perhaps most intriguing spectroscopic observation of these alloys has been the opposite trends exhibited by the Mossbauer isomer shifts and the photoelectron Au 4f binding energy shifts on the basis of simple electronegativity predictions. A charge compensation model has been proposed to explain this discrepancy[1]. In this model, Au loses d charge and this loss is overcompensated by a gain of s charge so that the net charge flow onto the Au site is in accord with electronegativity predictions. The d charge depletion at the Au site in Cu-Au alloys has recently been confirmed by X-ray absorption measurements of the Au $L_{2,3}$ edge whitelines[2]. Despite these observations, the nature of charge redistribution at the Cu site is not fully understood, although electronegativity argument suggests that Cu is expected to lose charge. The objective of this experiment is to make high resolution measurements of the near edge structure of the Cu L-edge in a series of Au-Cu alloys. In this report, preliminary results are presented and their implications discussed.

X-ray absorption measurements were performed at the BL1A beamline which is equipped with a double crystal monochromator. A set of beryl crystals (2d= 15.965 Å) was used. At the Cu $L_{3,2}$ edge, the overall spectrometer resolution is $<$ 1 eV. Absorption spectra were simultaneously recorded in three modes: total electron yield (TEY) with specimen current, total electron yield with a multichannel plate (MCP) and X-ray fluorescence yield (FLY) with a gas (Ar/CH_4) proportion counter. Normal incidence of the photon beam onto the sample with the fluorescence detector and the MCP positioned at 45 degree from the incident beam was used to record the data. Both TEY give identical spectra while TEY and FLY exhibit a drastic difference in the sensitivity of sampling depth with FLY being more sensitive to the bulk.

Samples of Cu, Cu_3Au (order and disordered), CuAu (ordered and disordered) and $CuAu_3$ have been studied. The specimens are metal foils of which the surface was scraped prior to their introduction into the vacuum chamber and was scraped again in-situ with a diamond file before each measurement. Fig.1 shows the Cu L-edge of a Cu_3Au sample before and after scraping. It is apparent that the surface is covered with oxide before scraping and after scraping the TEY spectra are still sensitive to the oxide remaining on the surface while the FLY spectrum is essentially bulk-like with no detectable oxide.

Fig.2 shows the Cu L-edge TEY spectra of several clean samples. It can been seen from fig.2 that the Cu L-edge has rich structures with an apparent whiteline at the threshold. These structures are often not seen in low resolution spectrum[3]. The presence of the whiteline (first peak in the $L_{3,2}$ edge) is not totally surprising since there exists some unoccupied densities of d states above the Fermi level due to s-p-d rehybridization, and a p

it can be revealed that the Cu deposit is dispersed and contains a mixture of CuO, Cu_2O and Cu with mostly oxide on the surface. This is deduced from the comparison of the TEY (more surface sensitive) and the FLY (more bulk sensitive) spectra. This observation is not surprising since the oxidation reduction reaction (hydrogen is oxidized in this case) was carried out in solution in ambient atmosphere and the Cu/porous silicon samples had been stored in ambient atmosphere prior to the measurement. The feature at ~ 57.2 deg Bragg angle (~920 eV) is the signal from the Si substrate due to second order radiation. Detailed analysis is now in progress.

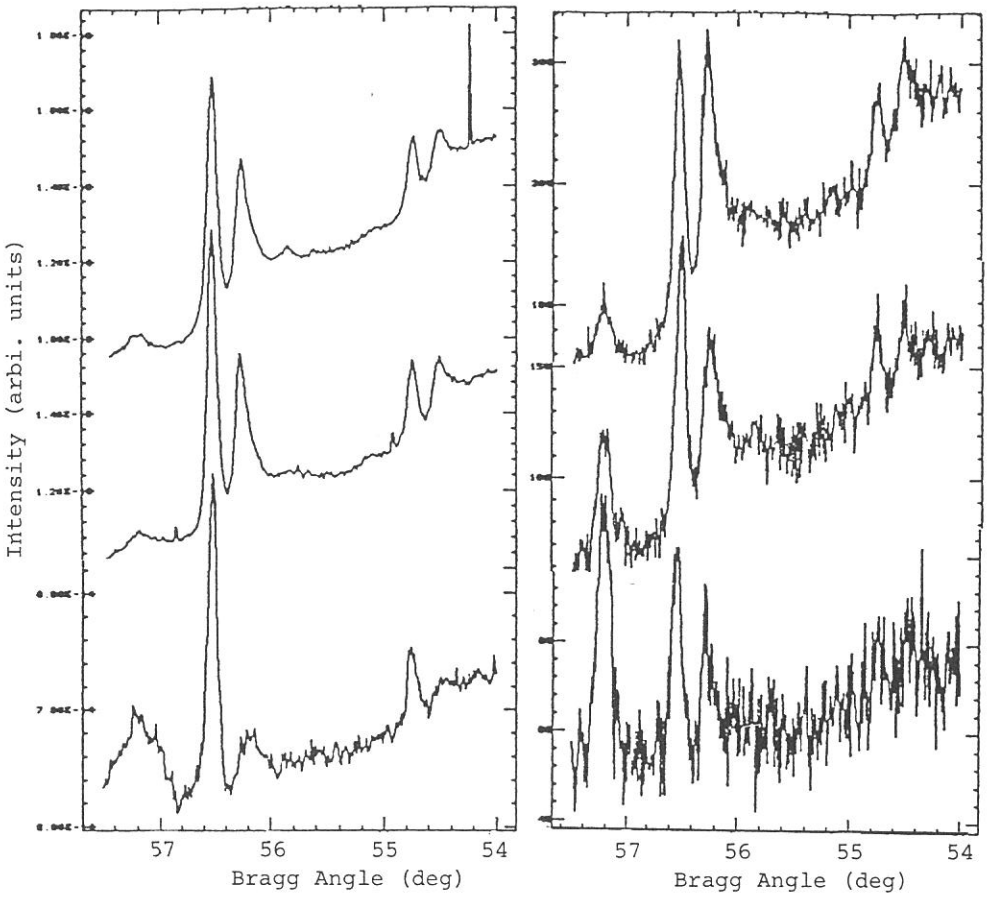

Fig.2 TEY (left panel) and FLY (right panel) spectra of copper on porous silicon. The initial concentrations of copper sulphate are (from top to bottom): 0.1 M, 0.01 M and 0.001 M

* JSPS (Japan Society for the Promotion of Science) Visiting Fellow, 1992.

1. M.J Sailor and K.L. Kavanagh, Adv. Mater. 4, 432(1992).
2. L.T. Canham, Appl. Phys. Lett., 57, 1046(1990).
3. I. Coulthard, J.W. Lorimer and T.K. Sham, Abstract 824RNP, 118th Meeting, The Electrochemical Society, Toronto, Oct. 1992; and to be published.

Reductive Dispersion of Cu on Porous Silicon: A Cu L-edge Study

T.K. SHAM[1,2,*], A. HIRAYA[1], and M. WATANABE[1]

1. UVSOR, Institute for Molecular Science, Myodaiji, Okazaki 444
2. Department of Chemistry, University of Western Ontario, London, Ontario, N6A 5B7 Canada

Porous silicon, silicon with high porosity and nano-crystalline structures has recently attracted much attention[1] partly because of its intense luminescence in the visible[2] and partly because of the fact that it is easy to make electrochemically. We became interested in porous silicon in connection with synchrotron light induced optical luminescence and its potential application in optoelectronics as well as the reductive dispersion of Cu and noble metals on the vast surface area of porous silicon[3].

In this report, we present preliminary results of the Cu L-edge spectra of a series of Cu films dispersed on porous silicon substrate from aqueous solution of $CuSO_4$. The measurements were carried out at the BL1A beamline using beryl crystals as the monochromator (2d = 15.965 Å). Porous silicon was prepared electrochemically on a p-type Si(100) wafer with a current density of 20 mA/cm^2 for 20 minutes. Cu films were prepared by immersing the specimen into $CuSO_4$ solutions with concentrations of 0.1 M, 0.01 M, and 0.001M[3]. Total electron yield (TEY) and fluorescence yield (FLY) were simultaneously used to record the Cu absorption spectrum at the Cu $L_{3,2}$ edge. Cu, Cu_2O and CuO were used as model compounds. The corresponding spectra are shown in Fig.1

Fig. 2 shows the TEY and FLY spectra of Cu deposited on porous silicon. A couple of features are noted. First, there is a significant amount of Cu on the porous silicon surface indicating the very large surface area. Second, comparing to Fig.1,

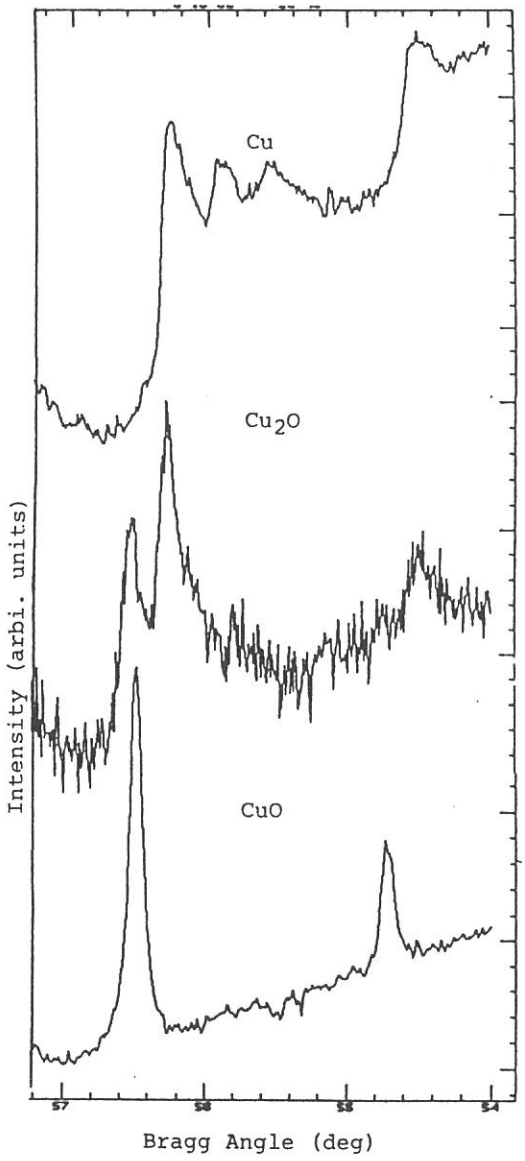

Fig 1. From top to bottom: Cu $L_{3,2}$ edge spectrum of Cu, Cu_2O and CuO.

to d dipole transition probes the d character. Two features are noteworthy from Fig.1. First, the whiteline becomes slightly less intense upon dilution of Cu in Au indicating that Cu gains some d charge upon alloying. Since Au is the most electronegative metallic element and gains charge overall in Cu-Au alloys, this observation implies that Cu loses sp charge and this is partially compensated by a d charge gain. The trend however is less dramatic than observed previously at the Au site[2]. Second, the oscillations beyond the whiteline become closer in energy as Cu becomes dilute. The origin of this is presently under investigation.

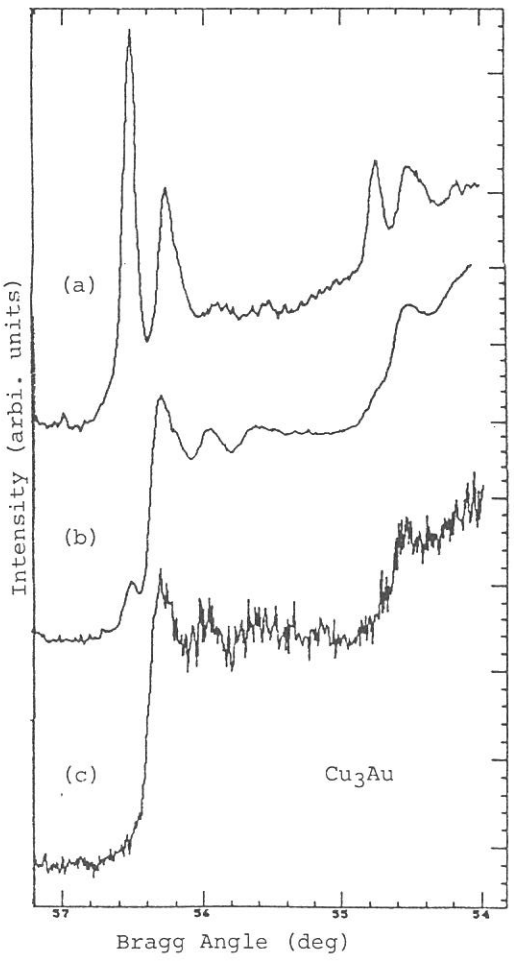

Fig.1 Cu_3Au spectra: (a) before scraping (TEY) (b) TEY and (c) FLY after scraping; Photon energy(eV)=776.5/sinθ

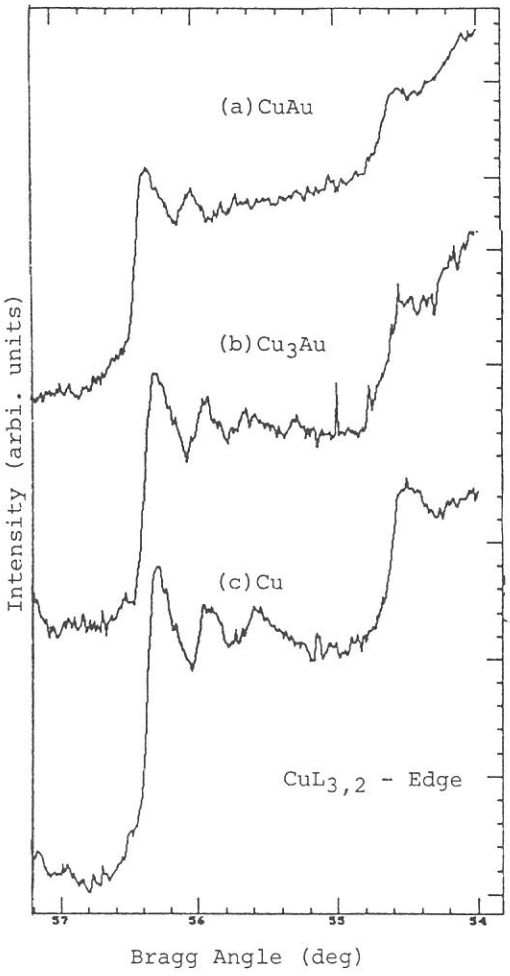

Fig.2 (a) CuAu, (b) Cu_3Au, (c) Cu; Photon energy (eV)= 776.5/sinθ

* JSPS (Japan Society for the Promotion of Science) Visiting Fellow, 1992

1. R.E. Watson, J. Hudis and M.L. Perlman, Phys. Rev. B4, 4139(1971).
2. T.K. Sham, Y.M. Yiu, M. Kuhn and K.H. Tan Phys. Rev. B41, 11881(1990).
3. G. Meitzner, D.A. Fischer and J.H. Sinfelt, Catalysis Letters, 15 219(1992).

Polarized Cu *L* Absorption Spectra of $Bi_2Sr_2Ca_{1-x}Y_xCu_2O_8$ (x=0.0,0.6)

Kimikazu SANO, Shun-ichi NAKAI, Atsushi KAMATA, Kunio MATSUDA,
Kazuhiro NOGUCHI, Hiroyoshi ISHII*, and Ikuyo SHIOZAKI*

Faculty of Engineering, Utsunomiya University, Utsunomiya 321
**Department of Physics, Tokyo Metropolitan University, Hachioji 192-03*

The cuprate oxide superconductors exhibit superconducting phenomenon when holes are doped into the compound. It is generally accepted that the doped holes are mainly located in O $2p_{x,y}$ and Cu $3d_{x^2-y^2}$ orbitals in the two-dimensional CuO_2 plane. The polarization dependency of X-ray absorption spectroscopy [1,2] (XAS) and high energy electron energy loss spectroscopy[3,4] (EELS) at O site, have shown the doped holes exist in the O $2p_{x,y}$ orbitals. On the other hand,concerning Cu $2p$ spectra which reveal information about Cu $3d$ orbitals, each experiment has shown different results. Bianconi et al.[5] and Abbate et al.[6] by using XAS measurements, have reported the peak energy shift about 0.3-0.5eV between Cu $3d_{x^2-y^2}$ and Cu $3d_{3z^2-r^2}$ components, though EELS by Nücker et al.[7] and XAS by Suzuki et al.[8] have shown no peak shift. These discrepancies are very important because the measurements provide direct information about unoccupied electronic states on the Cu $3d_{x^2-y^2}$ and the Cu $3d_{3z^2-r^2}$ orbitals. In order to clarify these discrepancies in the experiments, we have measured the linear polarized Cu $2p$ XAS spectra in $Bi_2Sr_2Ca_{1-x}Y_xCu_2O_8$ (x=0.0,0.6) single crystals.

The XAS measurement has been performed on the BL-7A at UVSOR facility with an energy resolution about 0.4eV at Cu *L* absorption peak. Spectra were measured by means of total electron yield from single crystal surfaces. The $Bi_2Sr_2CaCu_2O_8$ (x=0.0) is a superconductor sample which has a transition temperature of 80K, and non superconductor sample $Bi_2Sr_2Ca_{0.4}Y_{0.6}Cu_2O_8$ (x=0.6) shows a semiconducting behavior. These samples have been cleaved in a vacuum by pealing off with scotch tape to obtain clean surfaces.

Figure 1 shows the polarized Cu $2p$ XAS spectra of $Bi_2Sr_2CaCu_2O_8$(a) and $Bi_2Sr_2Ca_{0.4}Y_{0.6}Cu_2O_8$(b) single crystals. θ is the incidence angle of synchrotron radiation light, as indicated in figure 1. The spectra at θ=0° were taken for the polarization of electric field parallel to the CuO_2 plane and spectra at θ=80° were taken for almost perpendicular to CuO_2 plane. The spectra were normalized to the background below the absorption edge. In figure 1, both the spectra show the large polarization dependency and the energy shift between two incidence angles was about 0.5eV for x=0.0 and 0.3eV for x=0.6 sample. The intensity ratio was estimated to be about 7% and 22%, respectively. In our experiment, the energy shifts in the Cu $2p$ XAS spectra of both samples are commonly observed, therefore, it is considered that this effect is mainly related to the crystal structure of the sample.

Recently, C. T. Chen[9] measured Cu *L* XAS spectra for the same sample by means of total electron yield (TEY) and fluorescence yield (FY) method, and observed the peak energy shift in the TEY spectra but no shift in the FY spectra. Though TEY method is surface sensitive measurement, FY is bulk sensitive. Accordingly, our experimental results may not give information of bulk electronic structure in the sample. Therefore, the origin of the energy shift with angle is not fully understood at present. With respect to the intensity ratio with two incidence angles, our experimental results suggest a strong two-dimensionality of the electronic structure in $Bi_2Sr_2CaCu_2O_8$ as compared with $Bi_2Sr_2Ca_{0.4}Y_{0.6}Cu_2O_8$.

References
1) H.Matsuyama et al., Physca C160 (1989) 567.
2) C.T.Chen et al., Phys. Rev. Lett. 66 (1991) 104.
3) N.Nücker et al., Phys. Rev. B37 (1988) 5158.
4) H.Romberg et al., Phys. Rev. B32 (1990) 8868.
5) A.Bianconi et al., Phys. Rev. B44 (1991) 10126.
6) M.Abbate et al., Phys. Rev. B42 (1990) 7914.
7) N.Nücker et al., Phys. Rev. B39 (1989) 6619.
8) S.Suzuki et al., Phys. Rev. B44 (1991) 5381.
9) C.T.Chen, Private Communication.

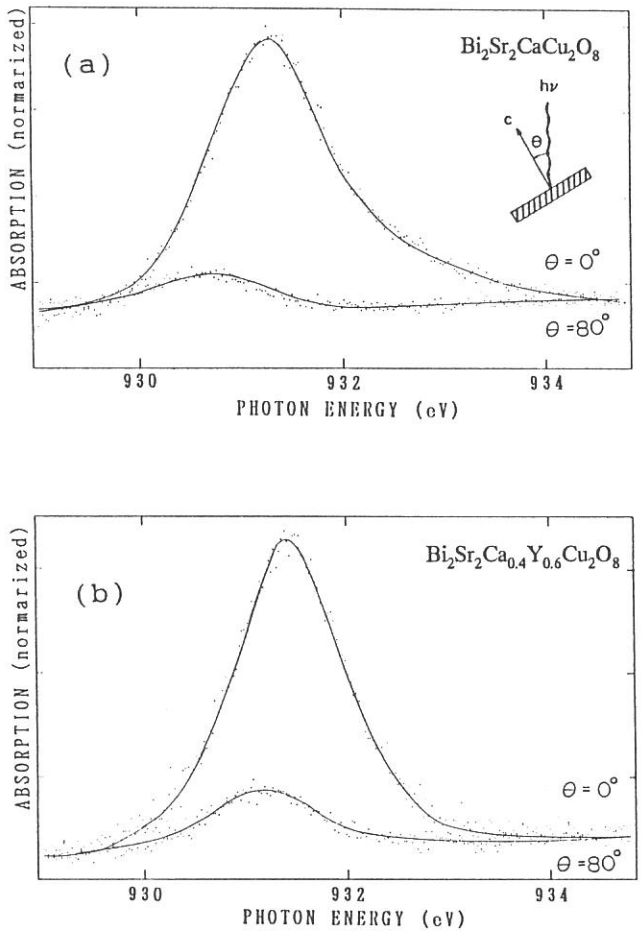

Fig.1 (a) Polarization dependency in the Cu 2*p* XAS spectra of $Bi_2Sr_2CaCu_2O_8$.

(b) Polarization dependency in the Cu 2*p* XAS spectra of $Bi_2Sr_2Ca_{0.4}Y_{0.6}Cu_2O_8$.

Cu $L_{III,II}$-EDGE X-RAY ABSORPTION SPECTROSCOPY STUDIES OF (Bi, Pb)-Sr-Ca-Cu-O: THE T_c VARIATION OF SUPERCONDUCTING COMPOUNDS

W. F. Pong,[1] H. L. Tong,[2] P.K. Tseng,[2] C. H. Chou,[2] J. B. Shi,[3] H. C. Ku,[4] A. Hiraya,[5] M. Watanabe.[5]

(1) Dept. of Phys. Tamkang U., Tamsui, Taiwan, (2) Dept. of Phys. Natl. Taiwan U., Taipei, Taiwan, (3) Dept. of Electronic Eng., Feng Chia U., Taichung, Taiwan, (4) Dept. of Phys., Natl. Tsing Hua U., Hsinchu, Taiwan, (5) Institute for Molecular Science, Okazaki, Japan.

We have measured the *x*-ray absorption spectra of Cu $L_{III,II}$-edge for the T_c variation of superconducting (Bi, Pb)-Sr-Ca-Cu-O compounds (Pb-BSCCO) at room temperature. The samples were measured using total electron yield mode with an electron multiplier under a base pressure of less than $5x10^{-8}$ torr, and the data was collected using a double-crystal beryl $(10\bar{1}0)$ monochromator.

Fig. 1 shows the Cu $L_{III,II}$-edge absorption spectra of the CuO and Pb-BSCCO compounds. The white line peak energies of CuO, Pb-BSCCO compounds, their corresponding full width at half maximum (FWHM), as well the relative integrated intensity of the peaks (from -2 to +2 eV relative to threshold of Cu $L_{III,II}$-edge) are summaried in Table I. The maximum white line peak of Cu $L_{III,II}$ in CuO are 931.3±0.3 and 951.2±0.3 eV, respectively. According to the dipole-selected transition rules, the origin of white line peaks at the Cu $L_{III,II}$ edges are attributed to atomic-like transitions from the ground state Cu 2p photoelectron being excited to the final state Cu 3d. This is due to hybridized Cu(3d) - O(2p) electron transfer which occurs from the 3d orbitals in Cu to the O atoms to give some unoccupied d states. For non-superconducting and various T_c superconducting Pb-BSCCO compounds, a sharp resonance white line denotes both Cu $L_{III,II}$ with a threshold similar to CuO, are evidently coincident with the prominent peaks at ~931 and ~951 eV. The main peaks in the spectra of the Pb-BSCCO are clearly similar to the CuO curve, this reveals a predominant Cu^{+2} ground state in Pb-BSCCO. Details of the *x*-ray absorption studies for Pb-BSCCO compounds will be reported in the future.

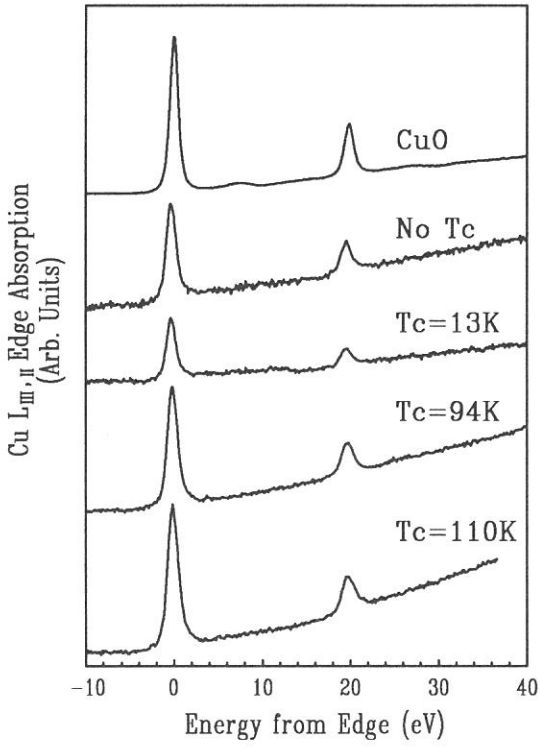

Fig. 1 Normalized Cu $L_{III,II}$ absorption spectra for CuO, and various T_c Pb-BSCCO compounds. The zero energy corresponds to 931.3 eV.

Compounds	$E_0(L_{III})$	FWHM	I_{III}	$E_0(L_{II})$	FWHM	I_{II}	$E_0(L_{II}) - E_0(L_{III})$	I_{III}/I_{II}
No Tc	931.0	1.3	102	950.9	1.3	36	19.9	2.9
Tc≈13K	931.0	1.2	59	950.9	1.5	18	19.9	3.3
Tc≈94K	931.1	1.3	128	951.0	1.6	38	19.9	3.4
Tc≈110K	931.1	1.4	151	951.1	1.7	50	20.0	3.0
CuO	931.3	1.1	1453	951.2	1.2	492	19.9	3.0

Tab. I Energy position (E_0) (±0.3 eV), full width at half maximum (FWHM) (±0.1 eV), and ($I_{III,II}$) relative integrated intensity of the white line peaks in the Cu $L_{III,II}$ near-edge absorption spectra.

TRIAL FOR MEASUREMENTS OF Ca K, Sr L, AND Cu L ABSORPTION EDGES FOR Bi-BASED HIGH-Tc SUPERCONDUCTORS

Rika SEKINE[1,2], Yasuhiro MURAKOSHI[1,3], and Maki KAWAI[2]

[1]Research Laboratory of Engineering Materials, Tokyo Institute of Technology, Yokohama, 227
[2]The Institute of Physical and Chemical Research (RIKEN), Wako, 351-01
[3]Tokyo Gakugei University, Koganei, 184.

The Tc values of high-Tc superconducting oxides are affected by the hole concentration. In the Bi 2212 phase, the hole carrier, which is controlled by the amount of oxygen, is supplied from the Bi-O layer to the Cu-O_2 layers through the Sr-O layers. Therefore, when the oxygen is reduced, not only the changes in hole carrier concentration but also changes in oxygen position may affect the mechanism of carrier supply and the Tc values. X-ray absorption spectra (XANES and EXAFS) of metal atoms can give us the information on the local structure of oxygen, i,e, coordination number and distance around each metal atom. In this study, we try to investigate the soft X-ray absorption edge regions, Ca K, Sr $L_{II,III}$, and Cu L_{III} for Bi2212 phases.

The Bi2212 samples ($Bi_{2.2}(Sr_{0.9-y}Ca_y)_2Ca_{1.0}Cu_{2.0}O_{8.1+\delta}$ with y=0, 0.4) were sintered in dry air for 144-240 hours at 810-840℃ as previously reported. [1] Some of the sintered samples were annealed in Ar at 600 ℃ for 48 hours and others in O_2 at 600 ℃ for 48 hours. Single crystal of Bi 2212 phase, which was supplied by Shigaki et al., was prepared by traveling solvent floating zone method. [2] Measurements were carried out at the beam line 7A of the UVSOR storage ring in the Institute for Molecular Science at room temperature in UHV chamber. Photon energy with the energy range of 900-4200 eV was used. Double crystal Ge(220), beryl, and InSb monochrometers are used for Ca K (3800-4200 keV), Cu L(920-980 eV), and Sr L(1920-2130 eV) edges, respectively. The X-ray absorption spectra have been measured by recording the total electron yield.

Figure 1 shows examples of Ca K-egde absorption spectra for (a) $CaCO_3$, which was used as a reference compound, and (b) Bi2212 sample with y=0.4. As shown in Fig.1(a), in higher energy regions than 4300 eV, the effects of harmonics could not be eliminated. Therefore, we focussed interests on only the XANES region in Fig.1(b). Since we cannot record spectra in sufficient S/N ration with the present equipment, we abandoned the measurement for the Ca K-edge region.

Figure 2 shows Sr $L_{II,III}$-edge spectrum for the single crystal of $Bi_{2.0}Sr_{1.8}Ca_{1.0}Cu_{2.0}O_{8+\delta}$. The L_{II} and L_{III} edges are

too near to separately discuss the EXAFS oscillations. Therefore, we only focused interests on the changes in the energy for Sr L_{III} edge. The edge energy was observed from 1943.01-1943.11 for each samples with different y values or different treatment, which is considered to be almost the same in limited energy resolution.

Figure 3 shows Cu L_{III} spectrum with emittance angle of 50 degree respect to perpendicular. There have been pointed out that at least two components exist for high-Tc cuprate compounds in Cu L_{III} region around 931 eV and 933 eV. Furthermore strong angular dependence in intensity ratio for these two peaks are also pointed out. However, we cannot clearly observe the latter peak or angular dependence. The peak energy for the former one changes from 931.4 to 931.6 eV for different samples, however, it seems that the shift depends not on the intrinsic energy state of each sample but on surface energy state which is sensitive to impurities or damages induced by air ambient or X-ray irradiation that samples are exposed during measurements.

The authors are indebted to M. Watanabe, O. Matsudo, and J.Yamazaki, UVSOR, the Institute for Molecular Science.

References

1 S. Kambe, T. Matsuoka, M. Takahashi, M. Kawai, and T. Kawai, Phys. Rev. B, 42 (1990) 2669.

2. I. Shigaki, K. Kitahama, K. Shibutani S. Hayashi, R. Ogawa, Y. Kawate, T. Kawai, S. Kawai, M. Matsumoto, and J. Shira fuji, Jpn. J. Appl. Phys., 29 (1990) L2103.

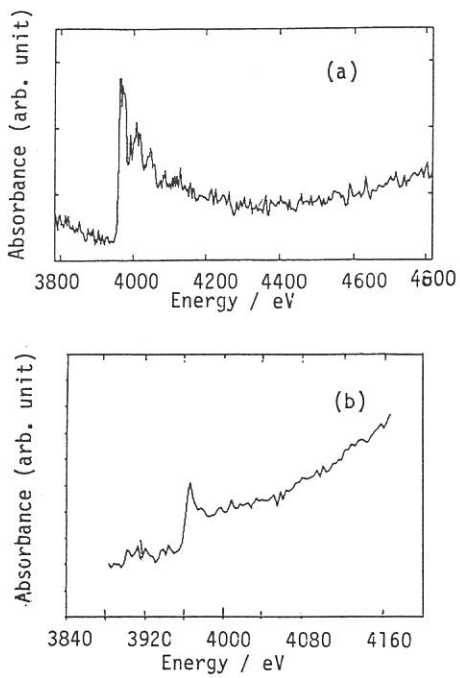

Fig. 1. Ca K-edge absorption spectra. (a)$CaCO_3$, and (b) $Bi_{2.2}Sr_{1.0}Ca_{1.8}Cu_{2.0}O_{8+\delta}$.

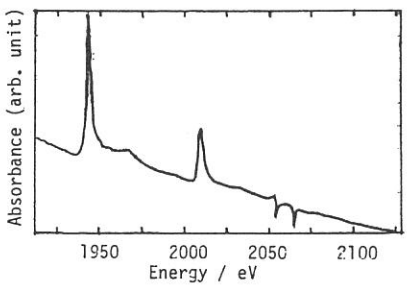

Fig. 2 Sr L_{II} (~2100 eV)- and L_{III} (~1940 eV)-edge absorption spectrum for single crystal of $Bi_{2.0}Sr_{1.8}Ca_{1.0}Cu_{2.0}O_{8+\delta}$.

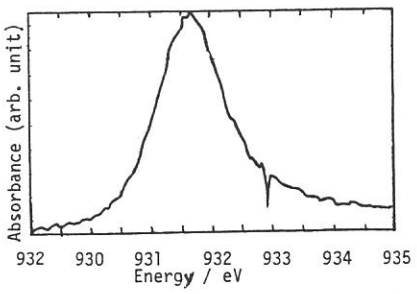

Fig. 3 Cu L_{III}-edge absorption spectrum for single crystal of $Bi_{2.0}Sr_{1.8}Ca_{1.0}Cu_{2.0}O_{8+\delta}$.

XAFS Study of Na-doped Nb_2O_5 Catalysts

Sadao Hasegawa*, Hirofumi Aritani* , Masahiko Morooka*, Yasue Sasaki* and Tsunehiro Tanaka**

*Department of Chemistry, Tokyo Gakugei University, Koganei, Tokyo 184

**Department of Hydrocarbon Chemistry, Faculty of Engineering, Kyoto University, Kyoto 606

1. Introduction

In our previous report[1,2], Na-doped Al_2O_3 catalyst has been exhibited a basic property. A sodium ion on the surface acts as an electron donor for the surface oxygen. It was deduced on the basis of XANES of sodium halides that the ionicity of a Na-O bond in that catalysts relates to the energy position of the primary peak, which is consistent with the catalytic performance.

In this report, the effect of Na-loading on the surface of bulk Nb_2O_5 and Al_2O_3-supported Nb_2O_5 catalysts have been investigated.

2. Experimental

Na-loaded Nb_2O_5 were prepared by impregnating niobium pentoxide with the ethanol solution of sodium ethoxide. Nb_2O_5 catalyst was prepared by the calcination of hydrated niobium pentoxide in air at 773K. Its structure was determined to be rhombic Nb_2O_5 by X-ray diffraction. Al_2O_3-supported niobium oxide catalysts were prepared by impregnating alumina powder (Nb_2O_5 10wt% on Al_2O_3) at 363K. All catalysts were followed by drying and calcining in air at various temperature.

The Na K-edge absorption spectra of the catalysts were measured at BL-7A soft X-ray beam line with UVSOR facilities, when used a beryl two-crystal monochrometer.

Table 1 Results of Isomerization of 1-butene. *1

catalysts	Composition / % 1-butene	2-butene cis-	2-butene trans-	selectivity*2
Nb_2O_5	50.4	26.0	23.6	1.1
Na/Nb_2O_5 *3	100	-	-	-
Nb_2O_5/Al_2O_3*4	27.1	27.6	45.4	0.6
$Na/Nb_2O_5/Al_2O_3$*4*5	65.6	28.5	5.9	4.9

*1 Reacted at 423K for 120min. *2 Value of cis/trans-2-butene.
*3 Na content is 10wt%. *4 Nb_2O_5 is 10 wt% on Al_2O_3.
*5 Na content is 2mmol/g.

3. Results and Discussion

Fig.1 shows the Na K-edge XANES pattern of Na-loaded catalysts. In the case of Na-loaded bulk Nb_2O_5, XANES pattern was different from the case of Na-loaded Al_2O_3 and no formation of basic site was observed on the surface, because cubic sodium niobate ($NaNbO_3$) was formed by calcination at 773K, which was determined by X-ray diffraction. This facts were agreed the results that no reactivity during 1-butene isomerization (Table 1) was observed.

In another case of Na-loaded Nb_2O_5/Al_2O_3, XANES pattern was different from Na-loaded bulk Nb_2O_5. It was exhibited a basic property by the reaction of 1-butene isomerization. As shown in Fig.2, Na-O bond length by the FT of k^3-weighted Na K-edge EXAFS in Na-loaded Nb_2O_5/Al_2O_3 was found to be 0.13nm. In the case of Na-loaded bulk Nb_2O_5, Na-O bond length was observed at 0.18nm. It posesses that the effect of Na-loading on Nb_2O_5/Al_2O_3 was not crystalyzed but formed nearly Na-O bond on the surface. These results possess that the bond length of Na-O in Na-loaded Nb_2O_5/Al_2O_3 catalyst was different from the case of cubic structure of sodium niobate, and existed the type of basic Na-O site on the surface. Such as Na non-loaded Nb_2O_5/Al_2O_3 catalyst was observed acidic property, in contrast, Na-loaded Nb_2O_5/Al_2O_3 was observed basic property.

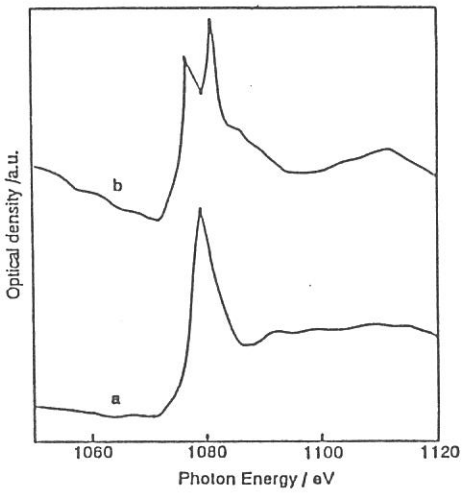

Fig.1 Na K-edge XANES pattern of sodium-loaded (a) bulk Nb_2O_5 and (b) Nb_2O_5/Al_2O_3.

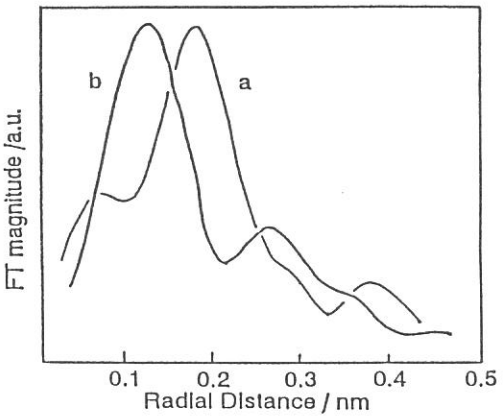

Fig.2 Fourier transform of k^3-weighted EXAFS of sodium-loaded (a) Nb_2O_5 and (b) Nb_2O_5/Al_2O_3.

1. N. Yoshihara, T. Kitagawa, I. Ihara, S. Hasegawa, T. Hasegawa, Bull. Chem. Soc. Jpn., 65 (1992) 1185.
2. S. Hasegawa, M. Morooka, H. Aritani, H. Yoshida, T. Tanaka, Jpn. J. Appl. Phys., in press.

X-RAY EXCITED LUMINESCENCE YIELD SPECTRA OF NaBr AND NaBr:Cu SINGLE CRYSTALS AT Na K-EDGE

Takatoshi MURATA, Katsuyuki HARADA, Atsunari HIRAYA[1], and Makoto WATANABE[1]

Department of Physics, Kyoto University of Education, Fukakusa, Fushimi, Kyoto 612

[1] *UVSOR, Institute for Molecular Science, Myodaiji, Okazaki 444*

The x-ray excited optical luminescence (XEOL) is one of the de-excitation processes following the excitation. The extensive study on the XEOL yield of CaF_2 has been performed by the present authors[1,2]. They found that the bi-directional edge jumps occur depending on the method of the preparation of the sample and also on the temperature. They succeeded to reproduce the observed yield spectra by the calculation using phenomenological theory proposed by Emura *et al.*[1,2]

The origin of the luminescence is the multiple production of the low-energy electrons by the incoming high-energy photons or particles. In some cases, it is possible to observe separated luminescence bands caused by the doped impurities and by the bulk. This means that there are different channels of the energy transfer of the produced low-energy electrons and holes with Auger effect. We present here examples of Cu-activated NaBr which emits two luminescence bands; one at 3.4 eV by Cu^+ impurities, and another at 4.5 eV by bulk NaBr, and non-activated NaBr which luminesces only 4.5 eV.

Luminescence yield measurements of NaBr and NaBr:Cu cleaved single crystal samples for the Na K edge excitation were performed at the BL1A, using a double crystal monochromator with two beryl flat crystals[3]. Interference filters were used to separate the emission band of the bulk and that from Cu impurities. Luminescence signal was detected with a Hamamatsu R955 photomultiplier.

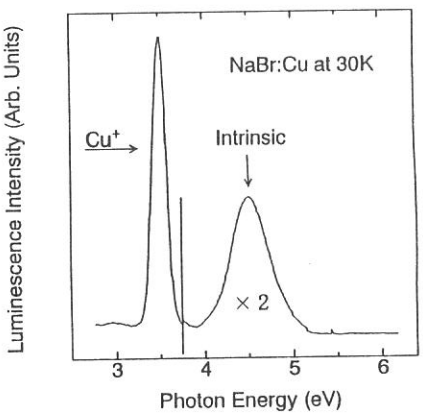

Fig. 1 Optical luminescence spectrum of NaBr:Cu at 30K.

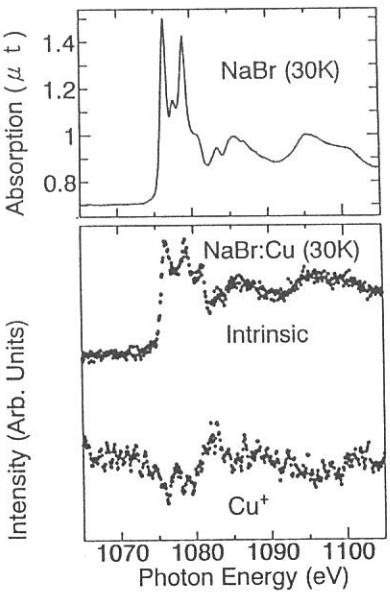

Fig. 2 Absorption spectrum of NaBr and yield spectra at 30 K.

Figure 1 shows the optical luminescence spectrum of NaBr:Cu at 30 K. The shape of the spectrum does not change with exciting x-ray energy. The emission band at 4.5 eV ($\sim$ 275 nm) is the intrinsic luminescence caused by the electron-hole recombination of the relaxed excited states. The band at 365 nm ($\sim$ 3.4 eV) is due to the transition from $3d$ to $3s$ state of Cu^+ ion. Figure 2 shows the luminescence yield spectra of the sample of the NaBr:Cu crystal with Na K-edge-excitation at 30 K. The absorption spectra of NaBr[4] is shown at the top. Although the signals of the yield spectra are noisy, both spectral features reproduce the absorption spectrum fairly well except for the direction of the edge-jump at the Na K-edge; it is normal for the intrinsic luminescence, and inverted for the impurity luminescence. In the case of NaBr pure crystal, a negative jump was observed as in the case of NaCl[3]. The total feature of these yield spectra is similar in the case of the Br K-edge excitation[5].

According to the phenomenological theory by Emura *et al.*[2], the ratio R of the luminescence intensities above and below the energy of the K absorption edge is expressed as follows:

$$R = \frac{1 - e^{-(\mu+\mu')t}}{1 - e^{-\mu t}} \times \frac{\mu + \mu' B}{\mu + \mu'}, \tag{1}$$

with $B \equiv \eta'/\eta$. Here μ and μ' denote the linear absorption coefficients due to the L-and K-edges, respectively, and η and η' are the effective yields of the luminescence for the excited electrons from L-shell and K-shell, respectively. The parameter t means the escape depth of the luminescence.

The negative features mean that the high-energy electrons excited from outer core states by x-rays at Na K-edge region contributes more to the optical luminescence than those from inner core states in ordinary cases. The positive jumps observed in the intrinsic luminescence yield for Cu-contained NaBr indicate that the contribution of the K-electrons is superior. The high energy electrons excited from L-states transfer energies mainly through the luminescence channel to the impurity. Accordingly, the relative contribution of the K-electrons to the intrinsic luminescence channel increases. Detailed discussion is made elsewhere[5].

REFERENCES

1) T. Murata, K. Harada, S. Emura, M. Nomura, K. R. Bauchspießand H. Maeda: To be published in Jpn. J. Appl. Phys. Suppl. (1993).

2) S. Emura, T. Moriga, J. Takizawa, M. Nomura, K. R Bauchspieß, T. Murata, K. Harada, and H. Maeda: To be published in Phys. Rev. B.

3) A. Hiraya, T. Horigome, N. Okada, N. Mizutani, K. Sakai, O. Matsudo, M. Hasumoto, K. Fukui and M. Watanabe: Rev. Sci. Instrum. **63** (1992) 1264.

4) T. Matsukawa S. Naoe, T. Murata and T. Mori: J. Phys. Soc. Jpn. **57** (1988) 2916.

5) T. Murata, K. Harada, S. Emura, M. Nomura, K. R. Bauchspieß, H. Maeda, A. Hiraya, and M. Watanabe: To be published in Jpn. J. Appl. Phys. Suppl. (1993).

Mg K-edge XANES Study of Mgnesium Oxide Species Supported on Silica prepared by Sol-gel Method

Hisao YOSHIDA, Tsunehiro TANAKA, Tomoko HANADA,
Takuzo FUNABIKI and Satohiro YOSHIDA

Division of Molecular Engineering, Kyoto University, Kyoto 606-01

It is widely known that catalytic activity of supported metal oxide is often different from that of the corresponding unsupported metal oxides. This has been understood to be due to not only the enlargement of surface area of metal oxide but also the qualitative change of active sites. The electronic and/or geometric state of active sites is presumably quite different from that in unsupported one. The effect of loading on its catalysis varies with kinds of material of support, loaded amount and the method of preparation. In the case of silica support, the difference of preparation method results in different activity.

Thermal change in the structure of an MgO/SiO_2 (MS) catalyst which show a high activity for fine chemical synthesis has already been reported[1]. In a previous study, we used silica as a support supplied by Fuji-Divison Chem. Co., while in the present study we prepared amorphous silica by hydrolysis of tetraethyl orthosilicate by a sol-gel method as described elsewhere[2]. Because the commercial silica contains inpurities which may lead us to a wrong conclusion about the property of silica, we adopted a sol-gel method to obtain pure silica. Here, we would like to clarify the effect of this silica support on the structure of surface magnesium oxide species by investigating Mg K-edge XANES.

The preparation of the samples and X-ray absorption experiments were carried out as described in the previous report[1]. The structure of MgO species in the highly loaded (> 20 wt%) MgO/SiO_2 was found to be the same as that of bulk MgO with rock salt structure by XANES analysis mentioned later, although XRD pattern showed a broad X-ray diffraction peak by the MgO (200) plane. In the case of low loaded (< 5 wt%) MgO/SiO_2, there were no appreciable peaks in the XRD pattern. Therefore, we have expected that the magnesium oxide is highly dispersed to form surface MgO species with a different structure from that of the bulk. The surface concentration of MgO estimated by XPS increased linearly with the loading of MgO up to 5 wt%, indicating that such highly dispersed MgO is dominant in the samples.

However, all the samples calcined at 500 °C in air (MS5) gave approximately the same XANES spectra regardless of the loading as those of Mg ions located at a center of a regular octahedron of oxygen ions as shown in Fig.1 a), b) and c). This suggests that magnesium ions are present in micro particles of MgO or in two dimentional array of MgO_6 octahedra even in the case of low loaded amounts of MgO. If MgO particles are formed, it is promising that the samples function as a solid base catalysts.

When the samples were calcined at 800 °C, 20MS8 and 5MS8 exhibited the

spectra identical to MS5 samples as illustrated in fig.1 d) and e). On the other hand, XANES feature of 1MS8 as shown in Fig.1 f) was appreciably different from that of 1MS5. In particular, resonance absorption at around 1325 eV was changed significantly. This change indicates that the structure of the MgO micro particle or the raft-like species has changed by calcination at 800 °C. We have recently found that on the 1wt% MgO loading sample evacuated at 800 °C, a new type of magnesium oxide species formed, which exhibited a photoluminescence spectrum with a fine structure[3] associated with an Mg-O bond in isolated MgO species interacted with the silica surface. Correspondingly, the change of XANES would result mainly from a distortion of coordination caused by the interaction of the isolated MgO species with silica surface in which Si^{4+} is coordinated tetrahydrally with oxygen anions.

In the previous study[1], drastic thermal structure-change of MgO species supported on the commercial silica by 17wt% was reported. However, in this study in which a sol-gel method was adopted for silica preparation, such change was not observed. The detailed study of the difference between these silica samples is now in progress.

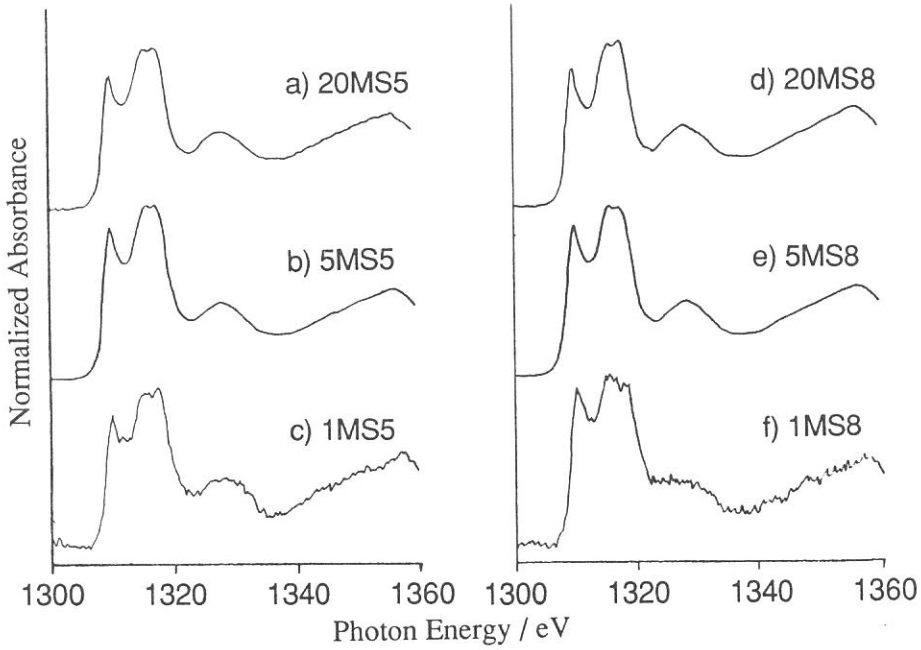

Fig.1 Mg K-edge XANES of the xMSy samples. x stands for loading amount (/wt%MgO), and y stands for calcination temperature (/100 °C).

1) T.Tanaka, H.Tsuji, G.Zhang, M.Sakuraba and H.Hattori, UVSOR ACTIVITY REPORT 1990,p81.

2) S.Yoshida, T.Matsuzaki, T.Kashiwazaki, M.Mori and K.Tarama, *Bull. Chem. Soc. Jpn.*,1974,**47**,1564.

3) T.Tanaka, H.Yoshida, K.Nakatsuka, T.Funabiki and S.Yoshida, *J. Chem. Soc. Faraday Trans.*, 1992,**88**,2297.

Mg K-EDGE STUDY ON ALKALI MODIFIED MgO CATALYSTS

HIDETO TSUJI, TSUKASA HISAZAKI, FUYUKI YAGI and HIDESHI HATTORI

Department chemistry, Faculty of Scienece, Hokkaido University, Sapporo, 060

INTRODUCTION Modification of MgO catalyst with alkali metal cations results in the activity higher than that of non-modified MgO for many base-catalyzed chemical reactions[1]. It is considered that the effect of modification by addition of guest ions on the catalytic property is caused by variation of reactive sites such as surface defects or change of partial charge on O anion of MgO surface. In any case the difference in electronic structure of MgO surface should be found. The considerable XPS studies on the electronic state of MgO surface with regard to the effect of alkali modification were carried out. However, the difference in the electronic state of matrix MgO caused by the modification with alkali was not observed clearly.

Previously we reported Mg K-edge XANES of MgO and Na^+ added MgO and found the distinct change of absorption edge structure[2]. In the present study, the electronic states of MgO influenced by addition of alkali metal cations, Li^+, K^+ and Rb^+, were investigated by Mg K-edge X-ray absorption spectroscory. We generalize the effect of alkali modification on MgO matrix and discuss the results in relation to base-catalytic actions.

EXPERIMENTAL The alkali modified MgO samples Li^+-MgO, K^+-MgO and Rb^+-MgO, were prepared by adding aqueous solution of LiOH, KOH and Rb_2CO_3 to MgO, respectively, followed by drying at 373K for 12h, and calcination at 873K for 5h in air. Total electron yield spectra were taken near the Mg K-edge at the soft X-ray absorption facility installed at the UVSOR BL7A Institute for Molecular Science. The monochromatizing crystal was a natural beryl with 2d=15.965Å. Fine powdered samples were evacuated at 823K for 2h, and placed on the first dinode of electron multiplier under N_2 atomosphere. All the measurements were performed below the pressure of ca 10^{-6}Pa and at room temperature.

RESULTS AND DISCUSSION Fig. 1 shows X-ray absorption spectra (total electron yield spectra) at Mg K-edge of MgO and Li^+-MgO, K^+-MgO, Rb^+-MgO. For alkali modified MgO, the fine structure of the spectra in the XANES region was similar to that of non-modified MgO. However, a significant difference in the intensity of the peak at the threshold was obviously observed.

In the absorption edge region, the fine structure of spectra reflects the distribution of unoccupied quantum state for absorbing atom. This sharp peak at absorption threshold can be assigned to a core exiton associated with the intra ionic allowed transition from 1s core state to 3p state of Mg[3]. Since the p state in the conduction band consists mainly of the electronic state of Mg cation in ionic crystal of MgO, a high peak at the absorption threshold for alkali modified MgO means that the partial charges of the Mg cation and O anion are extensively localized; an ionic nature of MgO is enhanced.

If MgO crystal becomes defective by addition of alkali metal cations, the charge localization between Mg cation and O anion on MgO must be weakened because Madelung potential decreases at coordinative unsaturated defects. Therefore, the enlargement of the peak at the absorption threshold shold not be caused by the contribution of defective sites.

As this spectral feature does not depend on the kind of alkali, it is adequate idea that the alkali of a low electron negativity compared with Mg interacts electrically with MgO matrix. X-ray absorption spectra at Mg K-edge revealed that the re-disribution of the charges on Mg cation, alkali metal cation and O anion take place around alkali added on MgO, and as a result, the electronic state of Mg becomes more cationic.

In fig. 2, X-ray absorption spectra at Mg K-edge of samples of Na^+-MgO prepared by adding aqueous solution of NaOH and ethanol solution of Na ethoxide are shown. The similarity of the fine structure of the spectra suggests that the qualitative change in the electronic state of MgO matrix is not influenced by the method of alkali modification.

In the chemical view point, it is concluded that a high base-catalytic performance of alkali modified MgO catalyst is owing to the increase in the ionicity on MgO surface; the highly localized partial charge on O anion of MgO surface contributes the enhancement of electron pair donor property.

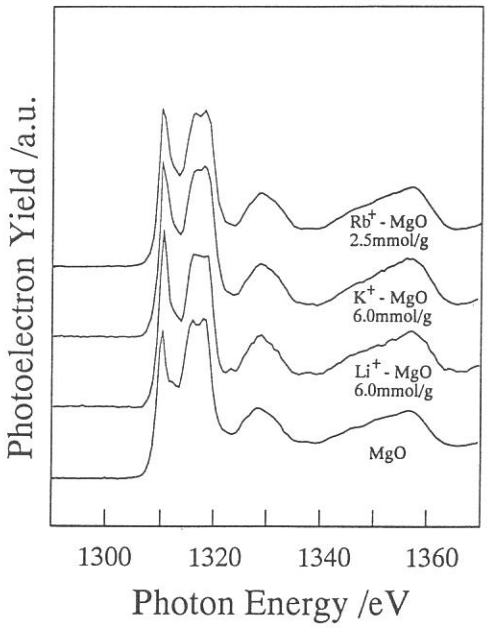

Fig. 1 Mg K-edge absorption spectra of MgO and various alkali modified MgO.

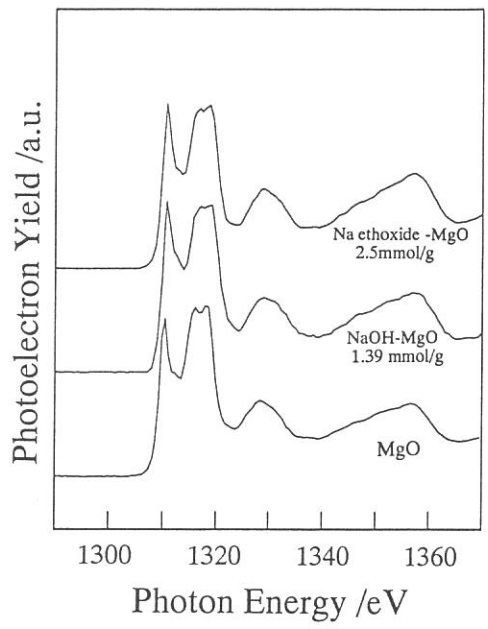

Fig. 2 Mg K-edge absorption spectra of MgO and Na+ modified MgO.

1) G. Zhang et al., Appl. Catal., 48 (1989) 63. 2) H. Tsuji et al., UVSOR activity report, (1990) 83.
3) T. Matsukawa et al., J. Phys. Soc. Jpn., 57 (1988) 2916.

Local Distortion of PO_4 Molecule in $KH_2(PO_4)_2$ Crystals

Hirofumi KASATANI, Yukio NODA[1], Hironobu MAEDA[2], Takashi UMEKI,
Yasuhiro YONEDA, Satoshi MURAKAMI[1], Yoshihiro KUROIWA[1] and Hikaru TERAUCHI

School of Science, Kwansei-Gakuin University, Nishinomiya 662
[1]Faculty of Science, Chiba University, Yayoi Chiba 263
[2]Faculty of Science, Okayama University, Okayama 700

1.Introduction

KDP family materials such as KDP(KH_2PO_4), ADP($NH_4H_2PO_4$), RDP(RbH_2PO_4) etc. show phase transitions at critical temperature T_c. When hydrogen atoms are replaced by deuterium atoms (abbreviated as DKDP), the transition temperature jumps up about 100K in these materials. So far, it has been believed that hydrogen ordering or softening of hydrogen tunneling mode plays an important role at the phase transition. However, recent works cast some doubts on the above tunneling model.

Hydrogen compound KDP transforms at T_c=123K. From the structural analysis, a PO_4 molecule distorts below T_c so that the bond length between P and O atoms splits to r_1=1.508Å and r_2=1.583Å from an undistorted state with r_0=1.538Å.[1)] Those numbers of DKDP are slightly different from ones in KDP, and it is known that T_c=213K, r_0=1.544Å, r_1=1.509Å and r_2=1.578Å.[2)]

The purpose of the present work is to investigate the local structure of PO_4 atoms to reveal the existence of disordering state by means of the XAFS technique. The key point we have to reveal is whether a PO_4 molecule distorts or not at high temperature phase. If the PO_4 molecule already distorts at above the transition temperature, the system must be treated as an order-disorder phenomenon of PO_4 molecules.

2. Experiments and Analysis

XAFS experiments around the K-absorption edge of phosphate atoms in KDP and DKDP were carried out at Wiggler beam line BL-7A of UVSOR. Since the energy of K-absorption edge of a phosphate is very low, special attention was paid to prepare the sample. Fine gel-like powder samples were made by dropping a saturated aqueous solution in to ethanol. The powder sample was entangled on a Cu-mesh and retained by collodion. Transmission XAFS measurements were performed in ultra high vacuum at various temperature. An InSb crystal was used as a monochromater. An example of an absorption coefficient observed in DKDP is shown in Fig.1a), in which XAFS signal around a phosphate atom and around a potassium atom is shown.

XAFS signal $k^3\chi(k)$ is obtained from the observed absorption coefficient by the standard procedure. The signal to noise ratio

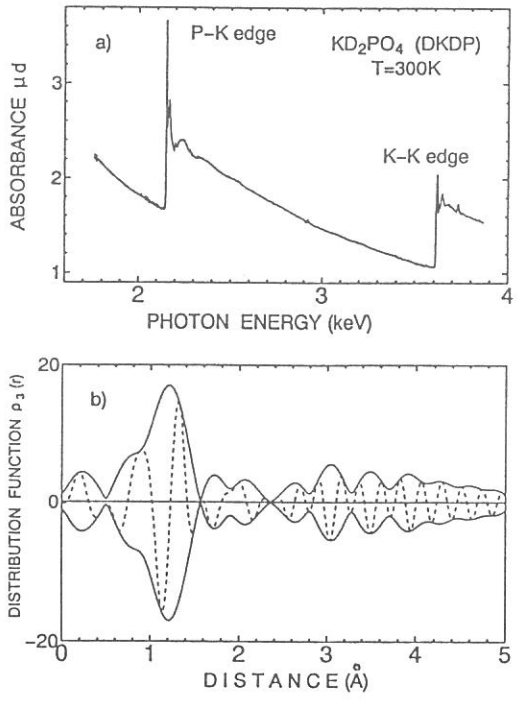

Fig.1 a) An example of XAFS signal in DKDP.
b) Fourier transformed distribution $\rho_3(r)$ of observed $k^3\chi(k)$ in DKDP at 199K.

is still poor so that we can use the k range from k=3.8Å^{-1}(with 2π unit) to 14.0Å^{-1} in $k^3\chi(k)$. In Fig.1b), Fourier transformed distribution function $\rho_3(r)$ of observed $k^3\chi(k)$ in DKDP at 199K is shown. The first peak reflects the oxygen atoms around the probed phosphate atom. Fourier filtered $k^3\chi(k)$ is recalculated by using the r range from r=0.32Å to 1.65Å in $\rho_3(r)$, and then this observed Fourier filtered $k^3\chi(k)$ is compared with two alternative models, one shell model and two shell model. For one shell model, the coordination number is fixed as N=4 and the bond length between P and O atoms(r_0) is a fitting parameter. On the other hand, in two shell model, the coordination numbers are fixed as $N_1=N_2=2$ and the bond lengths r_1 and r_2 are fitting parameters reflecting the local symmetry of the distorted PO_4 molecules.

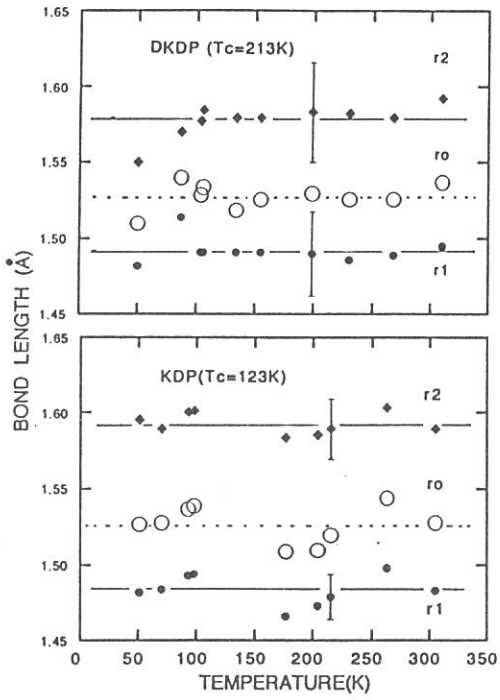

Fig.2 Bond length between P and O atoms in KDP and DKDP. r_0 denotes the bond length of undistorted PO_4 molecules, while r_1 and r_2 denote those of the distorted molecules.

3. Results and Discussion

Obtained bond lengths of KDP and DKDP are shown in Fig.2 as a function of temperature, for both one shell model and two shell model. Obviously, the PO_4 molecule in the low temperature phase distorts. However, least square fitting procedure gives almost the same discrepancy factor (R-factor) for two alternative models through all temperature region in KDP and DKDP. The ratio of R-factor between R_1 of one shell model and R_2 of two shell model indicates that it is difficult to distinguish which model is favorable, partially because the XAFS data of KDP is still poor and we could not measure enough range in k space in order to obtain the sufficient resolution. The bond lengths obtained in this experiments, however, are well consistent with the data of structural analysis noted in the previous section, both in high temperature and low temperature phases. Averaged data given by the present experiments are r_0=1.527(10)Å, r_1=1.484(10)Å and r_2=1.593(8)Å in KDP and r_0=1.528(8)Å, r_1=1.492(8)Å and r_2=1.578(11)Å in DKDP.

It is hardly to conclude that a PO_4 molecule is in a disordered state in KDP because of the insufficient resolution in the present experiments.

References

1) G.E.Bacon and R.S.Pease : Proc. Roy. Soc. (London), Ser. **A230** (1955) 259.
2) J.Nakano, Y.Shiozaki and E.Nakamura : Ferroelectrics **8** (1974) 483.

EXAFS STUDY ON LOCAL STRUCTURES NEAR THE PHASE TRANSITION OF PEROVSKITES

Yasuo NISHIHATA, Osamu KAMISHIMA, Kenji OJIMA, Jianhua ZHUAN
and Akikatsu SAWADA

Faculty of Science, Okayama University, Okayama 700

Many cubic perovskite crystals undergo phase transitions, where they transform to slightly distorted structure from the ideal perovskite structure. The phase transitions are concerned with the condensation of phonon modes. However, an overdamping of the phonon mode and central peak suggest that these phase transition cannot be regarded simply as displacive type ones. Recently, structure refinements by diffraction study on some perovskites of single crystals ($BaTiO_3$, $SrTiO_3$ and $PbTiO_3$ [1,2]) suggest the disorder of atoms. The purpose of this work is to study local structure and reveal whether or not there is a disordered nature in the crystals by EXAFS (Extended X-ray Absorption Fine Structure) technique. We measured x-ray photoelectron yield spectra for some kinds of powder samples; $KMnF_3$, $KNbO_3$ and $KTaO_3$.

In $KMnF_3$, successive phase transition occurs at 186 and 91 K, and caused by the condensation of the zone-boundary mode associated with the rotation of the MnF_6 octahedra [3]. X-ray photoelectron yield spectra, I, were taken near the K-K edge by the use of the double crystal monochromator (DXM) constructed at BL-7A of UVSOR. The Ge(111) plane was used as a monochromator. Signals from the powder sample which was mounted on a cryostat was very weak. Then, the powder samples were put on the first dinode of a photomultiplier with carbon paste. Figure 1 shows the spectrum of $KMnF_3$ at room temperature. Here, the spectrum was normalized by the x-ray photoelectron yield spectra from Au, I0. The quality of EXAFS spectra is not good enough to analyze the local structure around K atom. The intense x-ray using a superconducting wiggler enables us to obtain well-defined EXAFS signals.

[1] K. Itoh et al., Ferroelectrics, 63, 29 (1985).
[2] R. J. Nelmes, R. O. Piltz, W. F. Kuhs, Z. Tun and R. Restori, Ferroelectrics, 108, 165 (1990).
[3] K. Gesi, J. D. Axe, G. Shirane and A. Linz, Phys. Rev. B5, 1933 (1972).

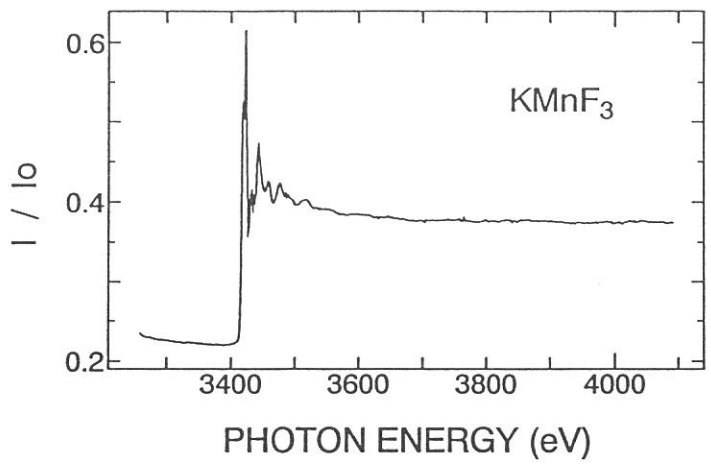

Fig. 1. X-ray photoelectron yield spectrum near the K-K edge of $KMnF_3$ at room temperature.

CORE ELECTRON ABSORPTION SPECTRA OF POLYESTER FILMS

Isuke OUCHI, Ikuo NAKAI, Masao KAMADA*, Shin-ichiro TANAKA* and Tsuneo HAGIWARA†

Department of Physics, Faculty of General Education, Tottori University,
Koyama, Tottori 680
*Institute for Molecular Science, Meidaiji, Okazaki 444
†Tokyo Research Laboratories, Teijin Limited, Hino, Tokyo 191

Polyethylene terephthalate (PET) is a typical polyester having a benzene ring in the main chain; its electronic spectra in UV region have been analyzed in detail[1] and its XPS have been reported[2]. In this work, the absorption spectra of core electrons of PET, together with those of polyethylene 2,6-naphthalate (PEN), were obtained; PEN has a naphthalene ring instead of benzene in the main chain.

The polymers for the samples were supplied from Teijin Limited. Thin amorphous films were made by casting a trichloro-hexafluoro-isopropanol solution. Uniaxially drawn films were obtained by stretching the cast films by an Instron tensile tester at 90°C. Biaxially drawn films of 0.7 microns were fabricated by Film Laboratories of Teijin Limited.

Absorption measurements were done at BL2B1 of UVSOR facilities. The samples were held between copper frames and put in a monochromatized radiation either normal to the beam or at 25° incidence. The transmited beam intensity through the sample or the blank was always corrected by detecting the photo-electrons from the Au mesh placed before the measurement chamber to eliminate the effects of the beam fluctuation and contaminations ; the absorbance of the sample was a ratio of the corrected blank intensity and the corrected sample intensity. The corrected blank intensity could change as much as ± 15% in a day: this was one of the sources of the possible errors.

The photon energy of the incident beam was corrected by the dips of the blank spectra without Au mesh correction at 284.7 and 291.0 eV originated from the carbon contamination, as described by Stohr et al[3].

The grating of the Grasshopper monochrometer had 600 lines per mm in the earlier experiments but later was replaced by that of 1200/mm; the resolution and the stray light were significantly improved. The comparison between the spectra obtained by use of these gratings is shown in Fig. 1.

The conspicuous absorption peaks at 285.5 eV and 289.1 eV of PET and PEN look to correspond to the absorption maxima at 285.5 eV and 287.4 eV, respectively, in the spectra of C_{60} [4]; they also correspond to the strong absorption of benzene adsorbed on Pt(111), peaking at 286 ev with a broad tail[5]. The absorption at 285.5 eV is consistent with the absorption at 285.5 eV of polycrystalline and microcrystalline graphites[6], amorphous carbons[7] and carbon films made by CVD [8]. These peaks have all been assigned to the transitions of C 1s to * state; therefore, the absorptions of PET and PEN at 285.5 eV and 289.1 eV must have occurred from the transitions of C 1s to *, although the peak at 289.1 eV

may be related not to C=C but to C=O.

The benzene ring in PET, as well as the naphthalene ring in PEN, tends to be alligned parallel to the film plane when drawn uniaxially, or, in particular, biaxially. If the parallelism be perfect, the normal incident light would not give rise to any intense peak at these photon energies; in actuality, there are small amount of non-parallel components even in the biaxially stretched films. Also, the films mounted oblique to the incident light exhibited stronger absorption at 289.1 eV. Therefore, the above assignment for these two peaks may be conceivable.

The other broad peaks at 293.4 eV, 296.6 eV and 304 eV should be related to * transitions, also after conjectured from the spectra of the above compounds.

The oxygen absorptions were found at 528.5 eV (shoulder), at 536.6 eV (main peak) and at 547 eV.

Detailed analysis is still to be made.

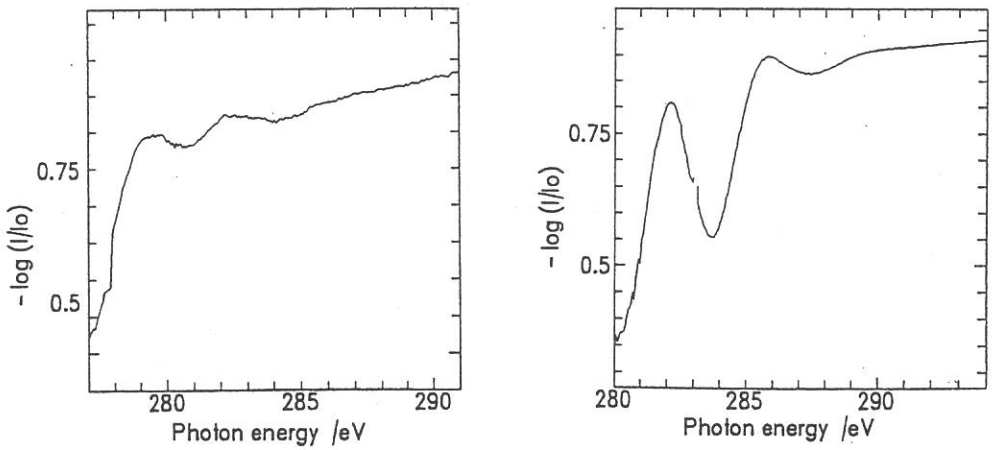

Fig.1 Comparison between the absorption spectra of biaxially oriented PET obtained by a monochrometer with a grating of 600/mm (left) and 1200/mm (right).

1) I. Ouchi: Polym. J. 15 (1983) 225.
2) ex. D.W. Dwight, J.E. McGrath and J.P. Wightman: J. Appl. Polym. Sci. Symp., 34 (1978) 35.
3) J. Stohr and R. Jaeger: Phys. Rev. B, 26 (1982) 4111.
4) H. Shinohara, H. Sato, Y. Saito, K. Tohji and Y. Udagawa: Jpn. J. Appl. Phys. 30 (1991) L848.
5) A.L. Johnson and E.L. Muetterties: J. Am. Chem. Soc. 105 (1983) 7183.
6) D. Denley, P. Perfetti and D.A. Shirley: Phys. Rev. B 21 (1980) 2267.
7) G. Commelli, J. Stohr, C.J. Robinson and W. Jark: Phys. Rev. B 38 (1988) 7511
8) K. Edamatsu, Y. Tanaka, T. Yokoyama, K. Seki, M. Tohnan, T. Okada and T. Ohta Jpn. J. Appl. Phys. 30 (1991) 1073.

PHOTOELECTRON-YIELD SPECTRA OF DYE-DOPED POLYMER SYSTEM

Masaya KAWASE+, Shunsuke NAKANISHI and Hiroshi ITOH

+Department of Chemistry and Department of Physics, Faculty of Education, Kagawa University, Saiwai-cho, Takamatsu 760

Organic dye-doped polymer system attracts much attention because of its optical properties and possibility of application for a functional optical memory. Optical dephasing of the dye-doped polymer system was reported previously[1,2].

In these studies using the incoherent photon echo technique, it was found that the optical dephasing time(T_2) of the doped dye molecule showed the host-dependence. That is, T_2 of the organic dye doped in the crosslinked polyvinyl alcohol derivatives (PVA-SbQ, PVA-SPPIα and PVA-SPPIIα) was longer than T_2 of the organic dye doped in polyvinyl alcohol (PVA). A study of Fourier-transform spectroscopy for photon echos, combined with the persistent hole-burning (PHB), has shown that the photon echo decay includes all information obtained in PHB [3]. This study suggests that the system with long T_2 shows the narrow hole-spectrum and is suitable for a functional optical memory.

As introduction of the cross-link in PVA was performed by photochemical reaction, there was the possibility to form the covalent bond between the doped dye and the host polymer. In order to investigate this point, we measured the soft X-ray photoelectron-yield spectra of the systems employed in this study.

In this report, we will present the results obtained by using BL7A.

As mentioned above, there is the possibility to form the covalent bond between the doped dye and the host polymer in photochemical reaction to crosslink the host polymer. In this study, DTCI was used as the doped organic dye. PPP-MO calculation showed that the frontier electron density was higher on hetero atom (S) than on other atoms around S atom. Therefore, if the covalent bond between the doped dye and the host polymer was formed in photochemical reaction, the soft X-ray photoelectron-yield spectra of S in the dye-doped crosslinked PVA systems must be different from that of the dye-doped PVA system [4]. The spectra of all systems tested in this study had the same shape displayed in Fig. 1. These results suggest that the covalent bond between the doped dye and the host polymer is not formed in the systems employed here. This study using BL7A shows that the host-dependence of T_2 is not caused

by the change of the structure of the doped dye molecule but that of the effective TLS density around the void space which entraps the dye molecule. Our model in the host dependent optical dephasing using the effective TLS density [1,2] is strongly supported by this study.

We would like to acknowledge Prof. Ichimura, Tokyo Institute of Technology, for providing us the crosslinked PVAs. We also thank to Dr. Watanabe, UVSOR, for his invaluable suggestion.

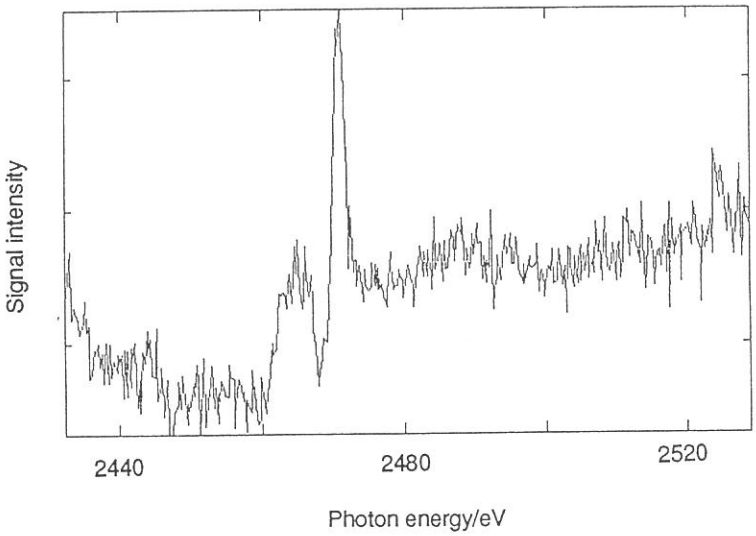

Fig. 1 Soft X-ray photoelectron-yield spectrum of the dye-doped polymer system

References

1. M. Kawase, S. Fujiwara, S. Nakanishi and H. Itoh, Chem. Phys. Lett., **194**, 268 (1992)
2. S. Nakanishi, M. Kawase and H. Itoh, in Ultrafast phenomena, in press.
3. S. Saikan, T. Nakabayashi, Y. Kanamatsu and N. Tato, Phys. Rev. B, **38**, 7777 (1988)
4. W. Gudat and C. Kunz, Phys. Rev. Lett., **29**, 169 (1972)

Photoemission Study of an Al-Pd-Mn Icosahedral Phase

M. MORI, S. HASEGAWA†, T. ISHIMASA, K. SAITO, S. MATSUO and H. INOKUCHI†

College of General Education, Nagoya University, Chikusa, Nagoya 464-01
†Institute for Molecular Science, Myodaiji, Okazaki 444

Since the discovery of an icosahedral phase (i-phase), there has been increasing interest in the electronic properties of icosahedral materials in spite of remaining the arrangement of the atoms unclear. Very recently, a dip-like anomaly in the DOS structure at E_F was confirmed with the UPS experiment. The dip-width and the depth were estimated to be 0.35eV and 70% of a normal DOS, respectively[1]. Successively, the CIS spectra at the binding energy region between 0 – 2eV show resonant characteristic[3]. The Fe 3d band is located in the region ranging from E_F to 2 – 2.5 eV below it with the maximum contribution at around 0.7eV in the binding energy. The smaller binding energy, exactly Fe 3d states sitting just below E_F, is consistent with Friedel's suggestion. The dip structure was interpreted in terms of the nearly-free-electron-like energy gap inferred from strong diffraction spots, which may be related to the stability of the i-phase. It has been known that in an Al-Pd-Mn alloy is a stable i-phase with a high quasicrystalline quality as well as an Al-Cu-Fe system[2]. This principal purpose is the check that the above-mentioned anomaly in DOS at E_F also exists in the Al-Pd-Mn i-phase.

An $Al_{68}Pd_{23}Mn_9$ i-phase specimen was a quasicrystalline ingot prepared by the method[2]. Preliminary checking of the sample was carried out by electron microscope and powder x-ray diffraction methods. The analyzer resolution was about 0.14eV at photon energy 35eV defined with a width of a Gaussian function. The clean surface of the specimen was obtained by scraping with a file in a vacuum of $2 - 4\times10^{-8}$ Pa. Immediately, the sample was transferred to the UPS experimental chamber and measured in a vacuum of $0.5 - 2\times10^{-8}$ Pa. A spectral dependence of incident radiation was determined from a photoelectric yield of gold which was prepared as a film.

UPS experiments were performed making a high resolution (0.14eV=ΔE defined as the width of Gaussian function) with the incident photon energy 35eV, in order to examine the detailed structure of DOS near the E_F. The dotted curve of Fig. 2 is the UPS spectum of Al-Pd-Mn i-phase sample. Well-defined Fermi edge of gold was observed, but Fermi edge of Al-Pd-Mn i-phase was not clearly observed as shown in Fig. 2, which has qualitatively a feature similar to the Al- Cu-Fe i-phase with the pseudo-gap structure[1].

Let us consider a model to reproduce spectra near E_F to obtain a quantitative estimation of the dip structure on the assumption that the observed spectrum is proportional to DOS and the DOS near E_F is linearly dependent on the energy. The DOS additionally has the dip of which shape is assumed to be a Lorentzian function having the center on E_F and a half width as showing in Fig. 1. The observed intensity $I(E)$ is given as follows.

$$I(E) = \int (ax + b) \cdot (1 - \frac{C\Gamma^2}{(x - E_F)^2 + \Gamma^2}) \cdot f(x) \cdot G\exp(-(x - E)^2/(\Delta E)^2)dx,$$

where $(ax + b) \cdot (1 - C\Gamma^2/\{(x-E_F)^2 + \Gamma^2\}$ shows the electronic DOS near E_F at energy x with the dip of the DOS near Fermi edge. In the case of C=0 a system has no anomaly (we call a normal DOS) and in the case of C=1 the system has no DOS at E_F; as C is the ratio of dip-depth and the normal, and C must be less than unity. $f(x)$ is the Fermi distribution function.

We consider the case of C=0 (the normal DOS case). We have tried to fit the spectrum of gold. The fitted was in good agreement with the observed curve using the energy resolution width ΔE=0.14eV and the fitting parameters a and b. But the calculated curve could not be fitted with the dotted curves as shown in Fig. 1, and it is noted that the calculated curve drops more abruptly near E_F than the experimental curve. At a final step, we tried to fit the spectrum of the Al-Pd-Mn i-phase, adding the additional fitting parameter C. The solid curve of Fig. 1 is the most adequately fitted calculation curve with C=0.67 and Γ=0.135eV. The solid curve of Fig. 2 shows that the calculated curve using this fitting model is in good agreement with the observed spectrum. Supposing the dip is approximately the Lorentzian function subtracting from the normal DOS structure, the dip-width is given as about 0.135±0.01eV and the DOS on E_F becomes 0.33±.05 of the normal DOS without the dip. The clear observation of the dip at E_F is consistent with UPS result of the Al-Cu-Fe i-phase[1]. These values should be taken as rough quantitative guess as to the dip width and depth because of somewhat arbitrary assumption of the Lorentzian form. Therefore, it is regarded that this 'dip' model is a good approximation to the DOS near E_F of this Al-Pd-Mn i-phase. A width of the dip is given as about 0.135 ±0.005eV and the DOS on E_F becomes 33±5% of the normal DOS. Comparing the UPS result of the Al-Pd-Mn i-phase with it of the Al-Cu-Fe i-phase, the dip depth is almost same and the width is sharper by the 3 times. The dip model is also supported by the present result. This non-well-defined Fermi edge is also an intrinsic property of this i-phase sample.

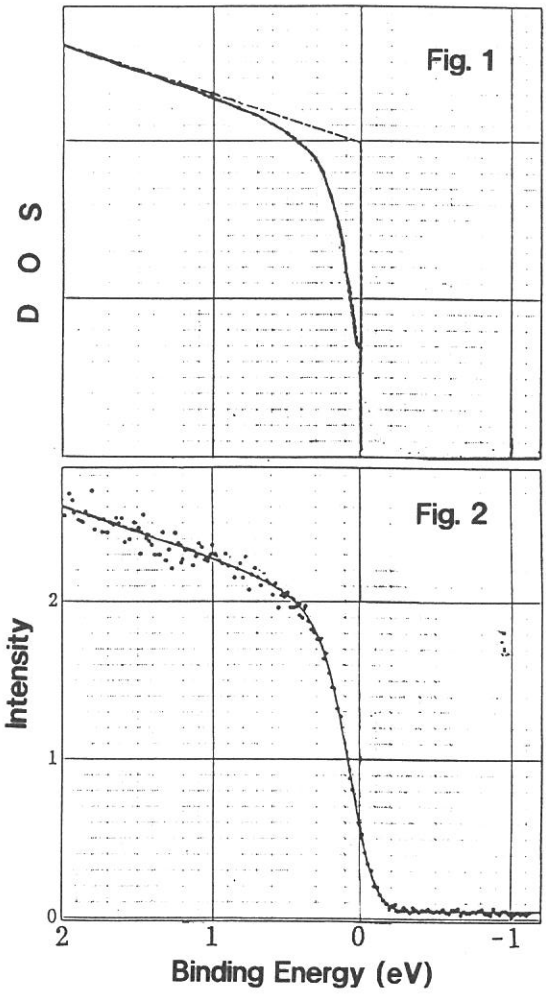

1) Mori M, Matsuo S, Ishimasa T, Matsuura T, Kamiya K, Inokuchi H and Matsukawa T, J. Phys.: Condens. Matter **3** (1991) 767
2) Ishimasa T and Mori M, Phil. Mag. **B66** (1992) 513
3) Mori M, Kamiya K, Matsuo S, Ishimasa T, Nakano H, Fujimoto H and Inokuchi H, J. Phys.: Condens. Matter **4** (1992) L157

FIG. 1. The DOS model of Al-Pd-Mn i-phase for fitting is made up at T=0K by subtracting the dip from the normal DOS (broken curve). Solid curve is in the case of C=0.67 and Γ=0.135eV.

FIG. 2. Dotted curve is the observed UPS near E_F for incident photon energy 35eV at room temperature. Solid curve is the calculated curve supposing that the DOS is like as the solid curve of Fig. 1.

UPS STUDY ON $NiPS_3$ CRYSTAL BY USING SYNCHROTRON RADIATION

H. Fujimoto
Department of Environmental Science,
The Graduate School of Science and Technology, Kumamoto University,
Kumamoto 860, Japan

H. Nakahama, M. Takashima, and K. Ichimura
Department of Chemistry, Faculty of Science, Kumamoto University,
Kumamoto 860, Japan

S. Hasegawa and H. Inokuchi
Institute for Molecular Science (IMS), Okazaki 444, Japan

Metal tricalcogeno-phosphate MPX_3 (M stands for a divalent metal ion and X is either S, Se, or Te) forms a large family of layered compounds. These compounds have attracted much attention due to their capability of intercalation with alkali metals and application to Li-based batteries [1]. Piacentini *et al.* [2] suggested that the Ni d states contribute primarily to the upper part of the valence band in the X-ray photoemission spectra. The resonant photoemission technique has been used to identify the origin of the valence band structures of $NiPS_3$ and $FePS_3$ [3,4]. In this report, we carried out a study of $NiPS_3$ crystals by ultraviolet photoemission spectroscopy (UPS) using synchrotron radiation to get further insight by carefully investigating the valence band electronic structure. We used the resonant-photoemission (RPS) and the constant-initial-state (CIS) spectroscopies to identify the contributions of each element to the valence band of $NiPS_3$.

All spectral measurements were performed at the UVSOR Facility of IMS. The photon energy ($h\nu$) was changed widely from 15 to 90 eV. The Fermi energy (E_F) of the instrument was determined by using the Fermi edge of gold films evaporated *in situ*. CIS spectra were obtained by measuring the $h\nu$ dependence of the electron counting rate and normalizing against the photon number. The photon number was determined by the emission current from a gold mesh placed in the light path and the emission yield of gold. $NiPS_3$ crystals were prepared from elemental mixtures of metal, phosphorus, and sulfur with the atomic ratio of 1:1:3 as reported previously [5]. The synthesized crystals were identified by means of powder X-ray diffraction and Raman spectroscopy. The elemental contents in the crystals were determined by an electron microscope analysis. The single crystal was fixed on a copper substrate by silver resin and was scraped by a diamond file or cleaved in vacuum. RPS and CIS spectra were measured on these clean surfaces.

The $h\nu$ dependence of UPS spectra is shown in Fig.1. Several features can be observed at 1.1, 2.1, 3.0, 4.2, 7.0, 8.2, and 10.0 eV from E_F. UPS spectra taken at high $h\nu$ are similar with the X-ray photoemission spectrum [2]. From the atomic subshell photoionization cross sections [6], the p character is enhanced at low $h\nu$. Taken into account of the atomic ratio between sulfur and phosphorus, the structure at 4.2 eV would mainly come from the sulfur 3p orbitals. Moreover, the structures observed at the high $h\nu$ can be assigned to the main and satellite bands of Ni 3d states.

Figure 2 shows CIS spectra of the valence band structures. Among the features of the valence band, the structures located at 2.1, 3.0, 7.0, and 10.0 eV show strong resonance at the 3d threshold energy of Ni; and the weak resonance is observed at the structures of 1.1 and 8.2 eV, and no resonance occurs in the features at 4.2 eV. The 4.2, and 8.2 eV structures are also

intensified at the photon energy of 30 eV. Therefore, the structures at 2.1, 3.0, 7.0, and 10.0 eV are mainly from Ni 3d orbitals, and the Ni 3d orbitals partly contribute to the features at 1.1 and 8.2 eV. Moreover, there is no 3d character in the 4.2 eV band.

From these observations, we conclude that the top of the valence band contains contributions from Ni atoms and P_2S_6 clusters. This is consistent with the observation that the photoionization threshold energy of $NiPS_3$ is almost same as that of $ZnPS_3$ and $FePS_3$.

References

[1]R. Brec, G. Ouvrard, A. Lousy, J. Rouxel, and A. Le Mehaute, *Solid State Ionics*, **6**, 185 (1982).

[2]M. Piacentini, F. S. Khumalo, G. Leveque, C. G. Olson, and D. W. Lynch, *Chem. Phys.*, **72**, 61 (1982).

[3]M. Piacentini, V. Grasso, S. Santangelo, M. Fanfoni, S. Modesti, and A. Savoia, *Il Nuvo Cimento*, **4D**, 444 (1984).

[4]M. K. Kelly, R. R. Daniels, G. Margaritondo, and F. Lévy, *Solid State Commun.*, **50**, 233 (1984).

[5]K. Ichimura and M. Sano, *Synth. Metals*, **45**, 203 (1991).

[6]J. J. Yeh and I. Lindau, *Atomic Data and Nuclear Data Tables*, **32**, 1 (1985).

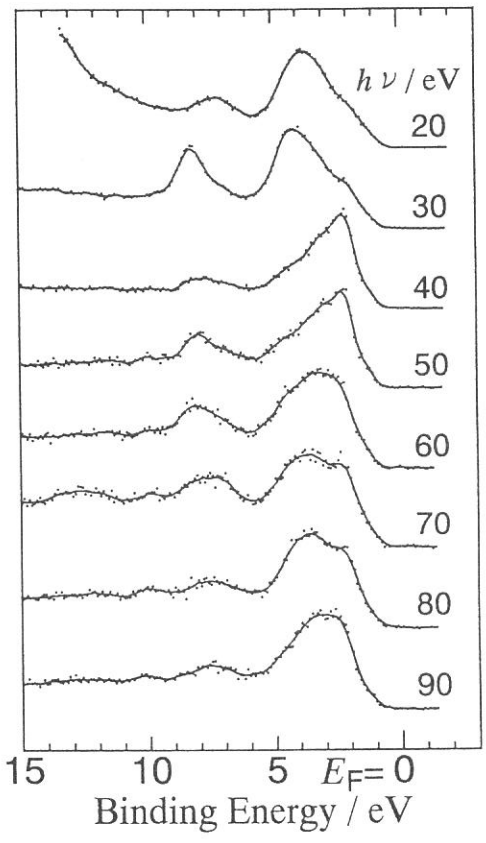

Fig.1 UPS spectra of the scaped $NiPS_3$ crystal.

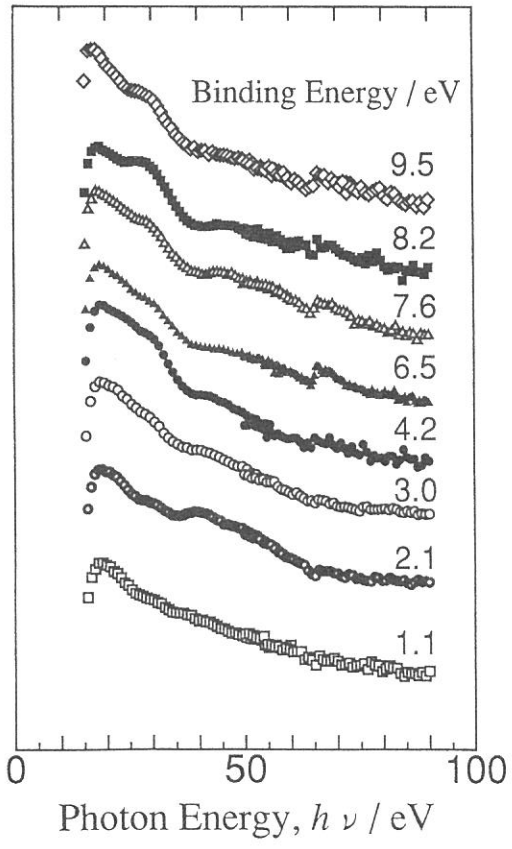

Fig.2 CIS spectra of the valence band structures.

Photoemission Study of $SrLaFeO_4$

Takahisa Omata, Naoyuki Ueda, Kazushige Ueda, Takuya Hashimoto, Hiroshi Kawazoe, Shinji Hasegawa* and Kazuhiko Seki**

Reseach Laboratry of Engineering Materials, Tokyo Institute of Technology, Midori-ku, Yokohama 227
**Institute for Molecular Science, Myodaiji, Okazaki 444*
***Department of Chemistry, Faculty of Science, Nagoya University, Chigusa-ku, Nagoya 464*

Electrical insulator of 3d transition-metal compounds are usually classified into Mott-Hubbard type or charge-transfer type. It has been clarified recentry that the compounds of Cu, Ni and Co are described as charge-transfer insulator. In this report, the electronic structure of $SrLaFeO_4$ with K_2NiF_4 structure has been studied by ultraviolet photoemission spectroscopy. It will be concluded that $SrLaFeO_4$ is a charge-transfer insulator if the bottom of the conduction band is composed of unoccupied Fe3d character.

Photoemission measurements were performed at the beam line BL8B2. The sample was a sintered pellet that was prepared by heating at 1500 °C for 48h in O_2 flow. It was scraped under a vacuum of 6×10^{-8} Torr with a diamond file. All spectra were normalized to the photon flux obtained from experimental and theoretical Au yield.

Fig.1 shows photoemission spectra in the valence band region for various photon energies of excitation. The valence band (2～12 eV band) consists of two feautures around 7.8 and 10.4 eV. The emission cross section of O2p steeply increases toward lower photon energies, while that of Fe3d emission becomes more dominant for higher photon energies ($h\nu$ > 40 eV)[1]. However, the line shape has unchanged for the whole photon energy in contrast with such different photon energy dependences of Fe3d and O2p. CIS spectra for various binding energies in the valence band spectra are shown in Fig.2. It is noted that the intensities of 7.8 and 10.4 eV bands steeply decrease toward higher photon energies and are enhanced for the excitation around $h\nu$～40 eV. Because of the fact that

Fe 3d cross section becomes maximum around $h\nu \sim 40$ eV, 7.8 and 10.4 eV bands are considered to be a mixture of Fe3d and O2p character. On the other hand CIS spectra for 4.0 and 5.0 eV bands do not show such enhancement and monotonously decrease toward higher photon energies. This suggests that O2p character is more dominant around valence band maximum rather than 7.8 and 10.4 eV bands.

Consequently we conclude that $SrLaFeO_4$ is a charge-transfer insulator if the bottom of the conduction band is composed of unoccupied Fe3d character.

1) J.J.Yeh and I.Lindau, At. Data Nucl. Data Tables, 32, 1(1985).

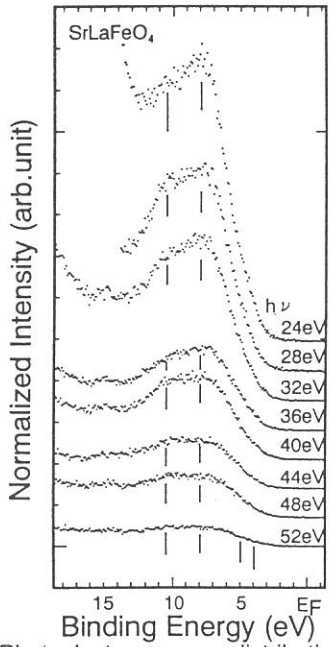

Fig.1 Photoelectron energy distribution curves taken at various photon energies on $SrLaFeO_4$

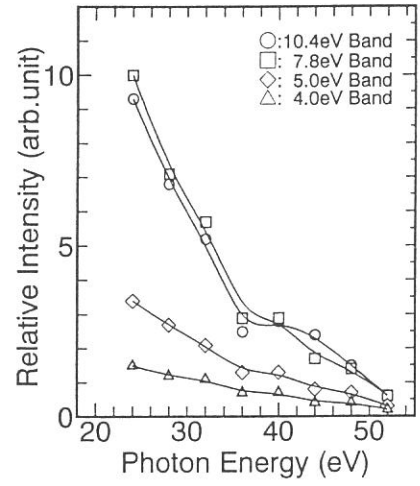

Fig.2 CIS spectra for various binding energies of the valence band spectra of Fig.1

Ultraviolet Photoelectron Spectra of C_{76} and K_xC_{76}

Shojun Hino
Department of Image Science, Faculty of Engineering, Chiba University, Chiba 260, Japan

C_{76} is one of the cage-like carbon compounds (fullerenes) isolated from carbon soot as C_{60}. Alkali metal dosed fullerenes often show high electric conductivity. The photoelectron spectra of both pristine and alkali metal dosed fullerenes will give a clew to understand the origin of their high conductivity. We have measured the ultraviolet photoelectron spectra of C_{76} and potassium dosed C_{76} at BL8B2.

Photoelectron spectra of pristine C_{76}

Figure 1 shows the photon energy dependence of the photoelectron spectra of C_{76}. Eight distinct structures denoted A – H in the figure are observed. There is no sudden appearance or disappearance of the structure in the spectra, as has often been observed in the UPS of the strict **k**-vector conserved system. The spectral onset locates at 1.3 eV below the Fermi level, which is smaller than those of C_{60} (1.9 eV) [1,2] and C_{70} (1.8 eV) [2,3] and the same as that of C_{84} (1.3 eV) [4].

The change of the spectral onset from C_{70} to C_{76} (only 6 atoms are added) is larger than that from C_{60} to C_{70} (10 carbon atoms increased). As the band gaps of fullerenes estimated from the photoemission spectra do not coincide with those estimated from their absorption spectra, the Fermi level of fullerenes does not seem to lie at the middle of the band gap. Actually inverse photoemission studies of C_{60} [5,6] and C_{70} [2] reveal that the Fermi level lies near the conduction band and the band gap is wider than the HOMO – LUMO gap.

A very strong intensity oscillation due to the incident pohoton energy tuning has been found in the first two bands of the spectra of C_{60} [1,7], C_{70} [2] and C_{84} [4]. However, there is no explicit intensity oscillation among the photoelectron structures induced by the incident photon energy change. The behavior of C_{76} seems to be different from the other fullerens.

A theoretically calculated density of states (DOS) of C_{76} using tight-binding approximation [8] expanded by 0.5 eV wide gaussian functions is also shown in Fig. 1. The calculated DOS is shifted so that both first bands coincide at the same energy position. The geometry used in the theoretical calculation is D_2 symmetry which was proposed by Ettl et al. from a NMR experiment [9]. The basis of their conclusion is 19 equal intensity lines in the NMR spectrum. As C_{76} has only one possible structure of D_2 symmetry, the structure of C_{76} is determined uniquely. The calculated DOS shows a very good correspondence with the photoelectron spectra. This agreement also supports the D_2 geometry of C_{76}.

Photoelectron spectra of potassium dosed C_{76}

Figure 2 shows the spectral change of the upper part of the valence band upon potassium dosing. At first stage of potassium dosing ($x = 0.13$ and 0.31), the valence band peaks shift far from the Fermi level by 0.15 eV, while the spectral onset shifts 0.1 eV. This peak shift dissolves at higher potassium dosage ($x = 3.0$). When potassium

dosage is 1.1, a new structure is observed as a small tail to the structure A. As the dosage increases, the new structure grows up between the structure A and the Fermi level to be observed as a distinct peak. At x = 2.1 and 3.0 the spectral onset is 0.15 eV, which is the closest position to the Fermi level in all the photoelectron spectra of potassium dosed C_{76}. The intensity of the new structure increases as the dosage increases. However, the spectral onset shifts away from the Fermi level. The spectral onset is about 0.2 eV at x = 3.6 – 5.5, and it increases to 0.3 eV at x = 6.5. Existence of a gap between the spectral onset and the Fermi level is a direct evidence of the band gap between the conduction and valence bands even though it is small. Therefore, K_xC_{76} is a narrow gap semi-conductor and may not be metallic or super-conductive.

REFERENCES

1. J. H. Weaver *et al.*,, Phys. Rev. Letters. **66**, (1991) 1741.
2. T. Takahashi *et al.*, Physica C **185–189**, (1991) 417.
3. M. B. Jost *et al.*, Chem. Phys. Letters. **184**, (1991) 423.
4. S. Hino *et al.*, Chem. Phys. Letters **190** (1992) 169.
5. P. J. Benning *et al.*, Science **252**, (1991) 1417.
6. T. Takahashi *et al.*, Phys Rev. Letters. **68**, (1992) 1232.
7. P. J. Benning *et al.*, Phys. Rev. B **44**, (1991) 1962.
8. S. Saito, S. Sawada and N. Hamada, Phys. Rev. B, in press.
9. R. Ettl *et al.*, Nature **353**, (1991) 149.

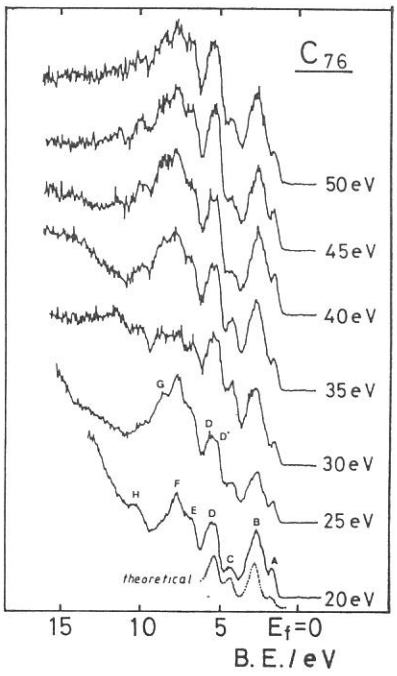

Fig. 1 The incident photon energy dependence of UPS of C_{76}.

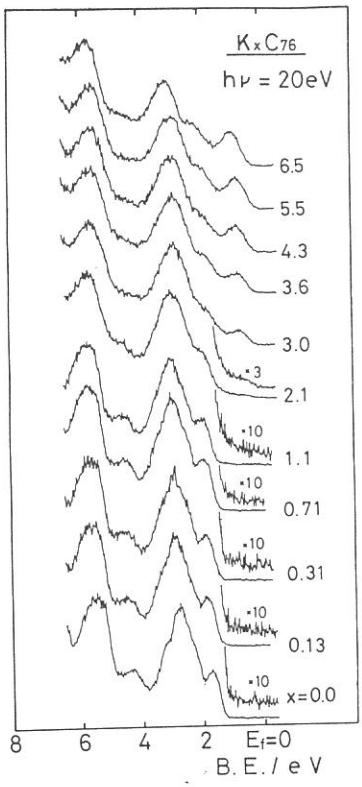

Fig. 2 Spectral change induced by potassium dosing.

Nonradiative decay processes of Cl 2p core exciton in LiCl and NaCl

K. Ichikawa, Y. Taguchi, K. Soda, K. Joda, S. Tanaka, O. Aita,
M. Kamada* and S. Tanaka*

College of Engineering, University of Osaka Prefecture, Gakuen-cho, Sakai 593
**Institute for Molecular Science, Okazaki 444*

We have investigated the nonradiative decay processes of the Li 1*s* core exciton in lithium halides[1,2] and the Na 2*p* core exciton in sodium halides[3,4] by using resonant photoemission. The enhancement of emission intensities of the valence band and the Auger peak was observed at the excitation energies of the Li 1*s* and Na 2*p* core excitons. In addition, kinetic energies of the Auger electron measured at excitation energy of the core exciton are slightly greater than those of ordinary one. The bottom of the conduction band is mainly composed of *s* states of alkali ions in LiCl and NaCl. Thus the Li 1*s* core exciton and the Na 2*p* core exciton are well localized in the alkali ion. On the other hand, the Cl 2*p* core exciton may somewhat be screened by valence electrons compared with the above excitons. The purpose of the present study is to investigate nonradiative decay processes of the Cl 2*p* core exciton in LiCl and NaCl. In this study, we anticipate different results from the previous studies on the core excitons well localized in the alkali ions.

A double stage cylindrical-mirror electron energy-analyzer at BL-2B1 was used to measure photoelectrons. Thin films of LiCl and NaCl were prepared *in situ* by evaporation onto gold substrates. The spectral distribution of incident radiation was determined from a photoelectric yield spectrum of gold.

Figure 1 shows the total photoelectric yield (TY) spectrum of NaCl. This spectrum shows sharp peaks at 201.4, 203.8, 205.9, and 208.2 eV and several broad peaks in the higher energy region. Early works on the absorption spectra have concentrated on interpretation of the first few peaks up to about 9 eV above the threshold. Because of the uncertainty of the absolute transition energies in calculations, the energy of the calculated band-structure has been shifted arbitrarily in order to get a reasonable correspondence between theoretical and experimental peaks. For this reason the first peak has sometimes been assigned to a transition to states in the conduction band[5] and sometimes to a core exciton.[6] At present, the first peak is interpreted in terms of excitation of a core exciton.

Figure 2 shows a set of energy distribution curves (EDC's) of NaCl obtained with the excitation photon energies around the Cl 2*p* threshold. Excitation photon energies ($h\nu$) are indicated on the right-hand side of each spectrum. The ordinates are proportional to the number of photoelectrons per photon flux. The abscissa represents the kinetic energy of electrons. The Cl $L_{2,3}VV$ Auger lines and Cl 3*s* levels are seen in this figure. The Cl 3*s* levels are indicated by arrows. It is noticed that the shape of Auger lines changes drastically with increasing the excitation energy. At $h\nu$ =200.4 eV, which corresponds to the low energy tail of the first absorption peak, the Cl 3*s* level is seen. Two Auger peaks are observed at 175 and 177 eV in the EDC's at $h\nu$ =201.0 and 201.4 eV, while four Auger peaks are seen at 172, 174.5, 175.5, and 178.5 eV in the EDC's measured between $h\nu$ =202.2 and 203.7 eV. At higher excitation energy than 220 eV a broad Auger line is always seen at the kinetic energy of 175 eV.

The change of the Auger shape is limited in the excitation energy range between the first and second peaks in the TY spectrum. The intensity of the 177-eV Auger peak has a maximum at $h\nu$ =201.4 eV which is the first peak energy in the TY spectrum as seen in Figs. 1 and 2. However, 178.5-eV Auger has its maximum intensity at $h\nu$ =202.8 eV

which does not coincide with TY peak. It is noted that the spin–orbit splitting of the Cl $2p$ level is about 1.6 eV from the photoelectron spectra and this value corresponds well to the difference of excitation energies where each Auger peak shows maximum intensity. But the energy separation between the first and second peaks in the TY spectrum is about 2.4 eV. Thus, the second peak in the TY spectrum is not a spin–orbit partner of the first peak and it can be assigned to a transition to states in the conduction band.

The 177-eV and 178.5-eV Auger peaks are observed only in the excitation energy region of the Cl $2p$ core exciton and on the higher energy side of the ordinary one by about 2 eV. These Auger peaks can be attributed to the decay of the core exciton. In the final state of the Auger-decay process of the core exciton, a photoexcited electron and two valence holes form some bound state and reduce the correlation energy from a two-hole state caused by the ordinary Auger transition. This bound state may split into a few levels and causes the 177-eV and 178.5-eV Auger peaks at the excitation energy of the core exciton.

In contrast to the Li $1s$ and Na $2p$ core excitons, no enhancement of the valence-band emission was observed at the excitation energy of the core exciton. Detailed analysis of the experimental results is under way.

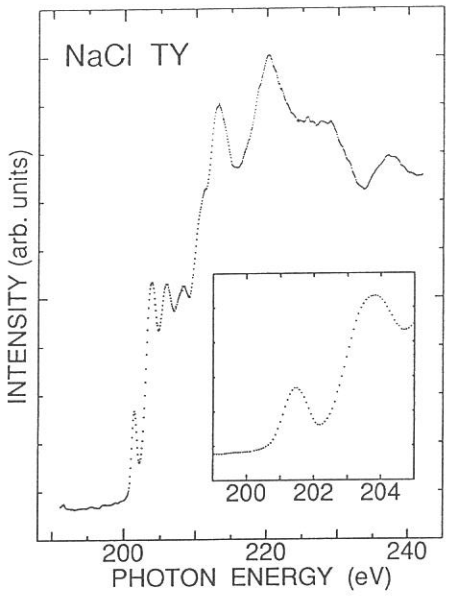

Fig. 1. Cl $L_{2,3}$ TY spectrum of NaCl. Inset shows the TY spectrum in the energy region of Cl $2p$ core excitons in expanded scale.

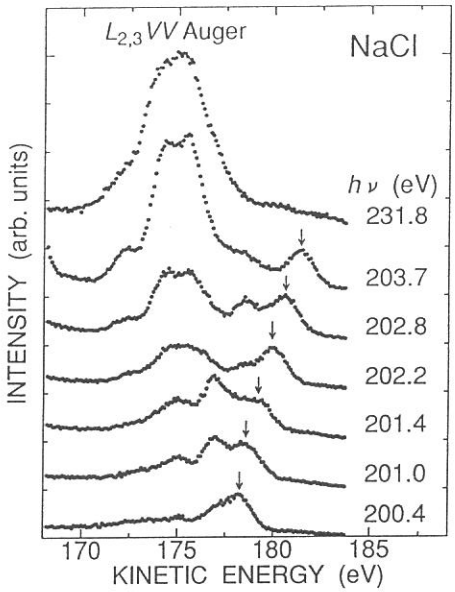

Fig. 2. A set of EDC's of NaCl. Excitation energies are indicated on the right-hand side of each spectrum. Arrows indicate the Cl $3s$ level.

1) M. Kamada *et al.* Phys. Rev. B **28**, 7225 (1983).
2) K. Ichikawa *et al.* Phys. Rev. B **32**, 8293 (1985).
3) M. Kamada *et al.* Phys. Rev. B **36**, 4962 (1987).
4) O. Aita *et al.* Phys. Rev. B **38**, 10079 (1988).
5) F. C. Brown *et al.* Phys. Rev. B **2**, 2126 (1970).
6) O. Aita *et al.* J. Phys. Soc. Jpn. **30**, 1414 (1971).

PHOTOEMISSION STUDY OF SUPERCONDUCTIVE AND NON-SUPERCONDUCTIVE ALKALI-DOPED C_{60}

Takashi TAKAHASHI[1], Takashi MORIKAWA[1], Shinji HASEGAWA[2], Hiroo INOKUCHI[2], and Yoji ACHIBA[3]

[1]*Department of Physics, Tohoku University, Sendai 980*
[2]*Institute for Molecular Science, Okazaki 444*
[3]*Department of Chemistry, Tokyo Metripolitan University, Tokyo 192-03*

Comparative photoemission measurements were performed on alkali (Rb , Cs) doped C_{60} to study the electronic structure, especially its change upon alkali-doping and the difference between the superconductor (Rb-C_{60}) and the non-superconductor (Cs-C_{60}). The photoemission measurement was done at BL2B. The photon energy used was 20 eV and the total energy resolution was about 0.15 eV.

Figure 1 shows the change of conductivity of a C_{60} film upon Rb- or Cs-doping. Pristine C_{60} film has a very low electrical conductivity in the range of 10^{-5} Scm^{-1} showing its insulating nature. However, upon the alkali-doping, the conductivity rapidly increases by 5 - 7 orders of magnitude until the calculated alkali content (x) reaches 3 - 4, then gradually decreases upon further doping.

Figure 2 shows change of photoemission spectrum in the vicinity of the Fermi level of C_{60} upon Rb-doping. As shown in the figure, the HOMO band located at about 2.3 eV, which originates in the six-fold degenerate h_u molecular orbital, shifts toward the high-binding-energy direction by about 0.3 eV upon a slight Rb-doping (from x=0.0 to x=0.5). The most striking feature in the spectrum upon the doping is appearance of a new band near the Fermi level, whose intensity is almost proportional to the doping amount. We ascribe this new band to the LUMO band of a C_{60} molecule which originates in the three-fold degenerate t_{1u} molecular orbital. We find that the density of states at the Fermi level gradually increases upon the Rb-doping in accordance with the growth of the occupied LUMO band near the Fermi level until x=3.7 (here, it should be reminded that the present study overestimates the x's by about 20 %, so that the actual composition is almost Rb_3C_{60} at x=3.7), then the density of states at the Fermi level decreases upon further doping as the occupied LUMO band gradually moves away from the Fermi level. This tendency of the density of states at the Fermi level shows a quite good correspondence to the change of the conductivity in Fig. 1.

Figure 3 shows the change of photoemission spectrum of C_{60} upon Cs-doping. The gross feature of change in the photoemission spectrum upon doping is similar between Rb and Cs, although one of them (Rb-C_{60}) becomes a superconductor while the other (Cs-C_{60}) not. In spite of the gross similarity, there is a small but distinct difference in the spectral intensity, namely the density of electronic states at the Fermi level. This is much more clearly seen in Fig. 4 where the photoemission spectra are displayed in an expanded scale. We find in Fig. 4 that the density of states at the Fermi level at the compositions of x=3 - 4 is much reduced (by a factor of about 5) in Cs-C_{60} compared with those in Rb-C_{60}. This is in good agreement with the conductivity measurement in Fig. 1 where the maximum conductivity in Cs-C_{60} is about a half order smaller than that of Rb-C_{60} at the composition of x=3 - 4. The observed lack of efficient density of states at the Fermi level would account for the absence of superconductivity in Cs-C_{60}.

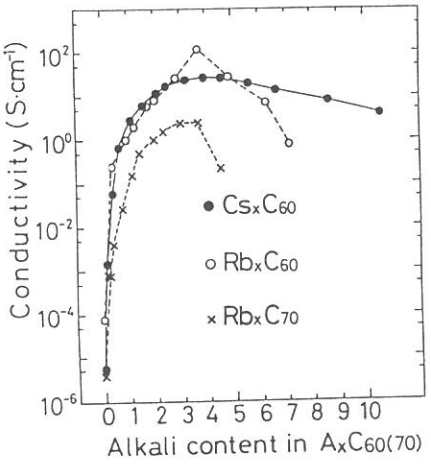

Fig.1 Change of the electrical conductivity of a C_{60} film upon Rb- or Cs-doping. The alkali content in film was calculated on an assumption that deposited alkali atoms distribute uniformly in the film.

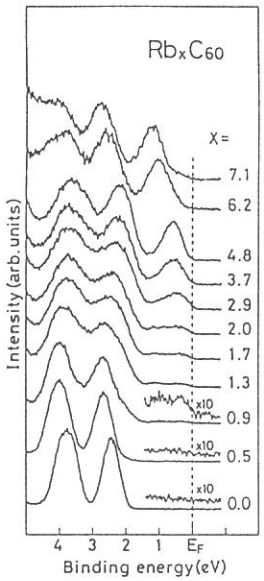

Fig. 2 Change of photoemission spectrum of C_{60} upon Rb-doping

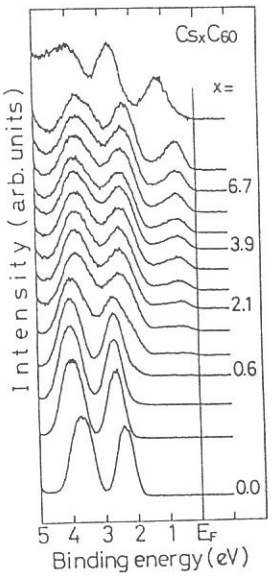

Fig. 3 Change of photoemission spectrum of C_{60} upon Cs-doping

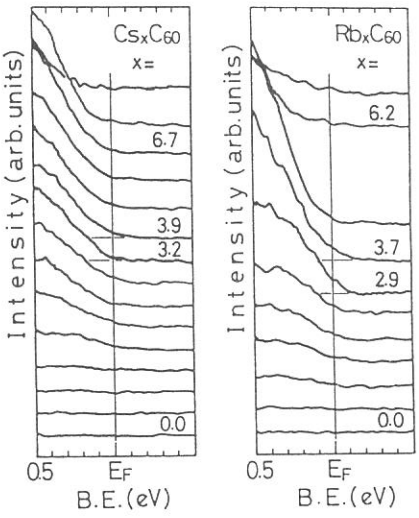

Fig. 4 Comparison of photoemission spectra in the vicinity of the Fermi level between Cs-C_{60} and Rb-C_{60}. The photoemission intensity is normalized with respect to the total intensity of the HOMO and HOMO+1 bands.

Molecular Orientation in Thin Films of Bis(1,2,5-thiadiazolo)-*p*-quinobis(1,3-dithiole) on Graphite Studied by Angle-Resolved Photoelectron Spectroscopy

S. Hasegawa, S. Tanaka, Y. Yamashita, H. Inokuchi,
H. Fujimoto[a)], K. Kamiya[b)], K. Seki[b)], N. Ueno[c)]

Institute for Molecular Science [a)]Department of Environmental Science, Kumamoto University [b)]Department of Chemistry, Nagoya University [c)]Department of Materials Science, Chiba University

Angle-resolved ultraviolet photoelectron spectra (ARUPS) using synchrotron radiation were measured for oriented thin films of bis(1,2,5-thiadiazolo)-*p*-quinobis(1,3-dithiole) (BTQBT) on cleaved graphite surface. The observed take-off angle dependence of photoelectron intensity was analyzed by using independent-atomic-center(IAC) approximation and MNDO molecular orbital calculation. The calculated results agree well with the experimental ones. From the comparison between these results, the molecules in the thin film are estimated to lie flat with the inclination angle $\beta \leq 10°$ to the HOPG surface. This analysis method is useful as a first step to a quantitative analysis for angular distribution of photoelectrons from thin films of large and complex organic molecules.

The experiments were carried out at UVSOR Facility (beamline 8B2). The incidence photon energy was hν= 40eV and the total energy resolution of the spectra was 0.15eV. The take-off angle (θ) dependence of photoemission intensity was measured at incidence angle of photons $\alpha = 0°$, BTQBT[1, 2] was carefully evaporated on HOPG substrate (Union Carbide ZYA-grade) at the deposition rate of 0.2 Å/min. The film thickness was estimated to be about 30 Å. The sample was then transferred to the measurement chamber ($\simeq 4 \times 10^{-10}$ Torr) under vacuum for *in situ* ARUPS measurements.

In Fig.1, the θ dependence of ARUPS spectra is shown in the binding energy region of $0 \sim 3.5$ eV. In this figure, three significant differences are observed: (1) the intensity of HOMO^{-1} band (A) exhibits a maximum at $\theta_{max} \simeq 37.5°$, while the HOMO (B) band gives a maximum at $\theta_{max} \simeq 45°$, (2) the maximum intensity of HOMO^{-1} band is more intense than that of HOMO band, and (3) the FWHM (full width at half maximum) of HOMO band is much larger than that of HOMO^{-1} band.

In IAC approximation by Grobman [3], a molecule is regarded as a set of independent atomic emitters. The total amplitude of photoemission is contributed to the atomic orbital coefficient of molecular orbital, the phase factor due to the difference in the path length to the detector from each atoms, and the atomic factor for optical excitation from an initial state to final continuum states. For the atomic factor, we used the values by Goldberg *et al.* [4].

In the calculation, we introduced the inclination angle β at which the molecular plane is inclined to the substrate surface and the molecular azimuthal angle ϕ_m specifying the azimuthal orientation in the molecular plane, as shown in Fig.2. In Fig.3 (a)$\sim$ (d), the calculated angular distributions of photoelecrtons for HOMO^{-1} state at inclination angles β= 0°, 5°, 10° and 20° are shown, where the dotted, broken and solid lines in each figure are the results at molecular azimuthal angles ϕ_m= 0°, 30° and 90°, respectively. The experimental results are also shown by open circles. The calculated distribution curve at β= 5° and ϕ_m= 90° (Fig.(b), solid line) give the best agreement

with the experimental results. By considering the experimental error and neglect of various scattering effects in the calculation, the BTQBT molecules were estimated to lie with the inclination angle $\beta \leq 10°$ to the HOPG substrate. The discussion for the HOMO band will be reported elsewhere[5].

For more complete analysis, it should be necessary to use exact values of atomic factors [4], and to take account of intermolecular interaction, surface barrier effect by inner-potential, and scattering of photoelectrons by neighboring atoms or molecules [6].

References

[1] Y. Yamashita, S. Tanaka, K. Imaeda and H. Inokuchi, Chem. Lett., 1213 (1991).
[2] K. Imaeda, Y. Yamashita, Y. Li, T. Mori, H. Inokuchi and M. Sano, J. Mater. Chem., **2**, 115 (1992).
[3] W. D. Grobman, Phys. Rev. B, **17**, 4573 (1978).
[4] S. M. Goldberg, C. S. Fadley and S. Kono, J. Electron Spectrosc. Relat. Phenom., **21**, 285 (1981).
[5] S. Hasegawa, *et al.*, (submitted to Phys. Rev. B).
[6] A. Liebsch, Phys. Rev. B, **13**, 544 (1976).

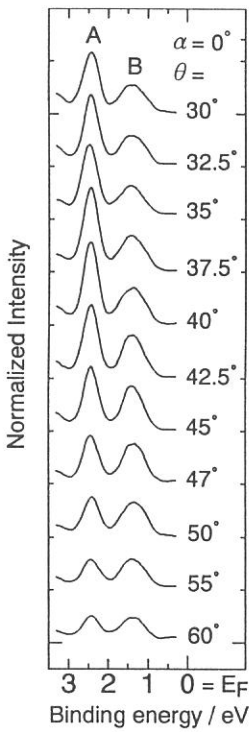

Fig. 1 The take-off angle (θ) dependences of ARUPS spectra. The HOMO^{-1} and HOMO bands are indicated by A and B.

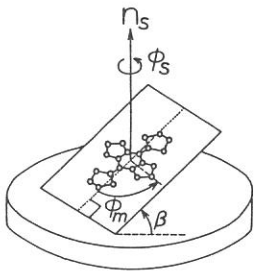

Fig. 2 Illustration of a BTQBT molecule with inclination angle β to the substrate. Molecular azimuthal angle ϕ_m is defined in the molecular plane.

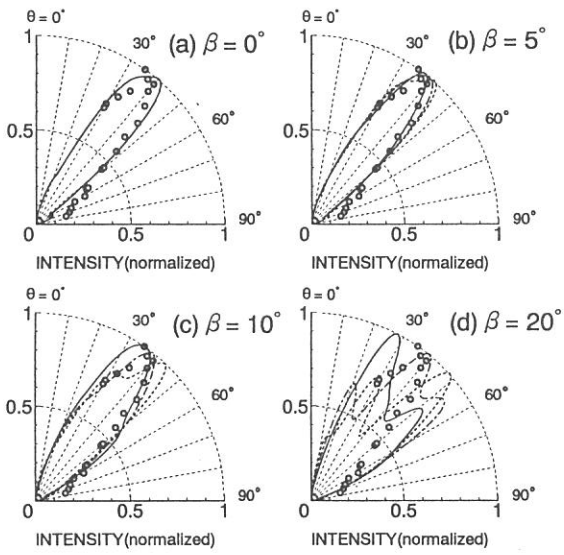

Fig. 3 The take-off angle (θ) dependences of photoemission intensities for the HOMO^{-1} band at $\alpha = 0°$.

Quantitative Analysis of Photoelectron Angular Distribution from Thin Films of Metal-Free Phthalocyanine

Nobuo UENO[a], Katsumi SUZUKI[a], Shinji HASEGAWA[b], Kazuhiko SEKI[c]
and
Hiroo INOKUCHI[b]

[a]*Faculty of Engineering, Chiba University, Yayoi-cho, Inage-ku, Chiba 263*
[b]*Institute for Molecular Science, Okazaki 444*
[c]*Faculty of Science, Nagoya University, Chikusa-ku, Nagoya 464*

The angular distribution of photoelectrons from thin films of organic crystals involves information on the molecular orientation in the film as well as on the wave functions of valence electron. Therefore, the quantitative analysis of the photoelectron angular distribution from a valence state gives a detailed information on the molecular orientation in ultrathin films of functional organic molecule, when the initial-state wave function is known. An advantage of the angle-resolved ultraviolet photoelectron spectroscopy (ARUPS) in determining the molecular orientation is that it introduces less radiation damages into the organic films in comparison with other surface sensitive techniques with electron beams. However, the quantitative analysis of the angular distribution from thin films of large organic molecules is very difficult, and no one has performed the quantitative analysis of the angular distribution after a challenging work by Permien *et al.* [1], which was reanalyzed by Richardson [2], on thin films of lead phthalocyanine. In our work on ARUPS of thin films of large organic molecules, we have found that the angular distribution calculated with the theoretical model used by Richardson [2] gave poor agreement with our experimental results on thin films of copper phthalocyanine.

In the present study, metal free phthalocyanine (H_2Pc) was selected as a sample, since (i) MNDO molecular orbital calculation is possible for this molecule, (ii) the molecule is large enough, (iii) phthalocyanine molecules were known to show flat-lie orientation on various single crystal surfaces [3,4], and the valence electronic states can be well approximated by those of isolated molecule because of the weak intermolecular interaction. For the calculation of the photoelectron angular distribution we used the independent atomic center (IAC) approximation presented by Grobman [5] and the initial-state wave function obtained by MNDO molecular orbital calculation.

Take-of-angle (θ) dependencies of the photoelectron spectra of H_2Pc film (8.6Å thick) on MoS_2 single crystal and HOPG graphite surfaces are shown in Figs. 1a and 1b for the normal incidence condition (the incidence angle $\alpha=0°$) at $h\nu=40$ eV. For both cases, the intensity of the peak A, which originates in the HOMO band consisting of single π orbital, shows prominent θ

dependence. In Figs. 2a and 2b, θ dependence of the intensity of the peak A is plotted for H_2Pc on MoS_2 and H_2Pc on HOPG, respectively. Sharp and similar angular distribution was obtained for both samples. It is notable that the angular distribution is very sharp and the angle θ_{max} giving the highest intensity is 34–38°. These characteristics can not be explained by the model calculation used by Permien *et al.* [1] and Richardson [2]. The angular distribution calculated by IAC approximation and MNDO molecular orbital calculation is also shown in Figs. 2a and 2b. In the calculation, the flat-lie orientation of the molecules and a complete polarization of the incidence photons were assumed, and the scattering of photoelectrons by the substrate and other molecules was neglected. An excellent agreement was obtained between the observed and calculated angular distributions, indicating that the analysis method using IAC approximation and molecular orbital calculation is successfully applicable to the quantitative analysis of the angular distribution of photoelectrons from thin films of large organic molecules.

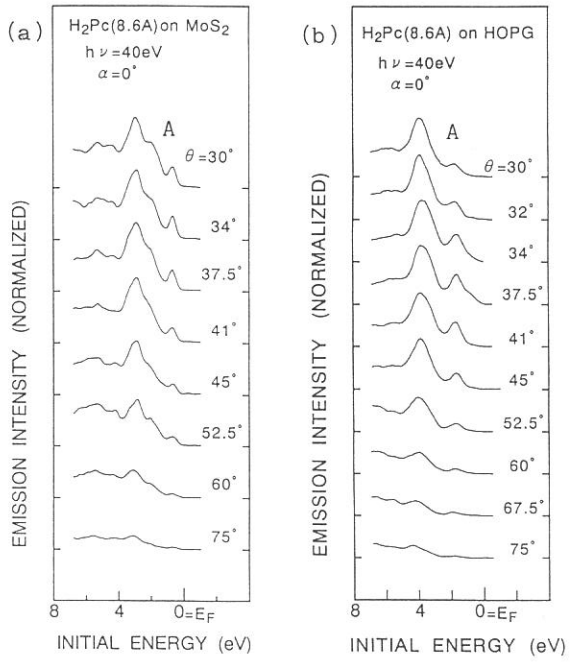

Fig. 1 Take-off-angle (θ) dependence of ARUPS spectra of thin films (8.6 Å) of metal-free phthalocyanine (H_2Pc) on MoS_2 (a) and on HOPG graphite (b) at hν=40eV and α=0°.

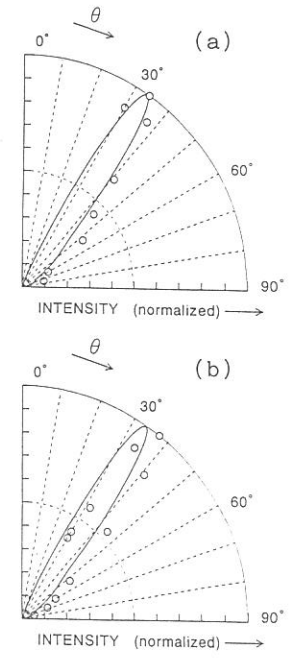

Fig. 2 Take-off-angle (θ) dependence of the intensity of HOMO band A. (a)H_2Pc on MoS_2. (b) H_2Pc on HOPG graphite. The calculated results are shown by solid curves.

References

[1] T. Permien, R. Engelhardt, C. A. Feldmann and E. E. Koch, Chem. Phys. Lett. **98** 527 (1983).
[2] N. V. Richardson, Chem. Phys. Lett. **102** 390 (1983).
[3] J. C. Buchholz and G. A. Somorjai, J. Chem. Phys. **66** 573 (1977).
[4] M. Hara, H. Sasabe, A. Yamada and A. F. Garito, Jpn. J. Appl. Phys. **28** L306 (1989).
[5] W. D. Grobman, Phys. Rev. B**17** 4573 (1978).

Photoelectron Spectroscopy of Polysilanes, Polygermanes, and Si-Ge Copolymers

Akira Yuyama, Satoru Narioka, Hisao Ishii, Toshihiro Okajima, Kazuhiko Seki, Shinji Hasegawa,* Masaie Fujino,**Hiroaki Isaka,** Michiya Fujiki,** Nobuo Matsumoto**

Department of Chemistry, Faculty of Science, Nagoya University, Chikusaku, Nagoya 464-01
**Institute for Molecular Science, Myodaiji, Okazaki 444*
***Basic Research Laboratories, Nippon Telegraph and Telephone Corporation, Midoricho, Musashino 180*

Polysilanes, which are polymers with Si backbones with organic substituents, have attracted attention as a new class of conducting polymers, photoresists, and also due to various interesting properties such as thermochromism. Such functions of polysilanes are not found in saturated organic polymers with C backbones. In this project, we have measured the whole valence band of five polysilanes, two polygermanes, and three Si-Ge copolymers by ultraviolet photoelectron spectroscopy (UPS) to investigate their electronic structures.

The UPS spectra were measured at BL8B2 of UVSOR. The samples were prepared by spin-coating on Cu substrates in a glove bag under N_2 flow. These films were transferred into the vacuum chamber without exposing to air, evacuated, and measured. The obtained spectra are of higher quality than those previously reported for several compounds[1] in showing fine structures and being free from charging.

The UPS spectra of a typical alkylpolysilane, PMPS (Poly(methylpropylsilane)), is shown in Fig.1(a). The abscissa is the binding energy relative to the vacuum level. To compare with the spectrum of PMPS, in Fig.1(b)-(f) we show the UPS and XPS spectra of propane[2)3)] and methane[4)], and the UPS spectrum of $Si_4(CH_3)_{10}$[5)] as a model compound of Si backbone. It is seen that the spectrum of PMPS corresponds well to those of constituent parts; the electronic structure of PMPS can be regarded as an overlap of those of methane, propane, and $Si_4(CH_3)_{10}$. The UPS spectra of polygermanes and block copolymer also correspond to those of $Si_4(CH_3)_{10}$ and $Ge_4(CH_3)_{10}$[6)] as in the case of polysilane, but the spectra of random polymers are not in so good correspondence to $Si_4(CH_3)_{10}$ and $Ge_4(CH_3)_{10}$ because of the contribution of Si-Ge bonding.

The UPS spectra of PMϕS (Poly(methylphenylsilane)), which is a typical arylpolysilane, is shown in Fig.2(a). Compared with PMPS, the spectrum of PMϕS is not in so good correspondence to $Si_4(CH_3)_{10}$ as for PMPS in the uppermost part of the valence band. We suppose that this is caused by σ–π interaction between the πHOMO states of benzene and the Si σHOVB states of the Si backbone. This result corresponds to that of theoretical band calculation reported by Takeda et.al.[7)]

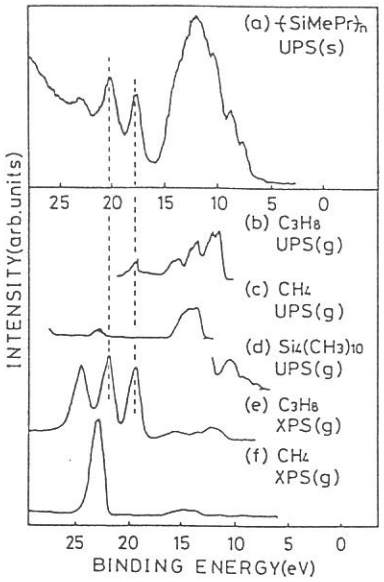

Fig.1 UPS and XPS spectra of PMPS and related compounds. (s) and (g) stand for solid and gaseous states, respectively.

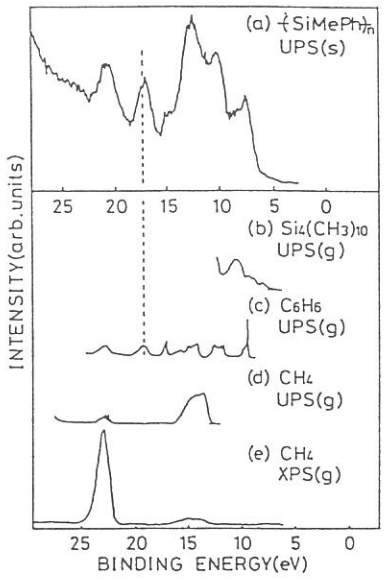

Fig.2 UPS and XPS spectra of PMϕS and related compouds. (s) and (g) stand for solid and gaseous states, respectively.

References

(1) G.Loubriel and J.Zeigler, Phys. Rev., B33, 4203 (1986)
(2) K.Kimura, S.Tatsumata, Y.Achiba, T.Yamazaki, and S.Iwata, Handbook of HeI Photoelectron Spectra of Fundamental Organic Molecules, Japan Scientific Societies Press, Tokyo (1980)
(3) J.J.Pireaux, S.Svenson, E.Basilier, P.Å.Malmqvist, U.Gelius, R.Coudano, and K.Siegbahn, Phys. Rev., A14, 2133 (1976)
(4) A.W.Potts, T.A.Williams, and W.C.Price, Faraday Disc. Chem. Soc., 54, 104 (1972)
(5) H.Bock and W.Ensslin, Angew. Chem. Internat. Ed., 10, 404 (1971)
(6) S.Tokura, K.Mochida, S.Masuda, Y.Harada, 63th Ann. Meeting of Chem. Soc. Jpn., 3 c 33 (Osaka, 1992)
(7) K.Takeda, H.Teramae, and N.Matsumoto, J. Am. Chem. Soc., 108, 8186 (1986)

TEMPERATURE DEPENDENCE ON THE FLUORESCENCE LIFETIMES OF HETEROGENEOUS TRYPTOPHAN RESIDUES IN HEAVY MEROMYOSIN POWDERS

Mieko TANIGUCHI and Masaya KATO
Department of Physics, Faculty of Science, Nagoya University, Chikusa-ku, Nagoya 464-01

Heavy meromyosin (HMM) is a subfragment of myosin which is one of the main proteins of muscle. HMM has an ability of ATP hydrolysis and interacts with actin filaments during muscle contraction. Therefore, it is important to get information whether any conformational changes take place in HMM. In most studies of protein conformation, temperature is a good indicator for monitoring their dynamical properties. The static and dynamic properties of tryptophan luminescence in HMM powders were investigated over wide temperature ranges under high vacuum conditions using synchrotron radiation from UVSOR. HMM was prepared from rabbit muscle. The apparatus was set up, as illustrated schematically in Fig. 1. A cryostat chamber was connected to a excitation monochromator in BL7B beam line. The vacuum pressure was about 1×10^{-7} torr. The samples were placed in a cryostat. A copper-constantan thermocouple was connected to the cell holder. The excitation and emission lights were focused by UV lens, respectively. Fluorescence decay times were measured by using the technique of time-correlated single photon counting under the single bunch operation. The signals from a microchannel plate photomultiplier were received by multichannel analyzer and then sent to microcomputer. Data were analyzed by a least-squares iterative convolution method. The fluorescence emission spectrum has a peak at 330 nm, when excited at 295 nm. The result means short-wavelength fluorescence from buried tryptophan residues. The decay times have three components (comp. 1 = 4.3-5.2 ns, comp. 2 = 2.5 ns and comp. 3 = 0.2 ns) and these values are independent of temperature. The fraction of these components depend on temperature. Fig. 2 show temperature dependence on the total and components of decay-associated emissions, respectively. The results show that the component 1 depends on temperature.

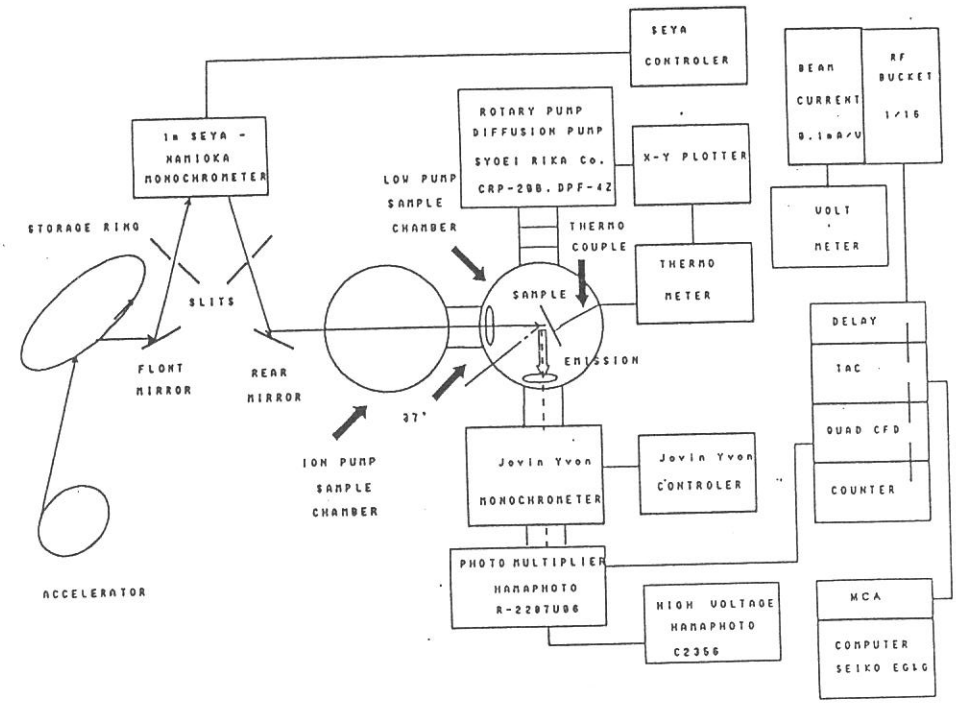

Fig. 1 A schematic drawing of apparatus for time-resolved fluorescence experiments.

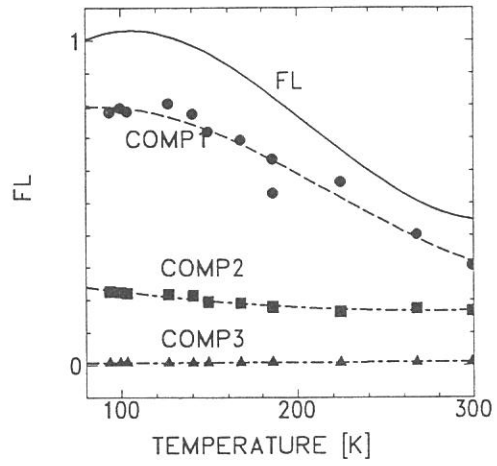

Fig. 2 Temperature dependence on the decay-associated emissions of HMM powders.
Excitation at 295 nm. Emission at 330 nm. ---, total intensity
Comp. 1 = 4.7-5.2 ns, comp. 2 = 2.5 ns, and comp. 3 = 0.2 ns.